

University of Illinois at Urbana-Champaign



ACRC

Air Conditioning and Refrigeration Center A National Science Foundation/University Cooperative Research Center

Comparison of R744 and R410A for Residential Heating and Cooling Applications

M. R. Richter, C. W. Bullard, and P. S. Hrnjak

ACRC CR-39

June 2001

For additional information:

Air Conditioning and Refrigeration Center
University of Illinois
Mechanical & Industrial Engineering Dept.
1206 West Green Street
Urbana, IL 61801

(217) 333-3115

The Air Conditioning and Refrigeration Center was founded in 1988 with a grant from the estate of Richard W. Kritzer, the founder of Peerless of America Inc. A State of Illinois Technology Challenge Grant helped build the laboratory facilities. The ACRC receives continuing support from the Richard W. Kritzer Endowment and the National Science Foundation. The following organizations have also become sponsors of the Center.

Amana Refrigeration, Inc.
Arçelik A. S.
Brazeway, Inc.
Carrier Corporation
Copeland Corporation
Dacor
Daikin Industries, Ltd.
DaimlerChrysler Corporation
Delphi Harrison Thermal Systems
Frigidaire Company
General Electric Company
General Motors Corporation
Hill PHOENIX
Honeywell, Inc.
Hussmann Corporation
Hydro Aluminum Adrian, Inc.
Indiana Tube Corporation
Invensys Climate Controls
Kelon Electrical Holdings Co., Ltd.
Lennox International, Inc.
LG Electronics, Inc.
Modine Manufacturing Co.
Parker Hannifin Corporation
Peerless of America, Inc.
Samsung Electronics Co., Ltd.
Tecumseh Products Company
The Trane Company
Thermo King Corporation
Valeo, Inc.
Visteon Automotive Systems
Wolverine Tube, Inc.
York International, Inc.

For additional information:

*Air Conditioning & Refrigeration Center
Mechanical & Industrial Engineering Dept.
University of Illinois
1206 West Green Street
Urbana, IL 61801*

217 333 3115

Abstract

In the first part of this report, experimental results are presented comparing a prototype R744 system with a commercially available R410A system in heating mode. When the heating capacity of the two systems is matched at the ARI heating capacity rating condition, the heating efficiency of the two systems is comparable. When the cooling capacity of the two systems is matched at the ARI cooling capacity rating condition, the heating efficiency of R744 is lower than R410A.

In the second part of this report, a theoretical comparison of R744 and R410A is made. The theoretical cycle performance of R410A and R744 is compared on the basis of the comfort of the conditioned space, which is determined by dehumidification in cooling mode and the supply air temperature in heating mode. Cycles are analyzed with both ideal and real compressors, and trade-offs between heat exchanger size and efficiency are presented.

In cooling mode, the relative efficiency of the two refrigerants is primarily a function of the airflow rate over the outdoor coil, since the indoor coil performance is constrained by the dehumidification requirement. The advantage for R744 in terms of slightly lower compression ratios and slightly higher evaporating temperatures is far outweighed by the thermodynamic advantage of R410A in terms of lower heat rejection temperatures at extremely high airflow rates. To reach its ideal thermodynamic efficiency, however, requires the subcritical R410A cycle have an infinite airflow rate. At the ARI rating condition, reducing the R410A airflow rate over the outdoor coil to match the finite rate required by R744, reduces the relative advantage of R410A by nearly 70%.

In heating mode, the R744 cycle is more efficient than R410A for supply air temperatures above 40°C, resulting primarily from the higher compression ratios required by R410A for elevated supply air temperatures. Additionally, for a compressors sized for equal capacity in cooling, the capacity of the R744 cycle is higher at lower outdoor temperatures, which has important practical benefits in terms of reduced dependence on lower efficiency supplementary heating.

Table of Contents

	Page
Abstract	iii
List of Figures	viii
List of Tables	xi
Chapter 1: Introduction	1
1.1 Background.....	1
1.2 Selection of baseline refrigerant	1
1.3 Basis of theoretical comparison	2
Chapter 2: Experimental Results of RAC1 System in Heat Pump Mode	3
2.1 Comparison of RAC1-R744 and baseline R410A systems.....	3
2.2 Test matrix and baseline results	5
2.3 Experimental heat pump results for R744 compared to R410A.....	5
2.4 Effect of varying indoor airflow rate on R744 performance	10
2.5 Effect of suction accumulator and indoor coil configurations on R744 results.....	10
2.6 Conclusions regarding experimental performance of R410A and R744.....	11
Chapter 3: Ideal Cycle Considerations	12
3.1 Ideal cycle description	12
3.2 Ideal heat pump cycle	13
3.3 Ideal air conditioning cycle	18
3.4 Ideal system performance	20
3.5 Ideal cycle conclusions.....	21
Chapter 4: Real Cycle Considerations	22
4.1 Cycle Assumptions.....	22
4.2 Compressor assumptions.....	24

4.2.1 Isentropic and volumetric efficiency	24
4.2.2 Variable vs. fixed displacement	25
4.3 Air conditioning cycle	28
4.4 Heat pump cycle.....	31
4.4.1 Cycle analysis	31
4.4.2 Supplementary heating options.....	33
4.5 Comparison of heat exchanger sizes required for heating and cooling.....	34
4.5.1 Indoor coil sizing	34
4.5.2 Outdoor coil sizing	38
4.6 Real cycle conclusions	41
Chapter 5: Seasonal Efficiency	43
5.1 Annual loads	43
5.2 Cycle assumptions.....	44
5.3 Results.....	45
Bibliography	48
Appendix A: System Configuration	50
A.1 R410A A/C & H/P System.....	50
A.1.1 R410A system instrumentation	50
A.1.2 Indoor Coil.....	51
A.1.3 Outdoor Coil.....	51
A.1.4 Filter Dryer.....	52
A.1.5 Mass Flow Meter	52
A.1.6 Compressor.....	52
A.1.7 Expansion Valve	52
A.1.8 Line Sets	52
A.1.9 Sight Glasses.....	52
A.1.10 Charging Conditions	52

A.2 R744 RAC1 System Components	52
A.2.1 System Overview and Schematics of RAC1.....	52
A.2.2 RAC1 Indoor Heat Exchanger.....	53
A.2.3 RAC1 Outdoor Heat Exchanger.....	55
A.2.4 Compressor and Compressor Motor.....	56
A.2.5 Line Sets	57
A.2.6 Sight Glasses.....	57
A.2.7 Suction Accumulator.....	57
A.2.8 Suction Accumulator Oil-Bleed Valve	58
A.2.9 Expansion Valve	58
A.2.10 Charging Conditions.....	58
 Appendix B: Effect of Suction Accumulator Configuration/Indoor Heat Exchanger Orientation on RAC1 R744 Heat Pump Performance	 59
B.1 System configuration	59
B.2 Experimental Results.....	60
B.3 Conclusion	63
 Appendix C: Indoor Chamber Energy Balance.....	 64
C.1 Determination of specific heat constants	64
C.2 Testing and results.....	64
C.3 Error analysis:	65
 Appendix D: Vapor Compression Cycle Control/Distribution	 69
D.1 Low pressure receiver in subcritical / transcritical cycle.....	69
D.2 High Pressure Receiver	70
D.2.1 Subcritical Cycle	70
D.2.2 Transcritical cycle	71
D.3 Flash gas bypass in subcritical / transcritical cycle	71

Appendix E: Psychrometrics and Sensible Heat Ratio	73
E.1 Sensible heat ratio in terms of log-mean differences.....	73
E.2 Psychrometric relationship.....	73
E.3 EES program.....	74
E.4 Results.....	75

List of Figures

	Page
Figure 2.1 Heating performance comparison with matched heating capacity	6
Figure 2.2 Heating performance comparison with matched cooling capacity	6
Figure 2.3 Effect of increased capacity of R744 at lower outdoor temperatures on overall heating efficiency (matched heating capacity).....	7
Figure 2.4 Effect of increased capacity of R744 at lower outdoor temperatures on overall heating efficiency (matched cooling capacity).....	7
Figure 2.5 R744/R410A cycle comparison.....	8
Figure 2.6 Frost pattern on outdoor coil indicating maldistribution.....	9
Figure 2.7 R744 gas cooler performance (indoor temperature 21°C).....	9
Figure 2.8 Compressor efficiency at matched cooling capacity.....	10
Figure 2.9 Effect of airflow rate reduction on R744 indoor coil (R410A baseline face velocity=1.55 m/s).....	10
Figure 3.1 Ideal subcritical cycle	12
Figure 3.2 R744 pressure enthalpy diagram.....	13
Figure 3.3 Maximum supply air temperature based on pinch point	14
Figure 3.4 Effect of pressure and refrigerant mass flow variations on maximum supply air temperature	15
Figure 3.5 Effect of increasing flow rate at a constant pressure on maximum supply air temperature and cycle efficiency for R744	16
Figure 3.6 Comparison of cycle efficiency based on maximum supply air temperature (both cycles with IHX)	16
Figure 3.7 Effect of decrease in evaporating temperature on heating cycle efficiency	17
Figure 3.8 Cooling cycle efficiencies (gas cooler exit temperature 35°C)	19
Figure 3.9 Effect of air flow rate on R410A cooling cycle efficiency (gas cooler exit temperature 35°C, evaporating temperature 12°C).....	19
Figure 3.10 Effect of fixed displacement compressor on ideal heat pump cycle capacity	20
Figure 3.11 Efficiency with finite displacement compressor.....	21
Figure 4.1 R410A compressor efficiency.....	24
Figure 4.2 R744 compressor efficiency.....	25
Figure 4.3 Load/capacity curve for system with fixed capacity compressor.....	26
Figure 4.4 Efficiency for system with fixed capacity compressor.....	27
Figure 4.6 Trade-off between increase in change in enthalpy and decrease in refrigerant mass flow rate as a function of gas cooler pressure for R744 ($T_{\text{evap}}=5.3^{\circ}\text{C}$).....	28
Figure 4.7 Dependence of evaporating temperature on sensible heat ratio	29
Figure 4.8 Effect of evaporating temperature on cooling cycle efficiency with unconstrained airflow rate over condenser/gas cooler.....	30
Figure 4.9 Effect of evaporating temperature on cooling cycle efficiency with matched air flow rates over condenser/gas cooler.....	30
Figure 4.10 Effect of internal heat exchanger on cooling cycle efficiency	31
Figure 4.11 Effect of real compressor and evaporating temperature on heating cycle efficiency.....	32

Figure 4.12 Refrigerant discharge temperatures for corresponding maximum supply air temperature with real compressor.....	32
Figure 4.13 Supplemental heating options.....	33
Figure 4.14 Comparison of fixed supply air temperature and variable supply air temperature supplementary heating configurations.....	34
Figure 4.15 Controlling air-side capacity in cooling mode by adjusting air flow rate over evaporator coil	35
Figure 4.16 Temperature profile in gas cooler	35
Figure 4.17 Effect of finite area gas cooler on heating cycle efficiency (real compressor, evaporating temp: 2.3 C)	37
Figure 4.18 Effect of finite area gas cooler on heating cycle efficiency (real compressor, evaporating temp: 2.3 C)	37
Figure 4.19 Conceptual diagram of indoor coil for reversible air conditioning and heat pump operation (side view). Slats at either end could rotate to increase the area for airflow by a factor of the number of passes, maintaining the air side heat transfer coefficient for large differences in flow rate.	38
Figure 4.20 Effect of airflow rate on heating cycle and system efficiency for 8.3°C outdoor heating condition, 40°C supply air temperature	39
Figure 4.21 Effect of heat exchanger area on system heating COP, 8.3°C outdoor heating condition, 40°C supply air temperature	40
Figure 4.22 Effect of airflow rate on cooling cycle and system efficiency for 45°C outdoor cooling condition, 12°C evaporating temperature	40
Figure 4.23 Effect of heat exchanger area on system cooling COP, 45°C outdoor cooling condition, 12°C evaporating temperature	41
Figure 5.1 Temperature bin data	43
Figure 5.2 Capacity normalization as function of heating capacity and outdoor temperature	44
Figure 5.3 Capacity load curve for sample system, 40°C supply air in heating.....	45
Figure 5.4 Comparison of overall annual efficiency as function of heating load requirement for 40°C supply air	46
Figure 5.5 Capacity load curve for sample system, 60°C supply air in heating.....	46
Figure 5.6 Comparison of overall annual efficiency as function of heating load requirement for 60°C supply air	47
Figure A.1 R410A facility layout showing location of instrumentation.....	50
Figure A.2 Diagram and specifications for the R410A A/C and H/P evaporator coil. This schematic shows the a side view of the evaporator as it is situated in the duct test section B.....	51
Figure A.3 Diagram and specifications of R410A A/C & H/P outdoor coil and compressor.....	51
Figure A.4 Schematic of RAC1 CO ₂ system	53
Figure A.5 Cross section of specially designed high pressure R744 heat exchanger header.	54
Figure A.6 Cross section of the microchannel tube used in the RAC1 R744 heat exchangers.....	54
Figure A.7 R744 indoor single pass microchannel heat exchanger slab shown on the top with the arrow showing the direction of refrigerant flow. The bottom schematic shows three single slab evaporators as they are placed in the duct test section.....	55

Figure A.8 R744 outdoor six pass microchannel heat exchanger slab.....	56
Figure A.9 R744 sight glass. Note the presence of liquid R744 at the bottom of the viewing area.....	57
Figure A.10 The R744 suction accumulator. The black tube pointed at the bottom of the viewing area is actually a fiber optic light source used to improve viewability	58
Figure B.1 Arrangement of suction accumulator for R744 RAC1 comparison with R410A: liquid-vapor lines intersect below level in accumulator.....	59
Figure B.2 Comparison of capacity and efficiency with re-orientation of indoor coil and adjustment of suction accumulator.....	60
Figure B.3 Compressor power for capacity/efficiency results.....	61
Figure B.4 Evaporating temperature (at inlet to evaporator)	62
Figure B.5 Ratio of calculated heat transfer in internal heat exchanger from high pressure side to low pressure side assuming no phase change.....	63
Figure C.1 Calculated concentration dependence on temperature with fixed density.....	66
Figure C.2 Calculated concentration dependence on density with fixed temperature	67
Figure C.3 Calculated specific heat dependence on concentration.....	67
Figure D.1 Low pressure receiver.....	69
Figure D.2 High pressure receiver.....	70
Figure D.3 Comparison of effect of high and low pressure receiver on ideal R410A subcritical cycle	71
Figure D.4 Flash Gas Bypass.....	71
Figure E.1 Graphic psychrometric determination of evaporator surface temperature	74
Figure E.2 Evaporating temperature dependence on inlet conditions for a given sensible heat ratio (R744)	76
Figure E.3 Capacity control for finite heat exchange area by varying air flow rate (R744).....	76

List of Tables

	Page
Table 2.1 Comparison of components for residential system	4
Table 4.1 Comparison of cycle assumptions based on the 8.3°C/21°C heat pump rating condition, dry coil, supply air temperature 40°C.....	23
Table A.1 Comparison of indoor heat exchanger specifications.....	54
Table A.2 Comparison of outdoor coil specifications for the three tested systems.....	56
Table C.1 Summary of energy balance results	65
Table C.2 Relative contribution to overall error from each source for the R410A baseline rating condition (8.3°C outdoor/21.1°C indoor).....	68

Chapter 1: Introduction

1.1 Background

Interest in R744 (carbon dioxide, one of the earliest-used refrigerants,) has recently been revived as a result of environmental considerations and modern heat exchanger manufacturing methods. Investigating the use of R744 in residential heat pump applications is a part of comprehensive program in transcritical R744 system and component research, which began by comparing the performance of R744 and R410A in cooling mode (Beaver et al., 1999a). In this report experimental results comparing the performance of R744 and R410A in heating mode are presented, as well as a theoretical comparison of the maximum operating efficiency in both heating and cooling mode of R744 and R410A subject to comfort constraints and real cycle limitations. By including the effect of comfort constraints and using R410A as a baseline, the theoretical portion of this report differs from earlier R744 cycle studies (Lorentzen and Pettersen, 1993; Hwang and Radermacher, 1998; and Robinson and Groll, 1998).

Much of the interest in R744 is due to the fact that it lends itself well to compactness. Several groups (including the ACRC) are investigating R744 for mobile applications, and it is possible that R744 systems could be marketed by the automobile industry by 2005. Recent studies have investigated the use of R744 in environmental control units for the military (Robinson and Groll, 2000), in which R744 is advantageous in terms of portability, refrigerant handling and worldwide availability. In residential systems, especially in the United States, compactness is not a driving concern. Rather, the comfort of a conditioned space and efficiency of the system under a variety of conditions is of overriding importance.

This report consists of four parts: first, experimental results comparing the first 3-ton R744 a/c system (RAC1) to a conventional baseline system in heating mode; second, a theoretical analysis of ideal transcritical cycles subject to comfort constraints in heating and cooling modes; third, an assessment of the effects of finite exchangers and a real compressor on cycle efficiency; and fourth, a comparison of annual efficiency as a function of climate.

Supplementary analyses are included in the Appendixes. The experimental facilities used for the experimental heat pump comparison are described in Appendices A-C. Appendix D discusses various vapor compression cycle control and distribution options that would be necessary in implementing the assumptions included in the theoretical analysis. Finally, Appendix E contains a discussion of psychrometrics and sensible heat ratio as they relate to the comfort constraint in cooling.

1.2 Selection of baseline refrigerant

The choice of the representative baseline system and refrigerant for the residential market is sensitive due to the variety of systems around the world. Pettersen et al. (1997) compared the simulated performance of an earlier R744 prototype with an R22 ductless split system designed for climate typical of Japan's. We have chosen a system typical of those used in the USA: a split system with an outdoor compressor/condenser unit and a ducted indoor heat exchanger. Comparisons are made against R410A as it is arguably the most efficient, and widely used HFC refrigerant commercially available.

For the experimental results, heat exchangers in the baseline R410A units are of a type commonly used in conventional systems: copper tubes and aluminum louvered and wavy fins. Due to higher operating pressures, the

heat exchangers for R744 require either smaller tube diameters or thicker walls. We have selected microchannel heat exchangers with specially designed headers to withstand the higher operating pressures.

1.3 Basis of theoretical comparison

The goal of the theoretical cycle comparison is to highlight important considerations with regard to R744 and R410A. These results should provide insight regarding heat exchanger design and cycle control for future work in improving the operating efficiency of practical R744 systems.

In a traditional ideal cycle comparison, the ideal Evans-Perkins (reversed Rankine) cycle is fully specified by setting the evaporation temperature and condenser outlet temperatures equal to those of the heat source and sink, respectively. For the ideal transcritical cycle, the gas cooler outlet temperature replaces the condenser temperature, and the pressure is set to the value that yields the maximum cooling or heating COP (Lorentzen and Petterson, 1996). In this report, the ideal cycles are defined differently, by introducing comfort constraints. For the indoor coil in cooling mode, the ideal evaporating temperature is set far enough below the wetbulb temperature of the indoor air, to ensure adequate latent cooling capacity at the specified operating condition. In heating mode, the refrigerant temperature at the exit of the indoor coil is set equal to the desired supply air temperature.

Theoretical calculations and experimental data reduction is done with EES (Klein and Alvarado, 2000). All refrigerant and air properties are based on internal functions within EES.

Chapter 2: Experimental Results of RAC1 System in Heat Pump Mode

2.1 Comparison of RAC1-R744 and baseline R410A systems

The original R744/R410A air conditioning experiments initially used a commercially available R410A A/C-only system as the baseline, because an R410A heat pump system had not yet become commercially available (Beaver et al., 1999). The heat exchangers in the R744 system were designed to match the geometry of the original R410A A/C-only system as closely as practical. As a result, they were not designed to fully capitalize on the properties of R744, nor were they designed for reversible (heating mode) operation. A detailed description of the experimental set-up can be found in Appendix A, while a comparison of the critical components of all three systems is shown in Table 2.1. Importantly, as compared to the R410A combined heat pump -A/C system used as the baseline for this comparison, the R744 system's outdoor coil has larger face area and refrigerant side area but less air side heat transfer surface. Similarly, its indoor coil has larger refrigerant side area but smaller face area and less air side heat transfer surface area.

The baseline system uses a hermetic scroll compressor. The R744 system uses a prototype semi-hermetic reciprocating compressor manufactured by Dorin. The compressor motor is rated at 3 kW at 380V/50 Hz, and the displacement of the compressor is rated at 2.7 m³/h at 1450 rpm. This is a different compressor than the open compressor used by Beaver et al. (1999a). The R744 compressor is controlled by a variable frequency drive so that the capacity can be adjusted. Three manual expansion valves, one for each slab on the outdoor coil, are used so that distribution between the slabs can be controlled. A suction line heat exchanger is used in the R744 system to obtain refrigerant- and cycle-specific performance improvements that are not available with R410A (Boewe et al., 1999).

Table 2.1 Comparison of components for residential system

Refrigerant		R410A-A/C Only	R410A-A/C & HP	R744
System	Type	Commercial	Commercial	Prototype
	Nominal capacity, A/C at 27/35, 50%	10.5 kW	10.3 kW	10.3 kW
	Nominal capacity, heat pump at 22/8.2, dry		9.8 kW	9.8 kW
Compressor:		Hermetic, Scroll	Hermetic, Scroll	Semi-Hermetic, Reciprocating
Expansion device:		Orifice tube: i.d. = 1.78 mm	Short tube orifice type	Manual valve
Outdoor coil	Description	One row, two circuits, fin pitch 1 mm (24 fpi), louvered wavy fins	Three circuits, two slab, fin pitch 1.3 mm (20 fpi), louvered wavy fins	Three brazed 6 pass slabs with 80 tubes each, connected in parallel for R744. Extruded 11 port micro-channel tube. (see fig.2)
	Face area	1.42 m ²	1.16 m ²	3*0.53 = 1.59 m ²
	Core depth	0.0185 m	0.0370 m	0.0165 m
	Core volume	0.026 m ³	0.043 m ³	3*0.0088 = 0.026 m ³
	Airside area	54.1 m ²	66.9 m ²	3*16.8 = 50.4 m ²
	Ref. Side area	1.5 m ²	3.38 m ²	3*1.37 = 4.1 m ²
	Material	Aluminum plate fins Cu tubes, od = 9.5 mm	Aluminum plate fins Cu tubes, od = 9.5 mm	Aluminum tube, folded louvered fins
Indoor coil	Description	Plate fins, three rows, six circuits, fin pitch 1.8 mm (14 fpi)	Louvered plate fins, three rows, six circuits, fin pitch 1.7 mm (15.2 fpi)	Three single pass slabs with 21 tubes each, connected in series for air flow, and in series for R744 h/p and parallel for R744 a/c. Brazed 11 port microchannel tube. (see fig. 3)
	Face area	0.32 m ²	0.42 m ²	0.36 m ²
	Core depth	.056 m	0.0565 m	3*0.0165 = .050 m ²
	Core volume	0.018 m ³	0.024 m ³	3*0.006 = 0.018 m ³
	Air side area	18.6 m ²	27.48 m ²	3*7.50 = 22.5 m ²
	Ref. Side area	1.0 m ²	1.31 m ²	3 * 0.91 = 2.73 m ²
	Material	Al. Wavy plate fins, Cu tubes, od = 9.5 mm	Al. Wavy plate fins, Cu tubes, od = 10 mm	Aluminum tube, folded louvered fins
Suction Line Heat Exch.	Description			Concentric tube, 2 parallel circuits in counterflow
	Length			2 m
	High Pressure Area			0.0377 m ²
	Low Pressure Area			0.0882 m ²
	Material			Aluminum

2.2 Test matrix and baseline results

The systems were tested at steady-state under dry conditions at indoor/outdoor temperatures specified in ARI standards. Those temperatures are a constant indoor temperature of 21°C (70°F) and outdoor temperatures of 16.7, 8.3, 1.7 and -8.3°C (62, 47, 35 and 17°F respectively). Results of the baseline R410A data were compared to data supplied by the manufacturer at the 8.3 and -8.3°C conditions. Dry conditions were run so that an easier comparison between the refrigerants could be made, and so that the results could be compared with computer models.

Experiments were conducted at two compressor speeds. First, the capacity of the R410A and R744 systems were matched in heating mode at the 8.3°C outdoor condition. The objective was to compare the performance of a system sized to provide the same heat pump capacity. Second, the capacity of the compressor was set so that the R744 system would have the same cooling capacity as the R410A system operating in air conditioning mode at 26.5°C indoors and outdoors at 34.9°C and 50% relative humidity. The objective of the second test was to simulate the operation of a combined air conditioning/heat pump system, having a single speed compressor sized for the cooling capacity rating condition. The appropriate compressor speed was calculated from the refrigerant mass flow rate and pressure ratio measured by Beaver et al. (1999) at the a/c rating condition using a different compressor, and the experimentally-determined volumetric efficiency of the Dorin heat pump compressor (84% at that operating condition).

$$COP_h = \frac{Q_{indoor}}{W_{compressor}} \quad (2.1)$$

Results of the tests are compared on the basis of cycle capacity and heating COP. Heating COP is defined as:

Fan power is not included in this cycle efficiency calculation, which tends to favor R410A.

Beaver et al. (1999a) showed the pressure drop over microchannel heat exchangers to be as much as 40% lower than the conventional round-tube, flat-fin heat exchangers used in the R410A system.

2.3 Experimental heat pump results for R744 compared to R410A

The results of the tests run with the capacity of the system matched in heat pump operation are shown in Figure 2.1. The results show that the heating COP of R744 is slightly lower than R410A at higher temperatures, but is matched at the lowest outdoor temperature tested. Additionally, the reduction of capacity at lower outdoor temperatures is not as significant for R744 as for R410A, resulting in a higher capacity for the R744 system at lower temperatures. Figure 2.2 shows the results of the tests run at matched air conditioning capacity. The heating COP of R410A is matched only at the lowest outdoor temperature by R744, however, the capacity of R744 is considerably higher.

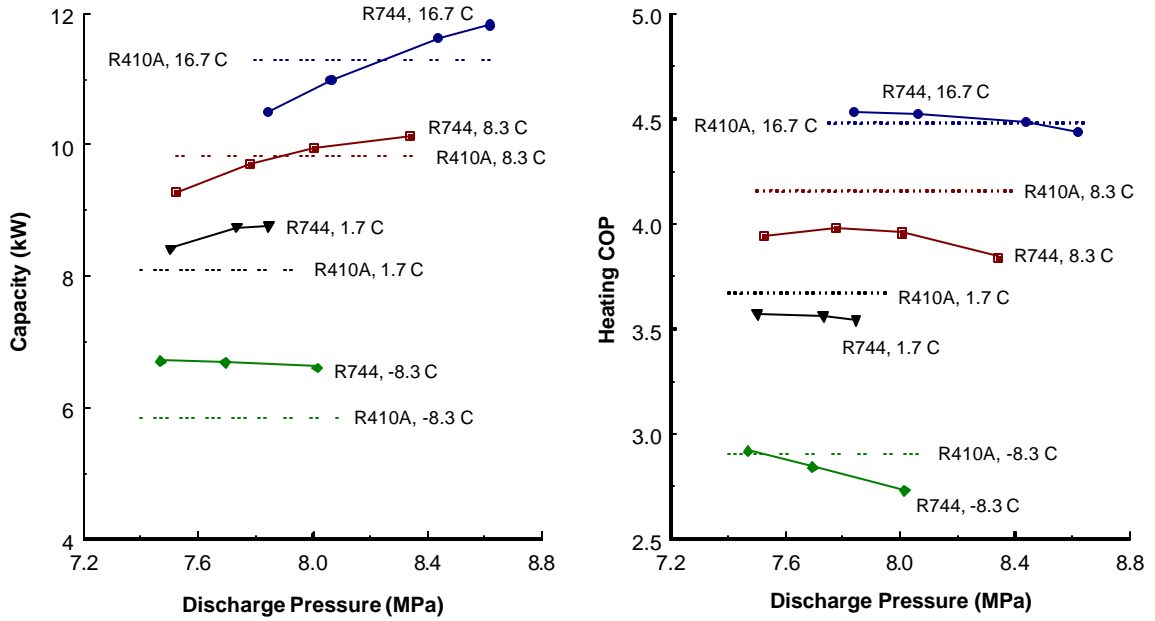


Figure 2.1 Heating performance comparison with matched heating capacity

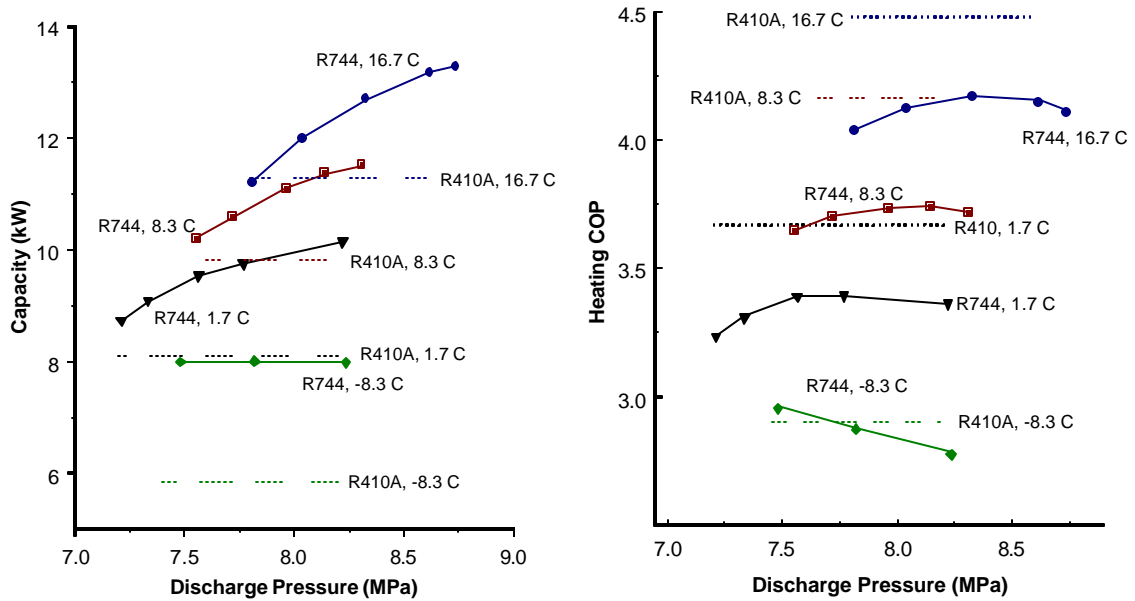


Figure 2.2 Heating performance comparison with matched cooling capacity

The higher capacity of the R744 system at lower outdoor temperatures becomes an important advantage when considering operation of a system in a typical residential application. A typical temperature-load curve is shown in Figure 2.3. Below the point that the load exceeds the capacity of the heat pump some sort of supplementary heating system would be required, typically electric resistance heaters. The higher capacity of R744 reduces the amount of supplementary heating required, which results in a higher overall system heating COP as compared to R410A. The points shown for R744 in Figure 2.3 are results from the tests when R744 compressor

speed was set to match the heating capacity of R410A. As shown in Figure 2.4, when the compressor speed was set to match the R410A cooling capacity: the higher capacity of R744 resulted in an even larger improvement in net heating COP at the lower outdoor temperatures as compared to when the heating capacities were matched. Because of the slight capacity/ heating COP trade-off at moderate temperatures, the R744 advantage could be increased depending on the application. A comparison of the thermodynamic cycle for R744 and R410A for the matched heat pump capacity at the 8.3°C outdoor temperature is shown in Figure 2.5.

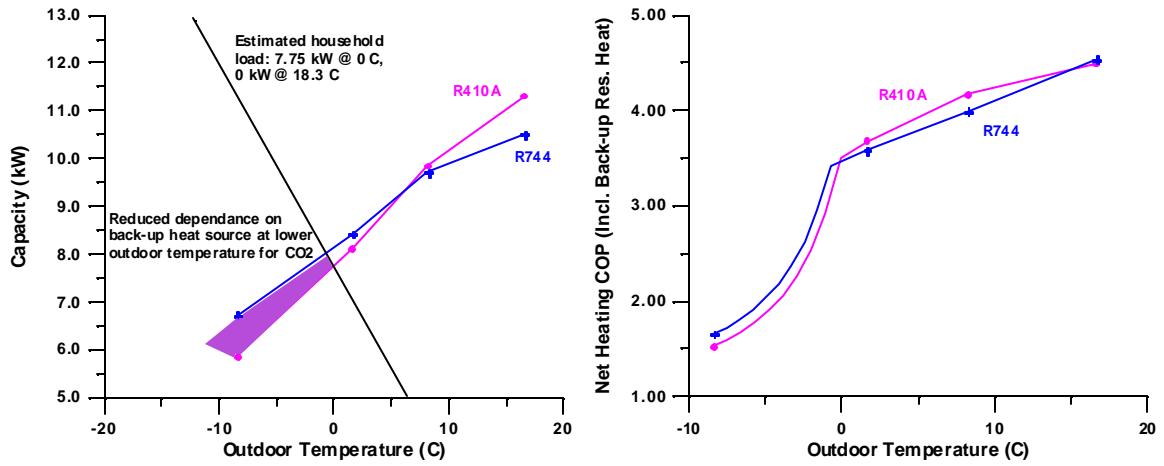


Figure 2.3 Effect of increased capacity of R744 at lower outdoor temperatures on overall heating efficiency (matched heating capacity)

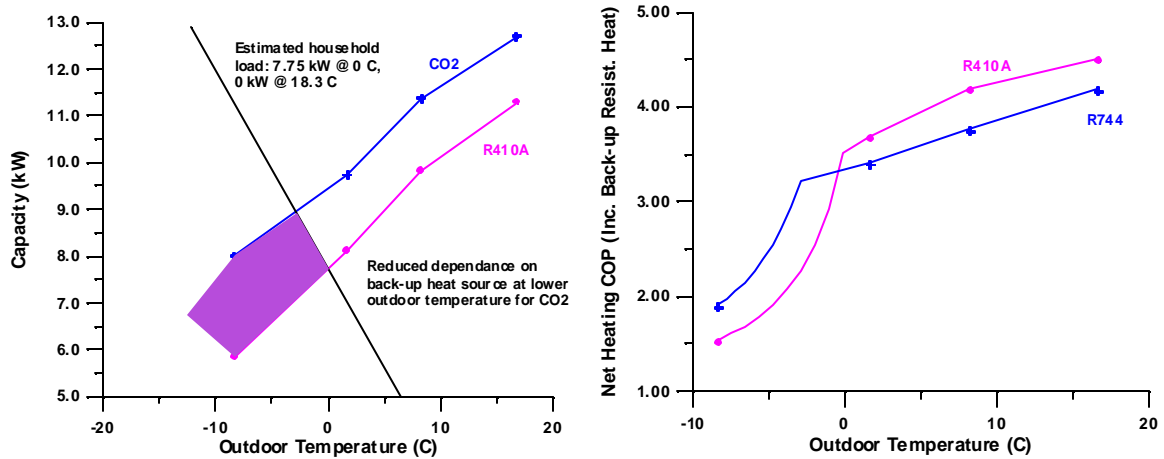


Figure 2.4 Effect of increased capacity of R744 at lower outdoor temperatures on overall heating efficiency (matched cooling capacity)

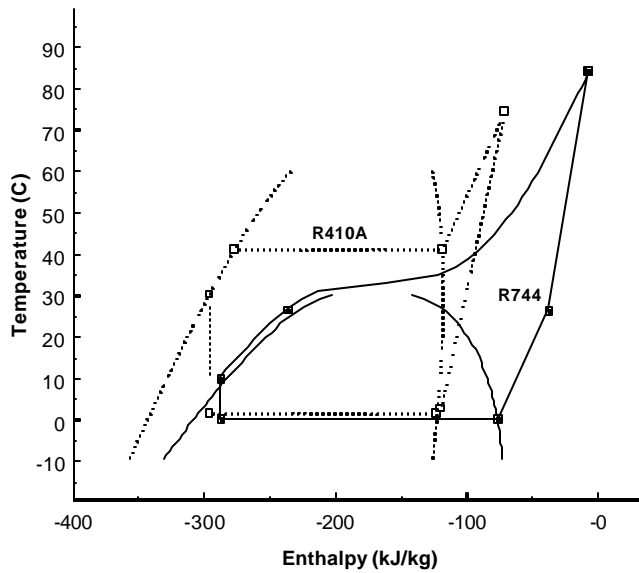


Figure 2.5 R744/R410A cycle comparison

Frost patterns on the outdoor coil suggested the presence of severe maldistribution in the prototype heat exchanger shown in Figure 2.6, which was to be expected since this multipass heat exchanger with vertical headers was never designed to operate as an evaporator (Song et al., 2001). It is likely that the next generation of heat exchangers can be designed to increase the evaporating temperature above that shown in Figure 2.5, thereby improving the system heating COP.

In Figure 2.7 the temperature of the refrigerant at the exit of the gas cooler is plotted as a function of discharge pressure. At low discharge pressures, the air/refrigerant temperature difference in the gas cooler is reduced, the effectiveness is lower and system capacity is decreased. As the gas cooler pressure is increased, the effectiveness and capacity of the gas cooler is increased. By comparing Figure 2.7 with the efficiency results shown in Figures 2.1 and 2.2 it can be seen that the benefit of increased heat rejection by the gas cooler outweighs the penalty of additional compressor work required to reach the higher discharge pressure, and the heating efficiency improves. At high gas cooler pressures, the air/refrigerant temperature difference is higher and the capacity of the evaporator becomes the limiting factor. As a result, maximizing the indoor coil effectiveness does not necessarily maximize cycle efficiency.

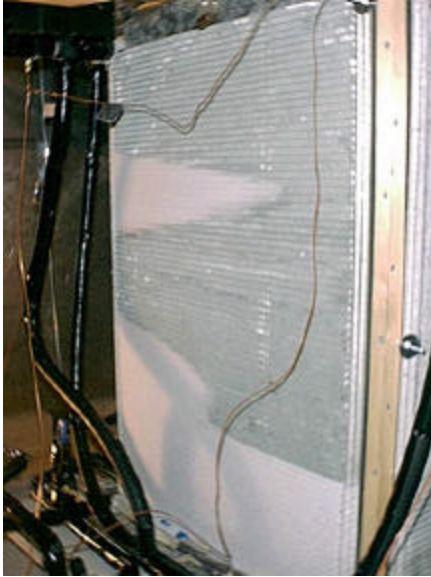


Figure 2.6 Frost pattern on outdoor coil indicating maldistribution

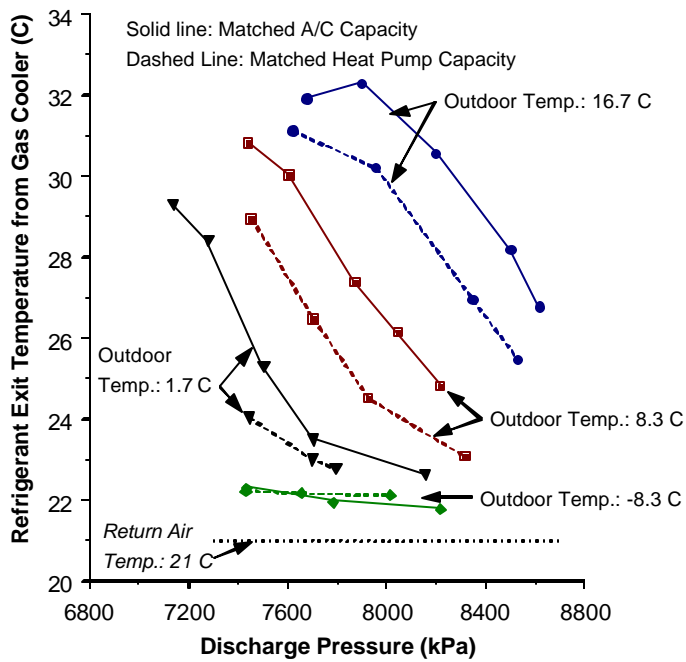


Figure 2.7 R744 gas cooler performance (indoor temperature 21°C)

The isentropic efficiency for the R744 compressor used in the heat pump system is shown in Figure 2.8. At equal compression ratios the efficiency of the R410A compressor is slightly higher. The four points plotted for R410A correspond to the compressor efficiency at each outdoor test temperature. The lowest compression ratio corresponds to the highest outdoor temperature (16.7°C) and the highest compression ratio corresponds to the lowest outdoor temperature (-8.3°C). Because the compression ratio for R744 is lower than for R410A at each operating condition, the compressor operating efficiency for R744 ends up being slightly higher.

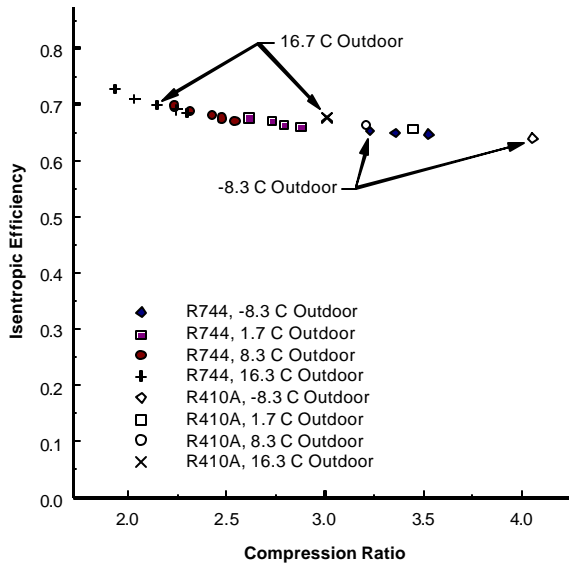


Figure 2.8 Compressor efficiency at matched cooling capacity

2.4 Effect of varying indoor airflow rate on R744 performance

In the experiments comparing the heat pump performance of R744 to the R410A baseline system, the airflow rate over the R744 indoor coil (gas cooler) was set to match that of the R410A system. Since R744 potentially has the advantage to deliver air at a higher temperature and reduced airflow rate, experiments were run at varying indoor flow rates to observe the gas cooler performance trade-offs. The results are shown in Figure 2.9.

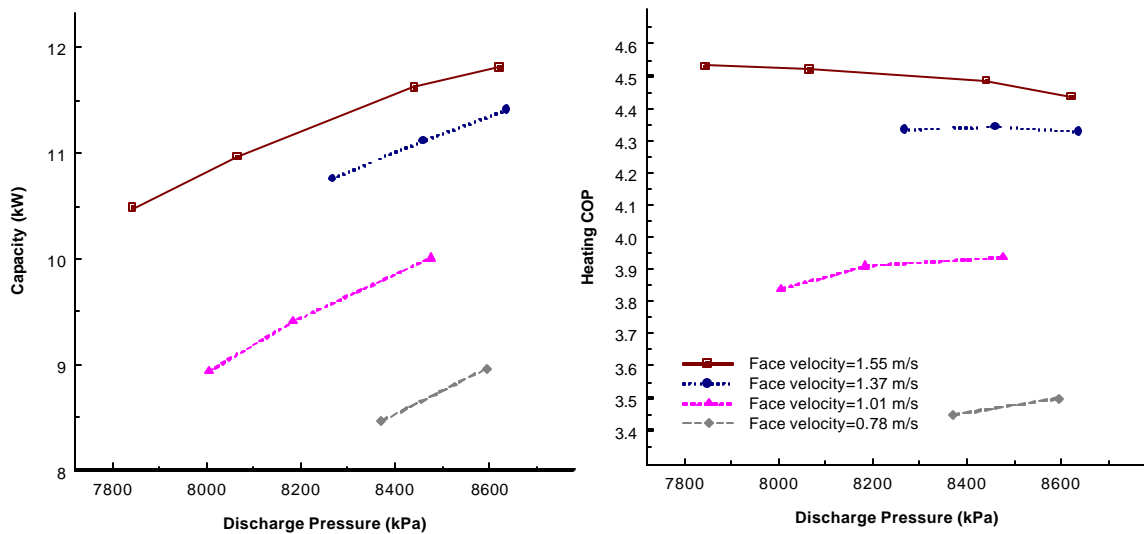


Figure 2.9 Effect of airflow rate reduction on R744 indoor coil (R410A baseline face velocity=1.55 m/s)

2.5 Effect of suction accumulator and indoor coil configurations on R744 results

Further experiments suggested that the R744 system might not have had full benefit of the suction accumulator.

The vapor line-liquid line intersection after the suction accumulator was, under certain conditions, below the level of liquid in the accumulator. As a result, this intersection was flooded with liquid defeating the purpose of the suction accumulator. Subsequent experiments with the suction accumulator reconfigured showed cycle COP improvement on the order of 5-10% above the COP_h values shown in the previous figures.

During these tests, however, the orientation of the indoor coil had also been changed. A study by Song et al. (2001) showed that the angle of the heat exchanger in the duct did not influence the heat transfer performance but did influence the air pressure drop across the coil. Based on these results the indoor coil was rotated 90° and placed perpendicular to the incoming air stream. As a result, it is not certain that the reconfigured suction accumulator was independently responsible for the improvement in efficiency.

A full discussion of the results is presented in Appendix B.

2.6 Conclusions regarding experimental performance of R410A and R744

These preliminary results from the R744 RAC1 system provide evidence that system performance is consistent with expectations based on thermodynamic cycle considerations. Using heat exchangers that are designed to match the packaging constraints of a conventional R410A air conditioning system, which has smaller heat exchangers than the baseline R410A heat pump system, we observed comparable cycle-COP and greater capacity at lower outdoor temperatures from the R744 system. The increased capacity of the R744 system at lower outdoor temperatures has considerable impact when calculating the overall system efficiency for an application, as the dependence on supplementary heating is reduced.

Chapter 3: Ideal Cycle Considerations

3.1 Ideal cycle description

A typical subcritical ideal vapor compression cycle is shown in Figure 3.1. Evaporation takes place at a constant temperature and pressure, with exit quality equal to one. At the entrance to the compressor, the enthalpy (h_1) and entropy (s_1) are calculated from the saturation properties of the refrigerant based on the evaporating temperature. The exit enthalpy from the compressor (h_2) is calculated based on isentropic compression from 1 to 2 with a compressor efficiency of one. Condensation is assumed to be isobaric, and the condenser exit quality is zero. From saturation properties of the refrigerant the exit enthalpy (h_3) can be calculated based on the condensation pressure and exit quality or temperature. As a result, the thermodynamic cycle can be completely described for a specified evaporating temperature and exit temperature from the evaporator.

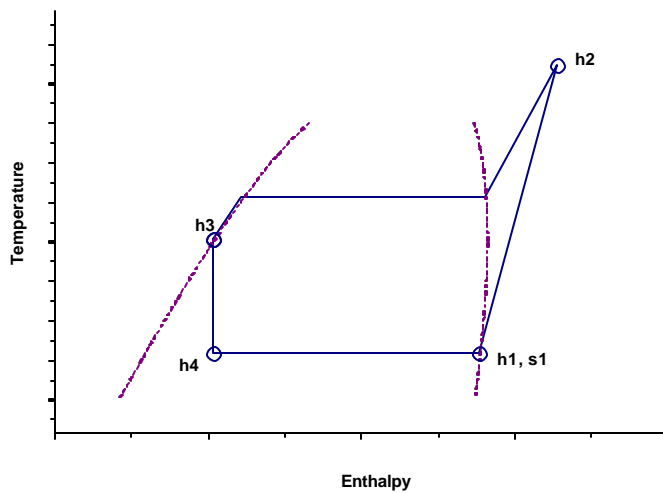


Figure 3.1 Ideal subcritical cycle

If the discharge pressure is higher than the critical pressure of the refrigerant then the cycle is transcritical. In the ideal transcritical cycle, the refrigerant can be cooled at constant pressure from a supercritical vapor to a saturated liquid without passing through a two phase region of condensation at constant temperature. The critical temperature and pressure is 31.1°C and 7380 kPa for R744, and 72.1°C and 4925 kPa for R410A.

Since the enthalpy at each state point is specified, the capacity of the system is a function only of the mass flow rate of refrigerant supplied by the compressor. The ideal system's heating and cooling capacities are:

$$Q_H = \dot{m}_{\text{refrigerant}} \cdot (h_2 - h_3) \quad (3.1)$$

and,

$$Q_C = \dot{m}_{\text{refrigerant}} \cdot (h_1 - h_3) \quad (3.2)$$

Respectively, the ideal cycle coefficient of performance, COP_c and COP_h for heating and cooling can be calculated as:

$$COP_c = \frac{h1-h3}{h2-h1} \quad (3.3)$$

$$COP_h = \frac{h2-h3}{h2-h1} \quad (3.4)$$

On the air side, assuming constant specific heat and neglecting latent heat transfer:

$$Q_{system} = \dot{m}_{air} \cdot c_{p,air} \cdot \Delta T_{air} \quad (3.5)$$

where, ΔT_{air} is the temperature difference between the return and supply air.

For a given cycle and specified capacity the required refrigerant mass flow can be determined from the equations above. The air-side mass flow rate for a given air inlet and exit temperature difference, or the air-side exit temperature difference for a given air mass flow rate and inlet temperature can also be calculated.

3.2 Ideal heat pump cycle

In a vapor compression cycle, minimizing the source/sink temperature and pressure difference maximizes cycle efficiency. In the subcritical cycle, because heat is rejected at a constant temperature, the condensing temperature can theoretically match the indoor air temperature. However, comfort considerations limit the extent to which the condensing temperature can be reduced. To provide a given capacity requirement at lower condensing temperature the airflow rate must be increased. The result is one of the primary drawbacks of heat pumps, that the higher flow rate of delivered air at a lower temperature results in a “drafty” environment in the conditioned space. Increasing the discharge pressure from the compressor can increase the supply air temperature, but a penalty is paid in cycle efficiency.

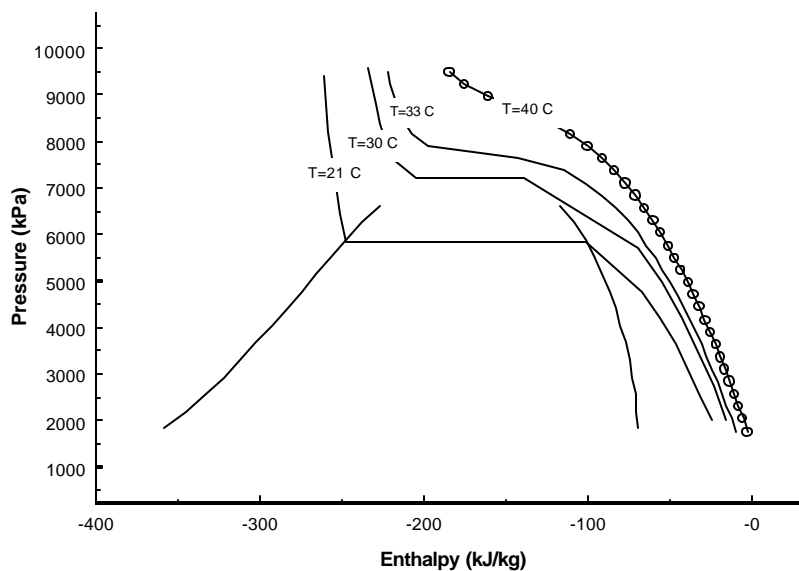


Figure 3.2 R744 pressure enthalpy diagram

The R744 cycle must operate near the critical point in order to deliver supply air at temperatures warmer than the human body. Under certain conditions an increase in pressure results in greater cycle capacity than the

increased power required by the compressor. As a result, the efficiency of the cycle improves and an optimum discharge pressure exists. Figure 3.2 is a pressure enthalpy diagram for R744. The 34°C isotherm shows a large change in slope between 7000 and 9000 kPa. In this range, there exists a discharge pressure that optimizes cycle efficiency for a given constant refrigerant exit temperature from the gas cooler. Typically, the region of refrigerant exit temperatures for which this phenomenon exists is too high for heat pump operation and primarily a consideration in air conditioning mode. The isotherm for 21°C is shown on Figure 3.2, and has a nearly constant slope in the supercritical region until it meets the saturated liquid line of the vapor dome. Additionally, since this isotherm is steeper than the line of constant entropy along which ideal compression would proceed, the lowest possible discharge pressure results in the highest cycle COP. Similarly with R410A: the lower the discharge pressure, the more efficient the cycle.

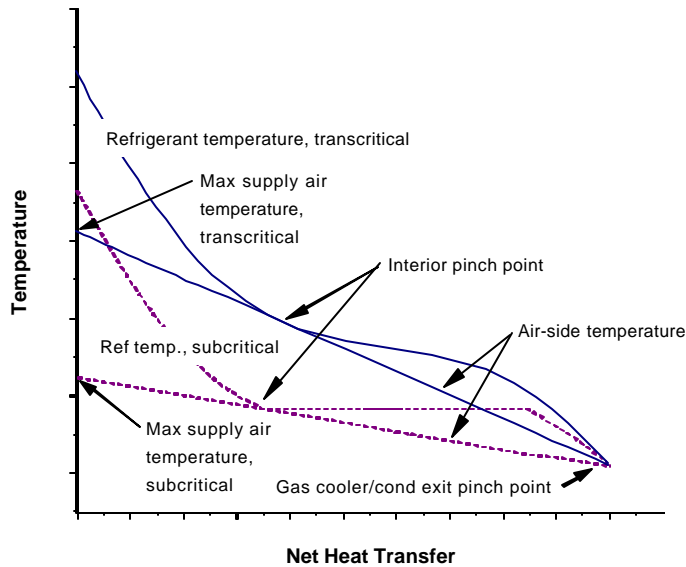


Figure 3.3 Maximum supply air temperature based on pinch point

The maximum possible supply air temperature (air exit temperature from the indoor coil) for an ideal transcritical cycle with a fixed capacity can be calculated based on the air/refrigerant temperature pinch point. This is shown in Figure 3.3 for a counterflow configuration. The temperatures of the air and refrigerant are plotted on the vertical axis versus the net cumulative heat transfer from the refrigerant on the horizontal axis. Assuming constant specific heat, the slope of the air side is linear and is equal to:

$$Slope = \frac{1}{\dot{m}_{air} C_{p,air}} \quad (3.6)$$

An airflow rate lower than the tangent to the pinch point would not meet the specified capacity. A higher airflow rate than the tangent would result in a supply air temperature lower than the maximum.

There are several ways to meet the same comfort constraint. A given capacity can be achieved at a specified supply air by adjusting the air flow rate and either increasing the high side pressure or increasing the refrigerant mass flow rate, as shown in Figure 3.4. For a specified heating capacity, increasing the refrigerant mass

flow rate increases the approach temperature difference between the refrigerant exit temperature from the heat exchanger and the air inlet temperature, which considerably reduces the efficiency of the ideal cycle, as shown in Figure 3.5. The solid lines in Figure 3.5 show the efficiency of the cycle, and the dashed lines show the corresponding refrigerant mass flow rate, and results for cycles both with and without a suction line heat exchanger are shown. The diamonds indicate the zero approach temperature condition; the lines coming off the diamonds show the effect of increasing the refrigerant mass flow rate at the noted pressure. Therefore, the ideal cycle which satisfies the supply air comfort constraint with the greatest efficiency is the one in which the mass flow rate is adjusted for a zero approach temperature. The high side pressure, which can be adjusted independently, determines the supply air temperature.

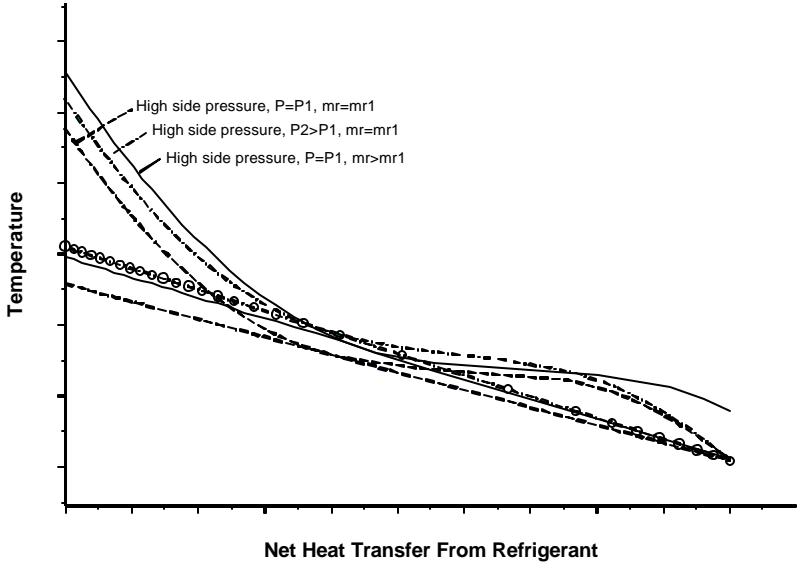


Figure 3.4 Effect of pressure and refrigerant mass flow variations on maximum supply air temperature

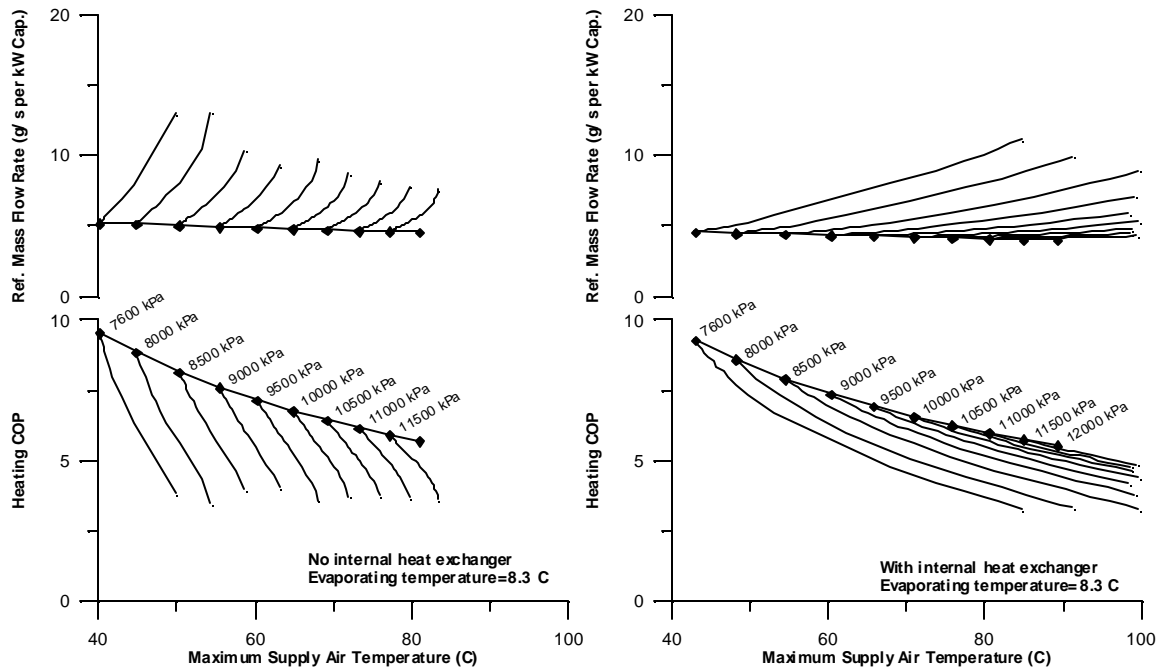


Figure 3.5 Effect of increasing flow rate at a constant pressure on maximum supply air temperature and cycle efficiency for R744

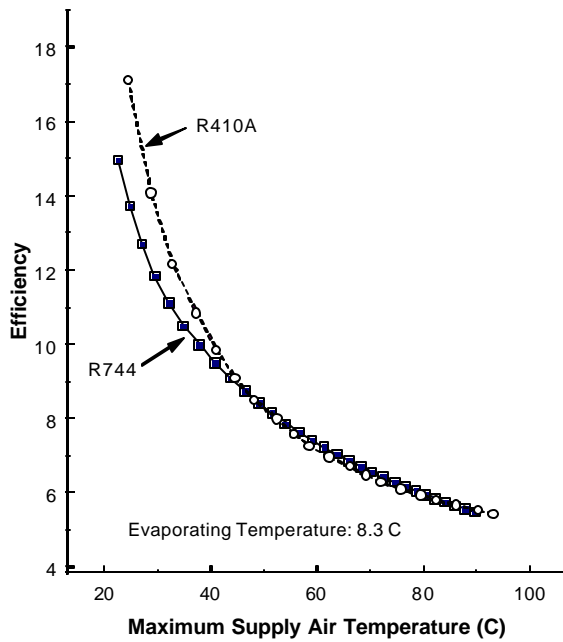


Figure 3.6 Comparison of cycle efficiency based on maximum supply air temperature (both cycles with IHX)

The slopes of the constant pressure lines in Figure 3.5 are considerably different in the cycle with the suction line heat exchanger as compared to the cycle without. In the cycle without an internal heat exchanger, since the evaporating temperature is fixed and the discharge pressure is constant, the discharge temperature from the compressor is fixed. As the refrigerant mass flow rate is increased, the air/refrigerant pinch point moves very little.

As a result, a large decrease in efficiency produces very little increase in the maximum supply air temperature. However, in the system with an internal heat exchanger the exit temperature from the compressor is not fixed. Since the effectiveness of the suction line heat exchanger is by definition one in the ideal cycle, an increase in refrigerant flow that raises the exit temperature of the refrigerant from the gas cooler also raises the refrigerant inlet temperature to the compressor. A higher inlet temperature to the compressor results in a higher exit temperature, and the pinch-point is moved. This accounts for the greater increase in maximum supply air temperature in the system with an internal heat exchanger for the same drop in efficiency as a system without an internal heat exchanger.

By correlating the heating COP for a given operating condition with the maximum supply air temperature, the energy cost of comfort can be quantified. The ideal cycle performance of R744 and R410A is shown in Figure 3.6 as a tradeoff between the heating COP and maximum supply air temperature. This plot is normalized to a system capacity of 1 kW, for an evaporating temperature of 8°C, a return air temperature of 21°C, a zero approach temperature and both cycles running with an internal heat exchanger (IHX). Under these conditions, for supply air temperatures greater than about 46°C, R744 and R410A have approximately the same ideal cycle efficiency. In the R744 cycle, the suction line heat exchanger begins to increase the cycle efficiency slightly when the supply air temperature is above 43°C, up to 6% when the supply air temperature is 80°C. In the R410A cycle, the suction line heat exchanger increases the cycle efficiency less than 2% over the supply air temperature range plotted. This illustrates that, at relatively low supply air temperatures with a properly controlled system, the internal heat exchanger could be bypassed with little effect on ideal cycle efficiency. However, as previously shown, the suction line heat exchanger diminishes the effect of a non-zero approach temperature on cycle efficiency.

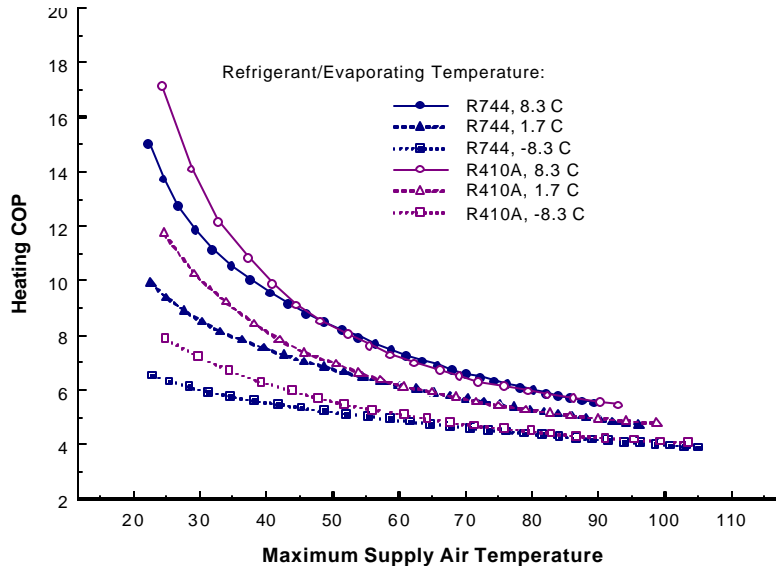


Figure 3.7 Effect of decrease in evaporating temperature on heating cycle efficiency

The effect of decreasing the evaporating temperature is shown in Figure 3.7. As the evaporating temperature decreases, so does the evaporating pressure. More work is required by the compressor to move refrigerant across the larger pressure difference, which is reflected in reduced heating COP. In all cases the efficiency of R744 is higher at the higher supply air temperatures. The breakeven supply air temperature increases

slightly with decreasing evaporating temperature, but remains around 40°C for the evaporating temperatures shown. The calculated refrigerant exit temperatures from the compressor range from 43-128°C for R410A, and from 46-143°C for R744.

3.3 Ideal air conditioning cycle

The comfort constraint in air conditioning mode is the dew point of the supply air. It can be met by reducing the evaporating temperature and/or the volumetric flow rate of air across the evaporator. Figure 3.8 shows the effect of evaporating temperature on cycle efficiency for an outdoor temperature of 35°C. As the evaporating temperature is dropped to decrease the dew point of the supply air, a significant efficiency penalty is paid.

While R410A shows a considerably higher ideal efficiency than R744 this advantage is tempered by practical airflow considerations. The ideal R410A cycle has a condensing temperature equal to the outdoor air temperature which, theoretically, would require infinite heat exchanger area and an infinite air flow rate to eliminate the air-refrigerant temperature difference. For R744, however, the effect of the temperature glide in the gas cooler is compatible with a relatively low airflow rate, and corresponding fan power requirements. This is shown in Figure 3.9, where the average air/refrigerant temperature difference and corresponding required air flow rate per kW of cooling capacity is plotted for an evaporating temperature of 12°C and an outdoor temperature of 35°C (the evaporating temperature is typical for a microchannel heat exchanger running with a sensible heat ratio of 0.75 at the 27°C/50% relative humidity indoor test condition). At that condition, the ideal cycle COP for R410A is 10.3, which would require an infinite air flow rate. The R744 gas cooler, on the other hand, requires only 5.0 m³/min/kW because the slope of the T-h curve is steeper for R744 than for R410A, which has a large horizontal region for condensation. Reducing the air flow rate to 5.0 m³/min/kW for R410A (for example to save fan power) reduces the ideal cycle efficiency from 10.3 to 7.5, which reduces R410A efficiency to 32% greater than R744. This compares with an efficiency for R410A that is 80% greater than R744 when air flow is unrestricted. Real R410A systems operate at air flow rates between 5.9 and 7.6 m³/min/kW cooling capacity, apparently using fan power to boost cycle COP and create the potential for saving more compressor power.

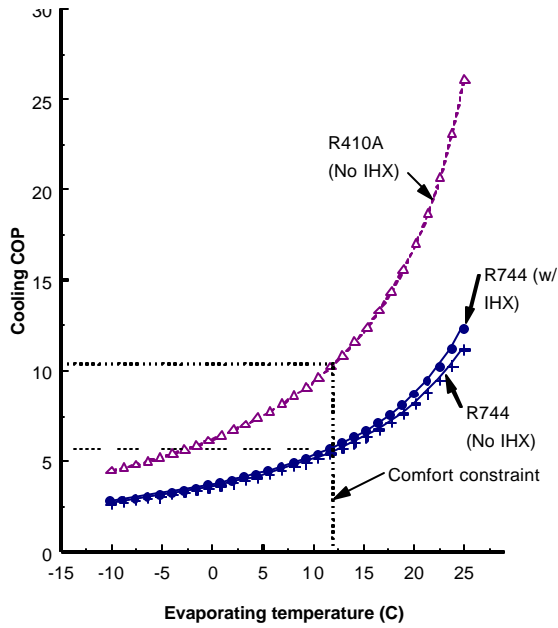


Figure 3.8 Cooling cycle efficiencies (gas cooler exit temperature 35°C)

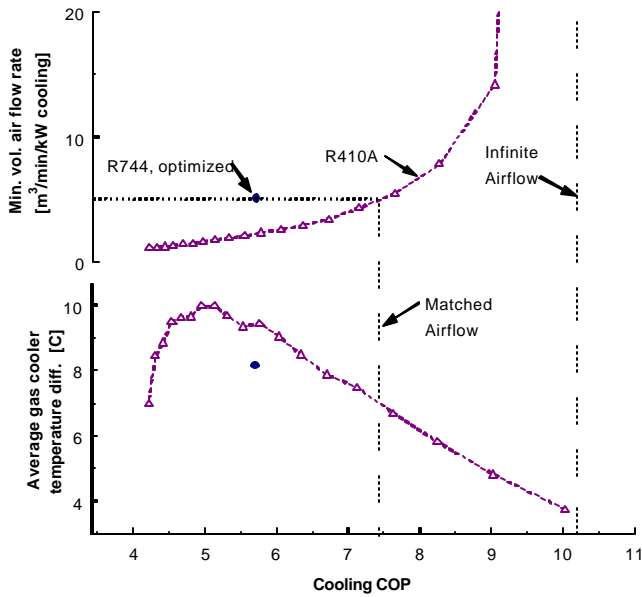


Figure 3.9 Effect of air flow rate on R410A cooling cycle efficiency (gas cooler exit temperature 35°C, evaporating temperature 12°C)

Additionally in Figure 3.9, there is a peak in the average air/refrigerant temperature difference. At higher efficiency with lower condensing temperatures the airflow rate is high and the temperature difference between the condensing temperature and the air stream is small. As the condensing temperature is increased, this difference increases. At lower efficiency with high condensing pressures, since the assumed air flow rate is minimized based

on the pinched condition, the temperature difference between the superheat region and the air stream is reduced, which decreases the overall heat transferred weighted average temperature difference.

3.4 Ideal system performance

The analysis to this point has considered the ideal cycle where the required system capacity is met by adjusting the refrigerant mass flow rate via a variable displacement compressor. In both heat pump and air conditioning mode the evaporator air temperature determines the most extreme operating conditions: warm outdoor conditions in air conditioning mode and cold outdoor conditions in heat pump mode require the highest compressor displacement to maintain capacity.

In a typical residential application, it is reasonable to base the maximum compressor displacement on the load requirements at the 45°C outdoor operating condition. In Figure 3.10 the ideal cycle capacity in heat pump mode is plotted for a supply air temperature of 21°C based on a fixed compressor capacity corresponding to the normalized compressor capacity required for a 12°C evaporating temperature and a 45°C sink temperature (0.54 m³/hr per kW cooling capacity for R410A and 0.21 m³/hr per kW cooling capacity for R744). The capacity of R744 is significantly higher than for R410A, which has significant practical implications in terms of overall heating efficiency. Because of the reduction in capacity inherent in heat pumps, heat pump systems require some sort of low-efficiency supplementary heating. The increased capacity of R744 at lower outdoor temperatures reduces the dependence on supplementary heating, which increases the overall heating efficiency. In Figure 3.11, the cycle efficiency corresponding to Figure 3.10 is shown.

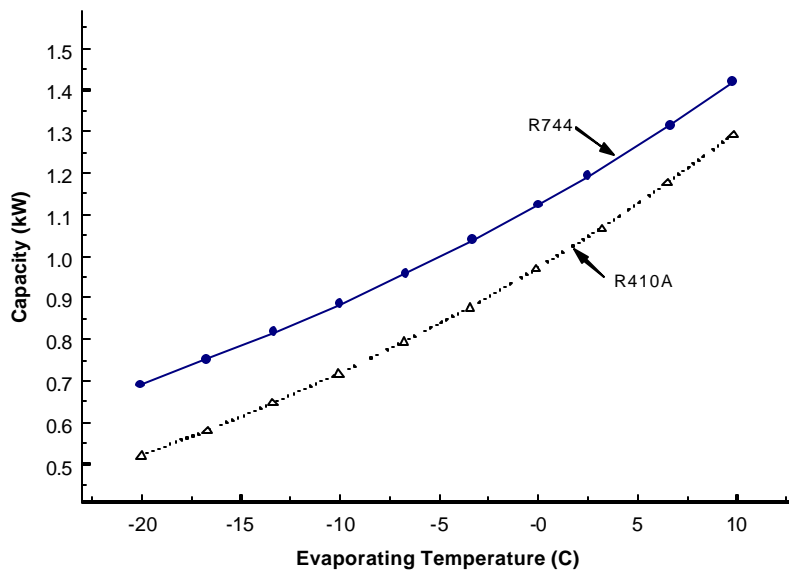


Figure 3.10 Effect of fixed displacement compressor on ideal heat pump cycle capacity

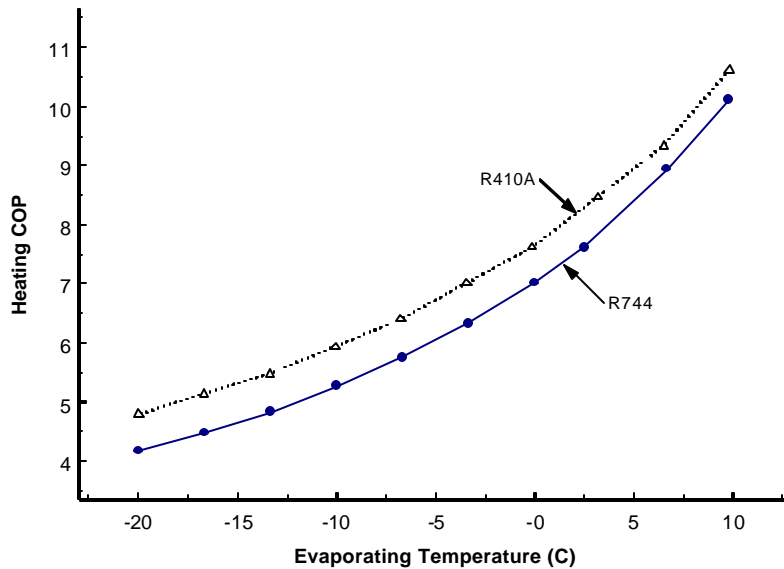


Figure 3.11 Efficiency with finite displacement compressor

3.5 Ideal cycle conclusions

For both transcritical and subcritical cycles, the thermodynamic cycle can be specified with only an evaporating temperature, a condensing pressure and a refrigerant exit temperature from the gas cooler. The supply air temperature comfort constraint in heating is met by increasing the condensing pressure or refrigerant mass flow rate, and in cooling the dehumidification comfort constraint is met by decreasing the evaporating temperature.

In cooling mode, R410A shows much higher efficiency than R744 for the same evaporating temperature. The difference between the two cycles is in their heat rejection temperatures, which is lower for R410A. The value of such a comparison is limited, however, because the subcritical cycle requires an infinite condenser air flow rate to approach the ideal cycle, while R744 can achieve it at a finite flow rate due to its supercritical temperature glide.

In heating mode, R410 and R744 have comparable efficiencies at high supply air temperatures, with R410A having higher efficiency at lower supply air temperatures. The supply air temperature at which the efficiency of R410A and R744 is matched depends on the evaporating temperature.

The primary advantage of R744 in the ideal cycle in heat pump operation is evident if the effect of a finite capacity compressor is included. Increased capacity of R744 at lower outdoor temperatures translates into reduced dependence on lower efficiency supplementary heating and higher overall heating efficiency.

Chapter 4: Real Cycle Considerations

4.1 Cycle Assumptions

The ideal cycle analysis in the previous chapter neglects practical considerations such as compressor losses and finite area heat exchangers. Based on several assumptions these effects can be included for a more realistic comparison of R410A and R744. The goal is to make assumptions that place practical limits on the cycle, but do not impose restrictions that would favor one refrigerant or the other. In this chapter the effect of using a fixed vs. variable capacity compressor with regard to cycle performance is briefly explored, then the trade-off between comfort, efficiency and heat exchanger sizing are more fully developed for the air conditioning and heat pump cycles independently.

As in the ideal cycle analysis the modeled heat exchangers are of a counterflow configuration. It is assumed that the heat exchange areas of the R410A and R744 heat exchangers are identical and in both cases microchannel heat exchangers are used. Except as noted the air and refrigerant side pressure drops are neglected since the optimum heat exchanger design for these parameters would be different depending on the refrigerant. In Table 4.1 the assumptions used in the following analysis are compared with parameters from a commercially available R410A system and a proposed prototype R744 system. Since many of the values given in Table 4.1 depend on operating conditions (pressure drop, area/kW capacity, etc.), the values given are based on the heat pump rating condition of an outdoor temperature of 8.3°C. The air side heat transfer coefficients are based on values typical for microchannel heat exchangers, 90 W/m² K at 0.052 kg/s airflow rate per kW capacity (Yin, 2000), and the assumption that the coefficient varies as $Re^{0.8}$.

In the following analysis the R744 cycle includes an internal heat exchanger where the R410A cycle does not. Compared to R410A, R744 has much higher evaporative heat transfer coefficients (Kirkwood et al., 1999 and Hihara, 2000), and, as a result, the temperature difference between the heat exchanger wall and the refrigerant would be smaller for R744 compared to R410A. This means that the evaporating temperature could be higher for R744 as compared to R410A. Based on the ratio of areas and heat transfer coefficients for the calculated R410A and R744 cycles with comfort constraints shown in Table 4.1, a 1.5°C refrigerant-wall temperature difference may be expected for R410A, while R744 could operate at an evaporating temperature more than 1°C higher. In practice, however, about 0.5°C of this difference would be dissipated due to pressure drop in a suction line heat exchanger, which would likely be present in an R744 system. Due to the slope of the vapor pressure curve for R410A, the pressure drop penalty would probably negate any COP advantage, so none is assumed to be present in the R410A analysis presented here.

Table 4.1 Comparison of cycle assumptions based on the 8.3°C/21°C heat pump rating condition, dry coil, supply air temperature 40°C

		<i>Calc R410A w/ comfort</i>	<i>Calc. R744 w/ comfort</i>	<i>R410A baseline</i>	<i>R744 RAC2</i>
Indoor Coil	Geometry	Ideal Counterflow	Ideal Counterflow	Three circuit, two slab, A- frame	
	Ref side area ¹ (m ² /kW)	-----	-----	0.10	0.314
	Air side area ¹ (m ² /kW)	-----	-----	1.88	2.27
	Air to Ref Area Ratio	7.8	7.8	18.8:1	7.2:1
	Ref side pressure drop (kPa)	Neglected	Neglected	19	8.1
	Air side pressure drop (kPa)	Neglected	Neglected	63.6	25.9
	Air Flow Rate (m ³ /sec)			0.57	0.55
Outdoor Coil	Geometry	Ideal Counterflow	Ideal Counterflow		
	Ref side area ¹ (m ² /kW)	-----	-----	0.45	0.65
	Air side area ¹ (m ² /kW)	-----	-----	8.87	6.68
	Air to Ref Area Ratio	10:1	10:1	19.7:1	10.3:1
	Ref side pressure drop (kPa)	Neglected	Neglected		33
	Air side pressure drop (kPa)	Neglected	Neglected	28.9	12.8
	Air Flow Rate (m ³ /sec)			1.26	1.25
Evaporator	Single-phase heat transfer coeff. (W/m ² K)	Dittus-Boelter	Dittus-Boelter ²	-----	Gnielinski
	Two-phase heat transfer coeff. (W/m ² K)	2500 ³	10,000 ⁴	-----	Rademacher Hwang ⁵
	Air side heat transfer coeff (W/m ² K)	90(Re/Re _{0.052 m/s}) ^{0.8}	90(Re/Re _{0.052 m/s}) ^{0.8}		
Gas Cooler/ Condenser	Single-phase heat transfer coeff.	Dittus-Boelter	Dittus-Boelter ²	-----	Gnielinski
	Two-phase heat transfer coeff	2500 ³	(Transcritical)	-----	
	Air side heat transfer coeff (W/m ² K)	90(Re/Re _{0.052 m/s}) ^{0.8}	90(Re/Re _{0.052 m/s}) ^{0.8}		106.7 ⁶
	Evaporating Temp at 8.3 C Heat Pump Rating Condition	2.3 C	2.3 C	1.5 C ⁸	0.8 C ⁴

1. Based on heat transferred by coil (outdoor=ht from envir.; indoor= ht from envir+comp pwr)
2. Most conservative (i.e. lowest calculated heat transfer coefficient) as compared to CO₂ specific correlations (Pitla et al., 1998)
3. Based on results from Kirkwood et al. (1999)
4. RAC2 simulation results (Yin, 2000)
5. Calculated values from Radermacher-Hwang range from 7500-22,600 for operating condition
6. Calculated from Chang-Wang correlation
7. Experimental R410A baseline results

4.2 Compressor assumptions

4.2.1 Isentropic and volumetric efficiency

To incorporate the effect of a real compressor into the cycle analysis a linear fit to compressor data is used for volumetric and isentropic efficiencies. The type of compressor selected for each refrigerant is: a commercially available hermetic scroll compressor for R410A and a semi-hermetic prototype reciprocating compressor for R744. The isentropic efficiency model for the R410A compressor is based on manufacturer's data for a 3 ton compressor, and this fit is compared with the measured performance of a similar compressor by Stott (1999) in Figure 4.1. The R744 fit is based on measured results of a 50 Hz prototype reciprocating compressor (Neksa, 1999). In Figure 4.2 its isentropic efficiency is compared with data from a very similar prototype compressor used in the RAC1 experimental results, which included losses of unknown magnitude attributable to a frequency converter. Experimental results from two open automotive compressors are also shown. In the cycle analysis it is assumed that no heat is rejected from the compressor to the surroundings.

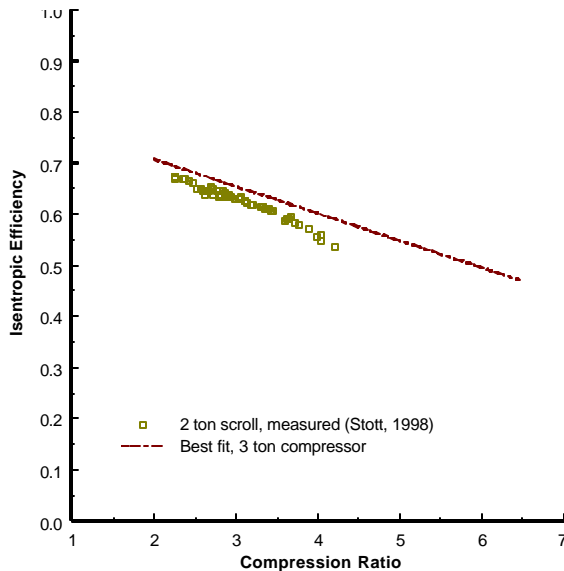


Figure 4.1 R410A compressor efficiency

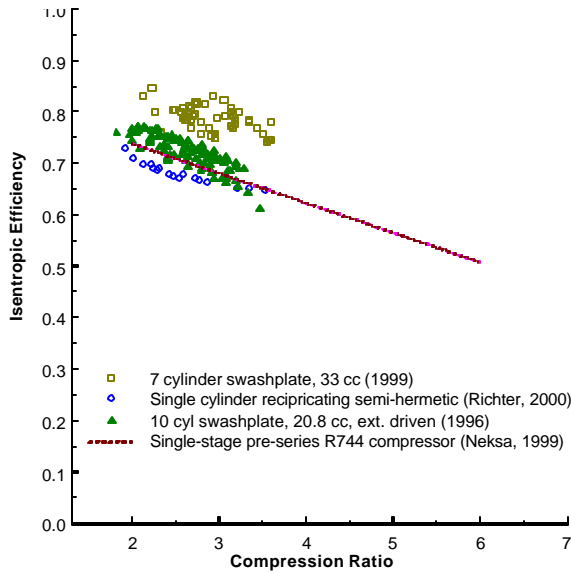


Figure 4.2 R744 compressor efficiency

The linear fits used are:

$$\text{R410A: } h_{isentropic} = 0.8134 - 0.05296 \cdot \left(\frac{P_{dis}}{P_{suc}} \right) \quad h_{volumetric} = 1.0214 - 0.0338 \cdot \left(\frac{P_{dis}}{P_{suc}} \right) \quad (4.1)$$

$$\text{R744: } h_{isentropic} = 0.8536 - 0.0577 \cdot \left(\frac{P_{dis}}{P_{suc}} \right) \quad h_{volumetric} = 1.028 - 0.097 \cdot \left(\frac{P_{dis}}{P_{suc}} \right) \quad (4.2)$$

The linear assumption breaks down at very low compression ratios, so this analysis is limited to conditions having a compression ratio greater than two. This limitation is not overly restrictive on the air conditioning cycle, because such conditions are encountered only momentarily at the beginning of the pulldown process when an air conditioner is first turned on. In the heat pump cycle, this assumption limits the lowest operating pressure of the condenser or gas cooler, and can constrain the theoretical minimum supply air temperature.

4.2.2 Variable vs. fixed displacement

Use of a variable displacement compressor is advantageous in that the flow of refrigerant can be adjusted to match the load condition. With a fixed capacity compressor, because efficiency depends on temperature (pressure) lift, the cycle has maximum capacity at the smallest indoor/outdoor temperature difference where the heating or cooling load is the smallest. As a result the load and capacity curves are “mirrored” from each other, with the highest load having the least capacity.

To illustrate this, Figures 4.3 and 4.4 show the capacity and efficiency of theoretical R744 and R410A systems with a fixed capacity compressor described by Equations 4.1 and 4.2. A linear relationship between the outdoor temperature and the required load is assumed. The efficiency shown is the maximum cycle efficiency, and, as such, the heat exchangers are assumed to be infinite. In heating mode, the evaporating temperature is assumed to be equal to the outdoor temperature and the results for two different supply air temperatures are shown. In cooling

mode, an evaporating temperature of 12°C is assumed to meet dehumidification requirements and the refrigerant exit temperature from the gas cooler is assumed to be equal to the outdoor temperature. The transition between heating and cooling occurs between 18 and 26.6°C, where it is assumed that ventilation can meet the cooling requirements (ASHRAE, 1997). The maximum air flow rate over either the outdoor coil is not restricted and the compressor is sized such that there is 1 kW cooling capacity at an outdoor temperature of 45°C (0.310 m³/hr for R744, 0.58759 m³/hr for R410A).

In both heating and cooling, while the peak loads occur at the most extreme outdoor temperatures, the peak capacity occurs when the outdoor temperature is closest to the indoor temperature. The increased capacity at these outdoor temperatures serves only to reduce the run duration during cycling. As a result, in order to avoid sacrificing efficiency, the heat exchangers would need to be oversized to accommodate the highest capacity. Achieving maximum efficiency at these conditions can be done without oversizing the heat exchangers if a variable displacement compressor is used.

The advantage of using a variable displacement compressor with respect to matching the load is shown in Figure 4.5. The compressor is assumed (for lubrication reasons) to have a maximum to minimum displacement ratio of three with efficiencies equal to those given in Equations 4.1 and 4.2 that are assumed to be independent of displacement. As a result, the corresponding cycle efficiency is the same as in Figure 4.4. With a variable displacement compressor the highest required capacity is lower than with a fixed capacity compressor, meaning the size of the heat exchangers can be reduced without sacrificing efficiency. In addition to efficiency advantages at a wider range of operating conditions, the cycle control that is gained by the use of a variable displacement compressor has important implications in terms of comfort control of the supply air. As will be discussed in the following sections, independent control of humidity and temperature requires the use of a variable displacement compressor and variable speed indoor blower.

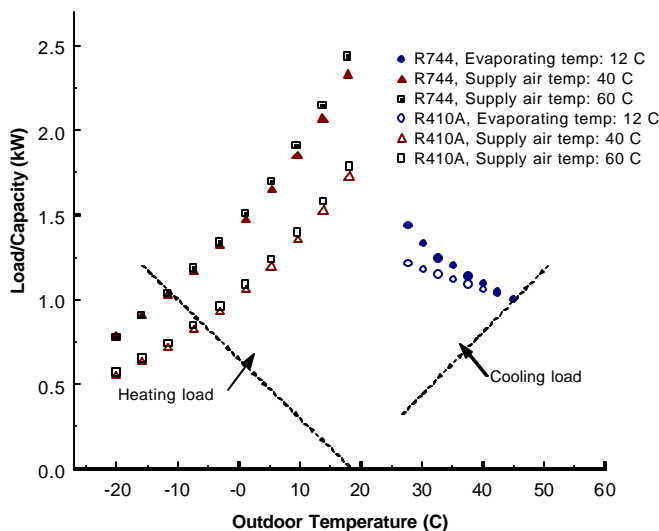


Figure 4.3 Load/capacity curve for system with fixed capacity compressor

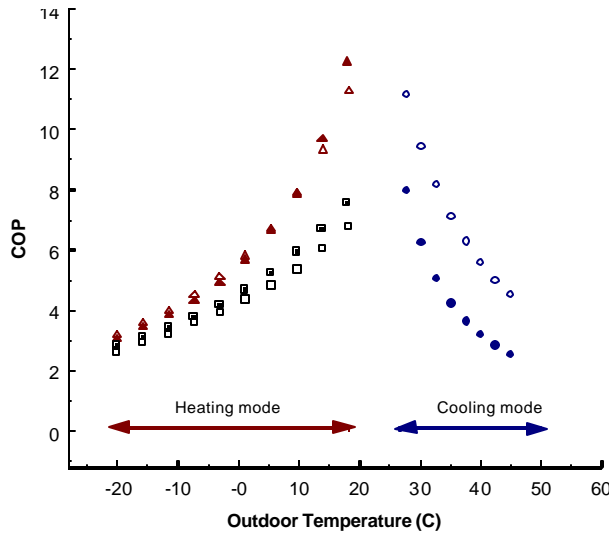


Figure 4.4 Efficiency for system with fixed capacity compressor

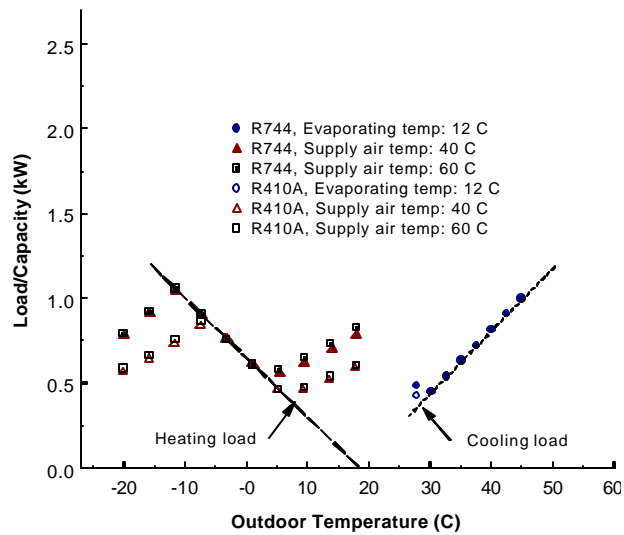


Figure 4.5 Load/capacity curve for system with variable capacity compressor

The differences in efficiency between R410A and R744 will be discussed in the following sections. However, one important difference between the two refrigerants that can be seen in Figures 4.3 and 4.5 is the change in capacity as a function of temperature. Similar to what was seen in the ideal cycle, with the compressors sized for equal cooling capacity at an outdoor temperature of 45°C, the heating capacity of R744 is approximately 40% higher than for R410A for both 40 and 60°C supply air temperatures. The efficiency of the two refrigerants is approximately equal for a 40°C supply air temperature; for a 60°C supply air temperature the efficiency of R744 is 5 to 10% higher than R410A. This increased capacity reduces the need for supplementary heating on cold days, which increases the overall seasonal efficiency.

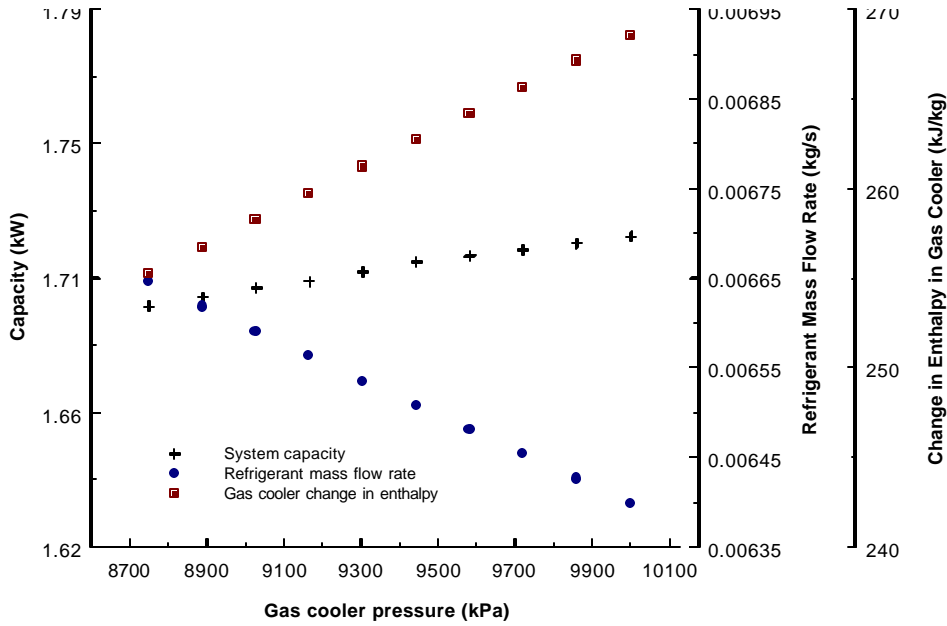


Figure 4.6 Trade-off between increase in change in enthalpy and decrease in refrigerant mass flow rate as a function of gas cooler pressure for R744 ($T_{\text{evap}}=5.3^{\circ}\text{C}$)

With both refrigerants, although the cycle operates at a higher pressure to deliver air at 60°C as compared to 40°C there is a negligible capacity difference, especially at lower outdoor temperatures. Since the inlet condition to the compressor is fixed, it would be expected that the mass flow rate of refrigerant would remain constant and increasing the gas cooler pressure would increase the change in enthalpy in the gas cooler, therefore increasing the system capacity. However, as shown in Figure 4.6, as the compression ratio increases the volumetric efficiency of the compressor decreases, reducing the mass flow rate of refrigerant. As the gas cooler pressure is increased from 8750 kPa (required for a minimum air delivery temperature of 60°C) to 10,000 kPa, the change in enthalpy increases by 5.2%, while the refrigerant mass flow rate decreases by 3.7%, resulting in a increase in capacity of only 1.3%. The result is that the increased change in enthalpy is offset by a decreased refrigerant mass flow rate and cycle capacity is limited.

4.3 Air conditioning cycle

In the air conditioning cycle the comfort of the conditioned space is determined by the relative rate of removal of sensible and latent loads, which is defined as the sensible heat ratio (SHR):

$$SHR = \frac{Q_{\text{sensible}}}{Q_{\text{total}}} = \frac{Q_{\text{sensible}}}{Q_{\text{sensible}} + Q_{\text{latent}}} \quad (4.3)$$

The sensible heat ratio is a function of only the airflow properties at the inlet to the evaporator and the surface temperature of the evaporator, and is independent of the airflow rate and total capacity of the cycle. As a result, the main effect is on the refrigerant side temperature difference. A full discussion of psychrometrics as related to SHR, as well as a listing of the EES program used to obtain results presented in this section is contained in Appendix E.

Assuming the same evaporator geometry and sensible and latent heat transfer for R410A and R744, the required evaporating refrigerant to wall temperature difference can be determined from the refrigerant side heat transfer coefficient alone. Based on the heat transfer coefficients listed in Table 4.1 ($2500 \text{ W/m}^2 \text{ K}$ for R410A and $10,000 \text{ W/m}^2 \text{ K}$ for R744), the refrigerant/wall temperature difference in the R744 evaporator would be need to be 25% of that needed for R410A. Because the same amount of heat could be transferred across a smaller temperature difference for R744, the cycle efficiency of R744 would be improved by operating at an evaporating temperature higher than R410A. This is shown in Figure 4.7 for a range of sensible heat ratios based on the assumptions listed in Table 4.1.

The effect that evaporating temperature has on cycle efficiency is shown in Figure 4.8 assuming two different outdoor temperatures: 35°C and 45°C . Over this range of outdoor temperatures the pressure ratios of R410A and R744 are both less than three, so the relative performance of the two cycles is changed little by considering the effects of a real compressor. As discussed in the ideal cycle, the higher efficiency for R410A results primarily from the fact that in Figure 4.8 the maximum outdoor airflow rate is unconstrained. In Figure 4.9 the effect of finite airflow rate is shown, assuming that the airflow rates over the outdoor coil are equal and determined by the pinched condition for R744. It is evident from Figures 4.8 and 4.9 that the operating point determined by the comfort constraint reduces significantly the overall efficiency of the system. For example, reducing the evaporating temperature to 12°C from 23°C reduces the efficiency by nearly half for most of the cases shown.

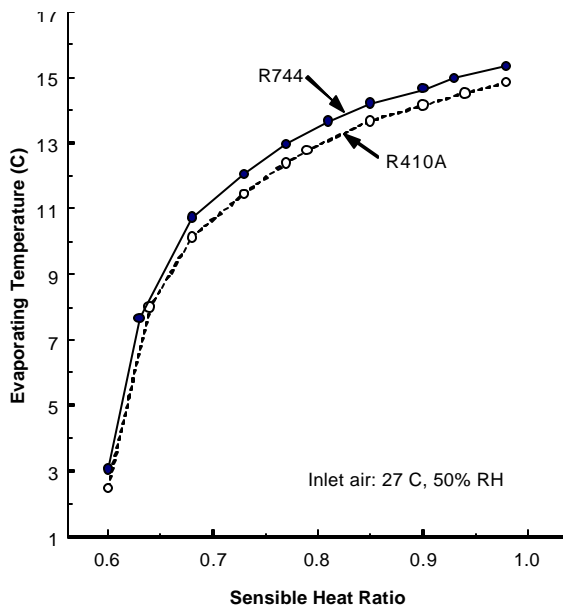


Figure 4.7 Dependence of evaporating temperature on sensible heat ratio

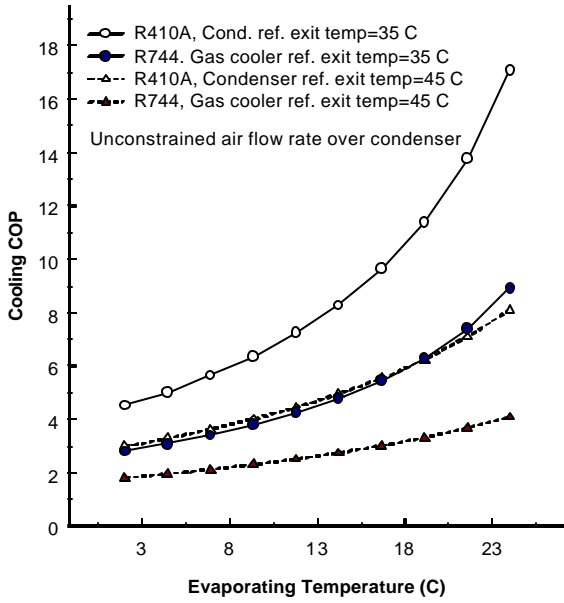


Figure 4.8 Effect of evaporating temperature on cooling cycle efficiency with unconstrained airflow rate over condenser/gas cooler

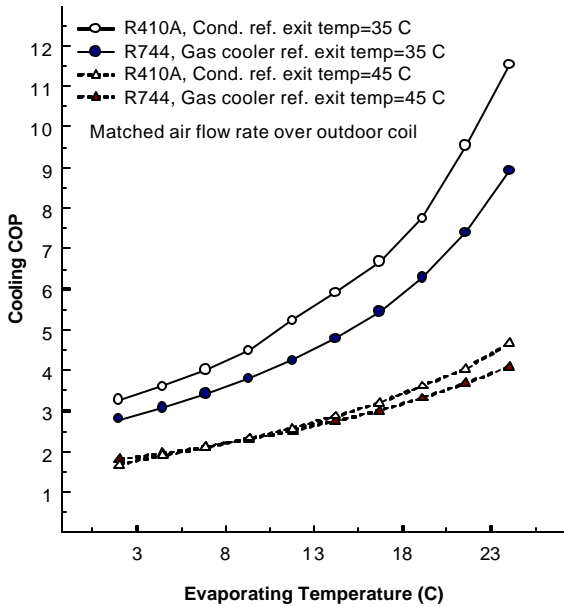


Figure 4.9 Effect of evaporating temperature on cooling cycle efficiency with matched air flow rates over condenser/gas cooler

Because the SHR is theoretically independent of capacity and airflow rate, a given capacity can be achieved for a finite area indoor heat exchanger by varying the airflow rate. Increasing the airflow rate increases the air/refrigerant temperature difference across the indoor coil resulting in a higher heat transfer rate. To maintain a surface temperature to meet a given SHR, the flow of refrigerant needs to be modulated by a variable capacity compressor.

This analysis assumes the presence of an internal heat exchanger in the R744 cycle, but not one in the R410A cycle. It was noted that the presence of an internal heat exchanger provided a benefit to the R744 cycle, where no benefit would be realized in the R410A cycle. In Figure 4.10 the cycle efficiency is plotted as a function of outdoor temperature for a fixed evaporating temperature of 12°C for both refrigerants with and without an internal heat exchanger. From the figure it is evident that the efficiency improvement using a suction line heat exchanger with R410A in cooling mode is minimal, and would probably be negative if pressure drop in the heat exchanger were considered. In the following heat pump cycle analysis, an internal heat exchanger is included in the R744 cycle, but not in the R410A cycle.

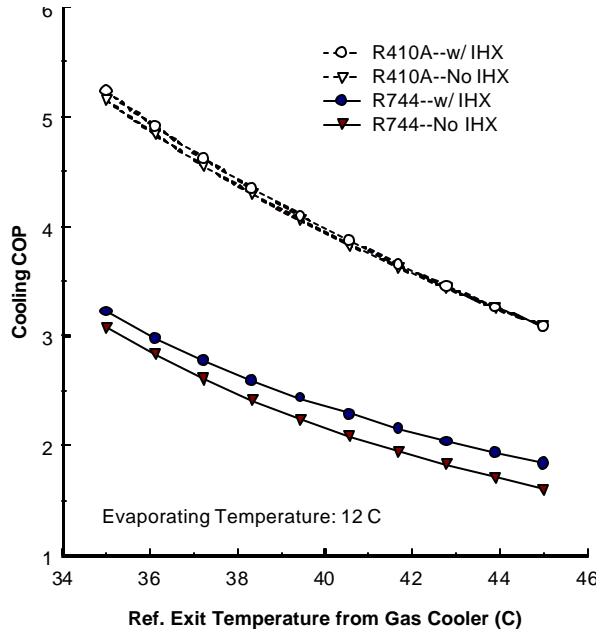


Figure 4.10 Effect of internal heat exchanger on cooling cycle efficiency

4.4 Heat pump cycle

4.4.1 Cycle analysis

The analysis in Section 3.2 of the ideal heat pump cycle neglected compressor inefficiencies and found that R410A was more efficient than R744 at lower supply air temperatures, and approximately equal at higher supply air temperatures. When compressor efficiency is included in the analysis, shown in Figure 4.11, R744 becomes more efficient at supply air temperatures above about 40°C, depending on the evaporating temperature. This relative improvement for R744 results from the fact that the compression ratios required for a high supply air temperature are much lower than for R410A, which translates into higher efficiency for the R744 compressor. Additionally, because R744 has a higher refrigerant side heat transfer coefficient, the evaporating temperature could be one-half degree higher for the same outdoor ambient temperature. This would result in approximately a 2% increase in the heating COP of R744 as compared to R410A for the same outdoor temperature (based on an evaporating temperature of 2.3°C, a supply air temperature of 40°C, and a refrigerant exit temperature of 21°C). Figure 4.12

shows only a small difference in the compressor discharge temperatures corresponding to the points plotted in Figure 4.11.

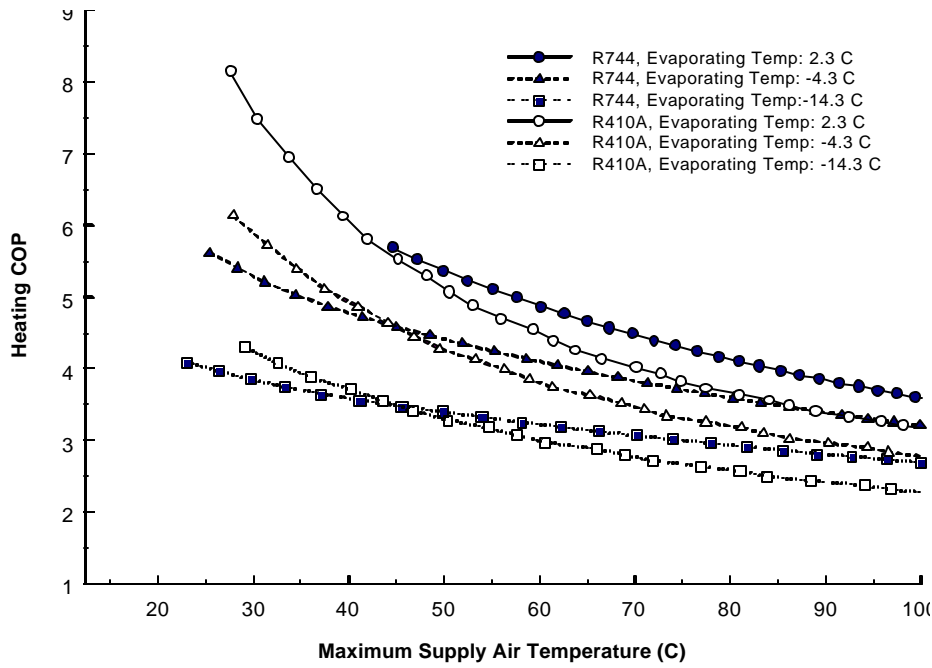


Figure 4.11 Effect of real compressor and evaporating temperature on heating cycle efficiency

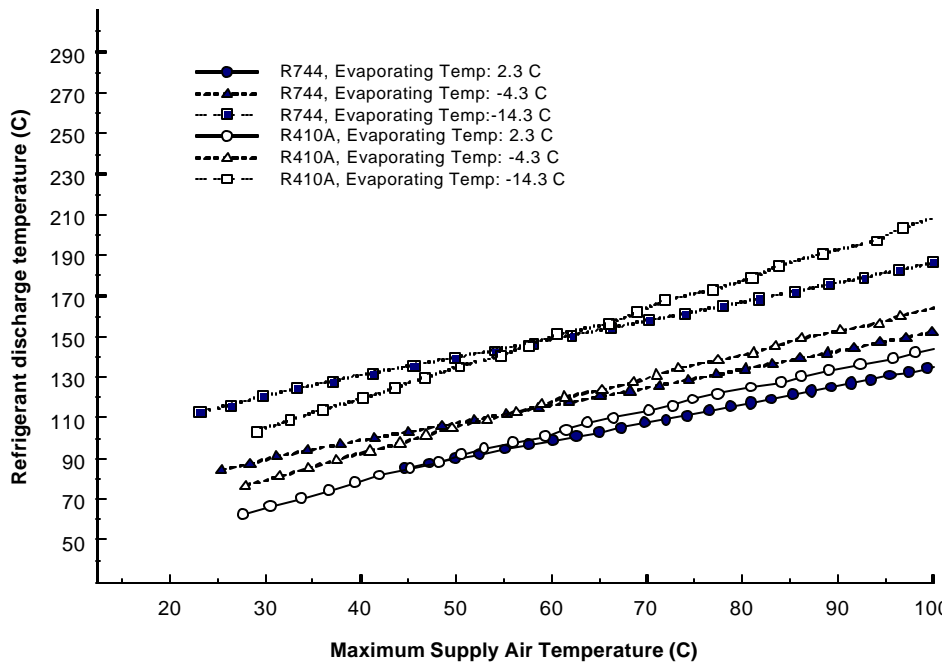


Figure 4.12 Refrigerant discharge temperatures for corresponding maximum supply air temperature with real compressor

4.4.2 Supplementary heating options

Below a certain outdoor temperature (the balance point), with the compressor displacement at its maximum, the capacity of the system cannot be increased to meet the requirements of the load and some sort of supplementary heating is required. Three possible air-side comfort control options are illustrated in Figure 4.13. For Option A, the air temperature would be raised below the comfort constraint in the gas cooler, then increased to the comfort constraint with the supplementary heat. With Option B, the air temperature is raised to the comfort constraint in the gas cooler, then above the comfort constraint by the supplementary heat. For Option C, the airflow can be split and the temperature of each stream raised such that when they are recombined the comfort constraint is met. Since, theoretically, any division of the airflow in Option C is possible, it is the least constrained case, making a meaningful analysis difficult. As a result, only Options A and B are compared, as shown in Figure 4.14 assuming a balance point temperature of -10.5°C . With Option A, the gas cooler pressure is reduced sharply as the evaporating temperature decreases. Because the low efficiency supplementary heating dominates the overall cycle efficiency, however, the advantage of the fixed supply air temperature case is not as high as might be expected. At an evaporating temperature of -20°C there is only a 3% improvement in delivering air at 60°C by fixing the supply air temperature (Option A) as compared to delivering air at 93°C by letting the air temperature vary (Option B). Since the hotter air would require less blower power, Option B could be the most efficient if adequate room air circulation could be maintained. Since the hotter air would require less blower power, Option B could be the most efficient if adequate room air circulation could be maintained.

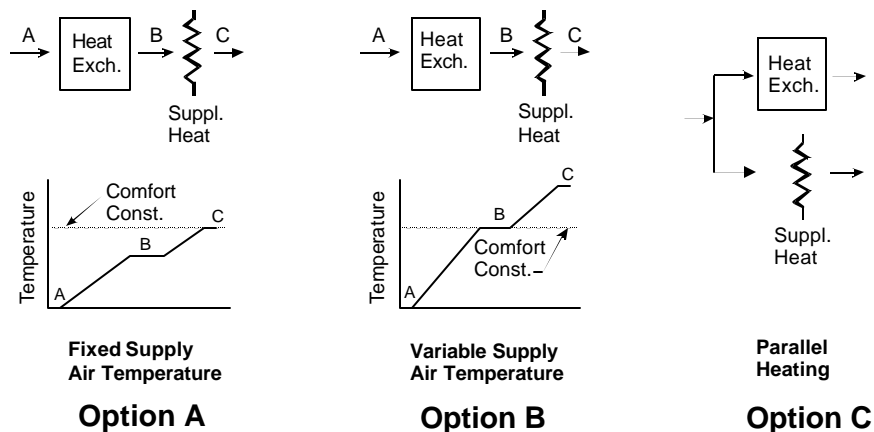


Figure 4.13 Supplemental heating options

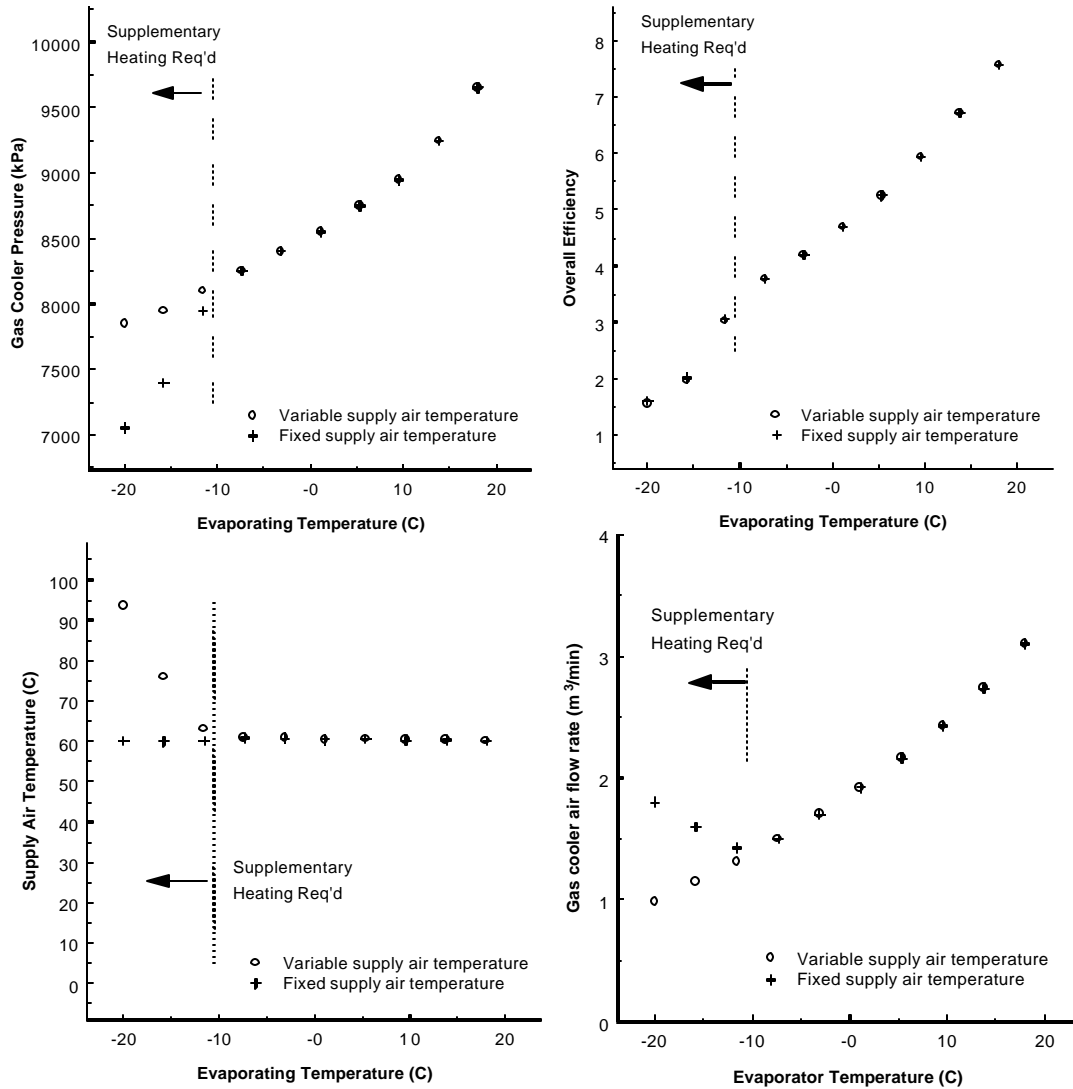


Figure 4.14 Comparison of fixed supply air temperature and variable supply air temperature supplementary heating configurations

4.5 Comparison of heat exchanger sizes required for heating and cooling

4.5.1 Indoor coil sizing

The challenge in designing a system to operate in both heating and cooling mode is optimizing the design of the heat exchangers to run well in both conditions.

In cooling mode, the dehumidification comfort constraint determines the evaporating temperature, and the heat exchanger area required is a function of the airflow rate. Based on the assumptions listed in Table 4.1 the relationship between indoor airflow rate and required indoor coil airside area is plotted in Figure 4.15 for a sensible heat ratio (SHR) of 0.75 and for capacities of 1 and 0.5 kW. Because such a large surface/air temperature difference is required to achieve a SHR of 0.75 based on air inlet conditions of 27°C and 50% RH, the heat exchanger area

required is on the order of $2 \text{ W/m}^2 \text{ K}$. The 0.5 kW capacity line shows the reduction in airflow that would be required to maintain the same SHR for a fixed area heat exchanger.

In heating mode, the airflow rate is fixed by the comfort constraint and the heat exchanger area required is a function of the pressure and mass flow rate of the refrigerant. Because the temperature difference goes to zero at the pinch points, the area required to accommodate heat transfer in this region accounts for the majority of the overall heat exchanger size. This is illustrated in Figure 4.16 which shows the air and refrigerant temperature profiles for an R744 counterflow gas cooler having 1 kW of capacity, supplying air at 60°C with approach and pinch point temperature differences of 0.2°C .

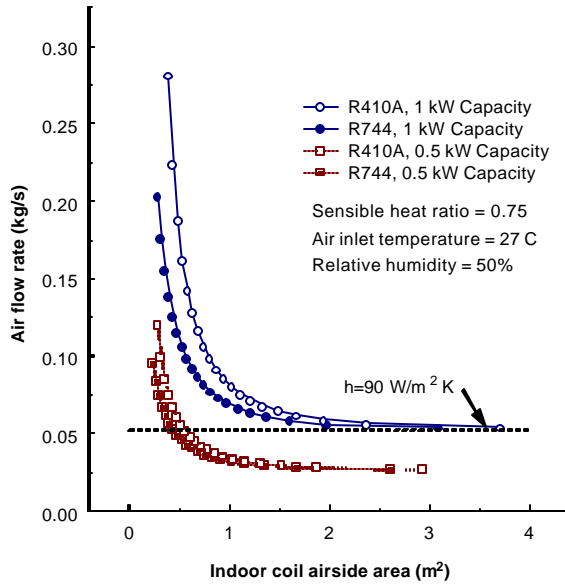


Figure 4.15 Controlling air-side capacity in cooling mode by adjusting air flow rate over evaporator coil

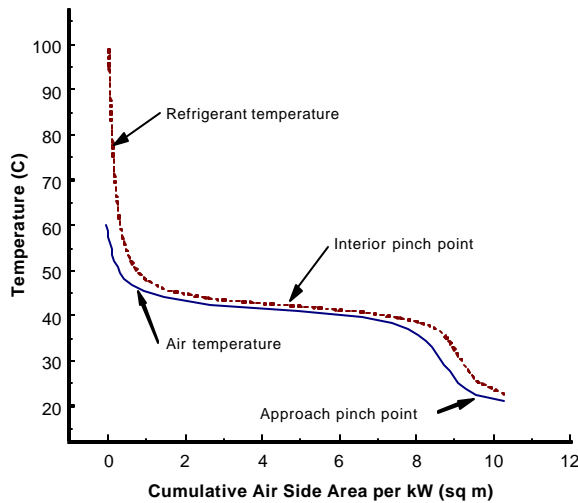


Figure 4.16 Temperature profile in gas cooler

Accepting a finite temperature difference at the pinch point and a non-zero approach temperature significantly reduces the required heat exchanger area. Figure 4.17 shows maximum heat pump cycle efficiency as a function of indoor heat exchanger size per kW for an evaporating temperature of 2.3°C and an air-side heat transfer coefficient of $90\text{ W/m}^2\text{ K}$ for both the 40°C and 60°C supply air temperatures. The points represent the highest efficiency obtainable by adjusting both the refrigerant mass flow rate and the high side pressure. In practice, the pinch point temperature difference would be controlled most directly by the high side pressure, and the approach temperature difference would be controlled most directly by the refrigerant mass flow rate. For reference, the size and efficiencies of the R410A baseline and R744 prototype systems listed in Table 4.1 are shown, respectively 26.3% and 12.7% below the ideal for the 40°C supply air condition. The lower efficiency of these two systems results from a departure from the ideal counterflow configuration and a lower evaporating temperature as listed in Table 4.1.

Figure 4.18 shows the effect on heat exchanger area of increasing the temperature difference at the pinch points near the refrigerant critical temperature and at the heat exchanger exit. Figure 4.17 is a composite of Figure 4.18, showing the highest efficiencies for a given length. Each series of points represents a specific exit temperature from the gas cooler, showing the effect of increasing the temperature difference at the gas cooler exit pinch point. The difference between points within the series shows the effect of increasing the temperature difference at the critical temperature pinch point by increasing the gas cooler pressure. Notably, the strategy for obtaining maximum efficiency depends on the size of the heat exchanger. For example, for an air-side area greater than $3.5\text{ m}^2/\text{kW}$ heating capacity, maximum efficiency is obtained by minimizing the refrigerant gas cooler exit temperature. However, for smaller heat exchangers, increasing the gas cooler exit temperature above the supply air temperature and increasing the condensing pressure to increase the temperature difference at the critical temperature pinch point maximizes efficiency.

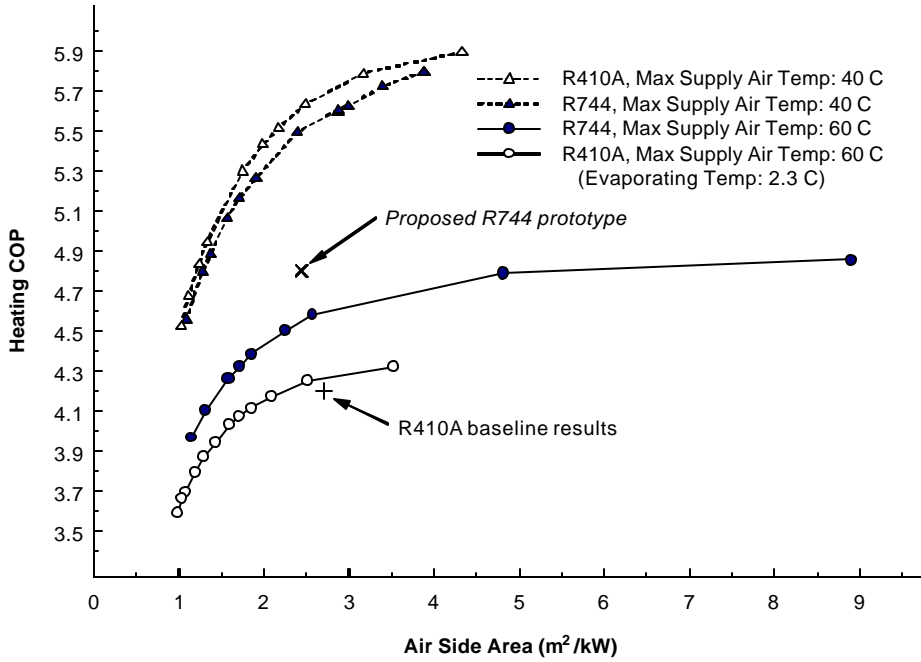


Figure 4.17 Effect of finite area gas cooler on heating cycle efficiency (real compressor, evaporating temp: 2.3 C)

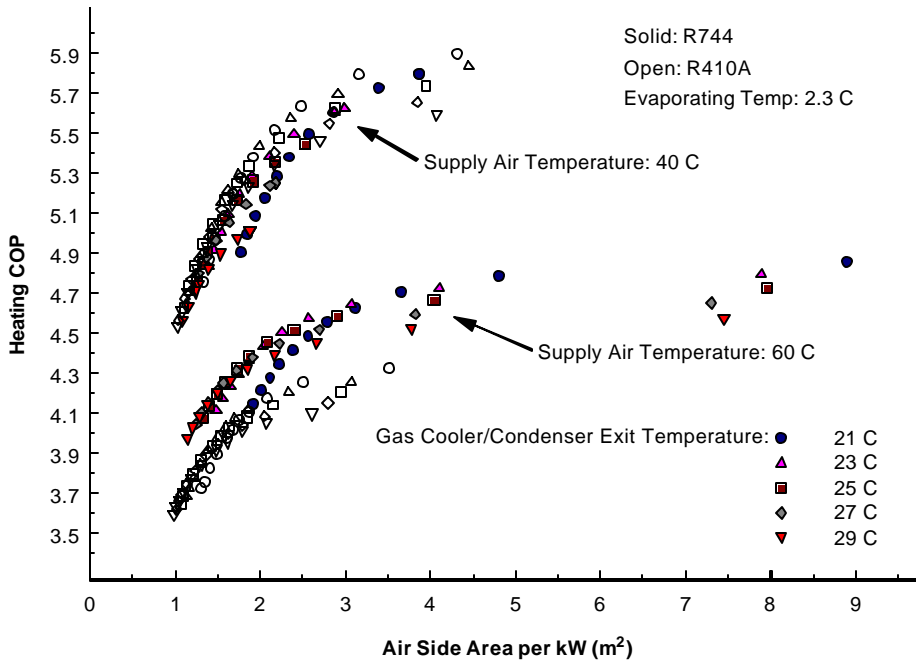


Figure 4.18 Effect of finite area gas cooler on heating cycle efficiency (real compressor, evaporating temp: 2.3 C)

In heating mode, an airflow rate of 0.052 kg/s per kW capacity is required to warm air from 21 to 40°C. In Figure 4.15, which showed the required airflow rate for a given capacity and airflow rate in cooling mode, it was assumed that the heat transfer coefficient was 90 W/m² K at a flow rate of 0.052 kg/s. As a result, the results from

Figures 4.15 and 4.18 can be correlated for the 40°C supply air case to estimate the reversible performance of an indoor coil of specified air-side area. Based on these results, an airside area of 2 m²/kW capacity would meet the heating capacity within 5% of maximum efficiency, and the cooling capacity within 5% of minimum airflow rate for both R410A and R744. As a result, the indoor coil sizing considerations are basically the same for both refrigerants.

For a supply air temperature of 60°C, the airflow rate required would approximately half per kW capacity as the 40°C supply air case (assuming an air inlet temperature of 21°C). Therefore, assuming a heat transfer coefficient dependence on $Re^{0.8}$, the heat transfer coefficient for a supply air temperature of 60°C would be 57% of that for a supply air temperature of 40°C. For R744 the airside area would need to be increased nearly 70% (based on the assumptions in Table 4.1) to compensate for the reduction in heat transfer area; for R410A the area would need to be increased by over 60%. As a result, for supply air temperatures of 60°C and reasonable efficiency, heating performance of the indoor coil would be the primary design consideration. Alternatively, indoor coil designs that adjust depending on if they are heating or cooling may need to be developed. A concept of this is shown in Figure 4.19.

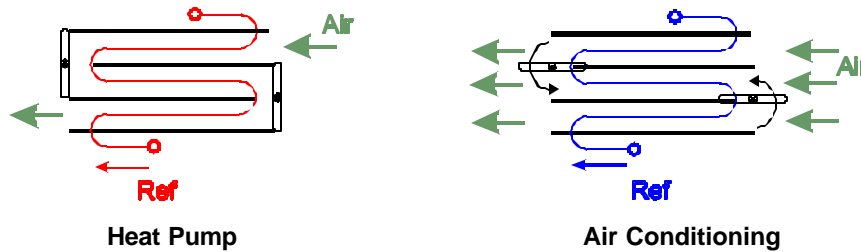


Figure 4.19 Conceptual diagram of indoor coil for reversible air conditioning and heat pump operation (side view). Slats at either end could rotate to increase the area for airflow by a factor of the number of passes, maintaining the air side heat transfer coefficient for large differences in flow rate.

4.5.2 Outdoor coil sizing

Because the airflow rate over the outdoor coil is not constrained (as it is for the indoor coil based on comfort) there is an additional variable in terms of required heat exchange area. Since the airflow rate effects the required heat exchanger area, the effect of fan power on system COP needs to be included in order to get an accurate assessment of the effect of heat exchanger size on system performance. In order to incorporate the effect of fan power on system COP the following relationships are used:

$$W_{fan} = \frac{\dot{v}_{air} \cdot \Delta P_{outdoor}}{h_{fan}} \quad (4.4)$$

$$COP_{system} = \frac{Q_{indoor}}{W_{fan} + W_{compressor}} \quad (4.5)$$

The fan efficiency (h_{fan}) is assumed to be 0.5. Similar to the assumptions regarding the air-side heat transfer coefficient in Table 4.1, the air side pressure drop over the outdoor coil ($DP_{outdoor}$) is assumed to be 45 Pa at an airflow rate of 0.15 kg/s, and is assumed to vary as Re^2 .

In heating mode the combination of the heat exchanger area and airflow rate determines the evaporating temperature (assuming that the exit quality is fixed by a suction accumulator and the refrigerant flow rate is determined by the indoor capacity requirements). As the airflow rate is increased the evaporating temperature increases which results in higher cycle efficiency. In Figure 4.20 the relationship between airflow rate, cycle and system efficiency is shown for the 8.3°C outdoor condition with a supply air temperature of 40°C. In Figure 4.21 the required heat exchanger area as a function of airflow rate is shown.

In cooling mode, the refrigerant pressure in the outdoor coil becomes an variable in addition to the airflow rate over the outdoor coil. In Figure 4.22 the optimum discharge pressure in terms of cycle efficiency is plotted as a function of airflow rate for the 45°C outdoor cooling condition with an indoor evaporating temperature of 12°C. The effect of airflow rate on system efficiency is also shown. For the transcritical R744 cycle, because the optimum discharge pressure is above the minimum possible, increasing the air flow rate does not effect the optimum discharge pressure. Therefore, the cycle efficiency is constant. For the subcritical R410A cycle, however, the optimum pressure corresponds to the minimum possible pressure. As a result, as the airflow rate is increased the optimum pressure decreases and system efficiency improves.

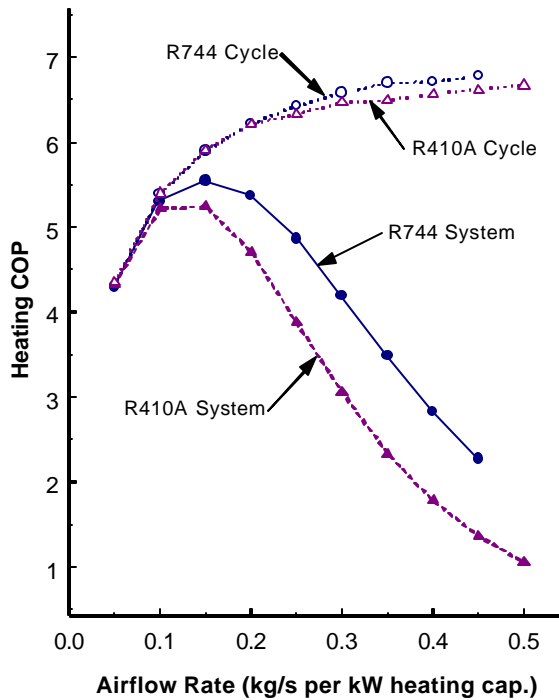


Figure 4.20 Effect of airflow rate on heating cycle and system efficiency for 8.3°C outdoor heating condition, 40°C supply air temperature

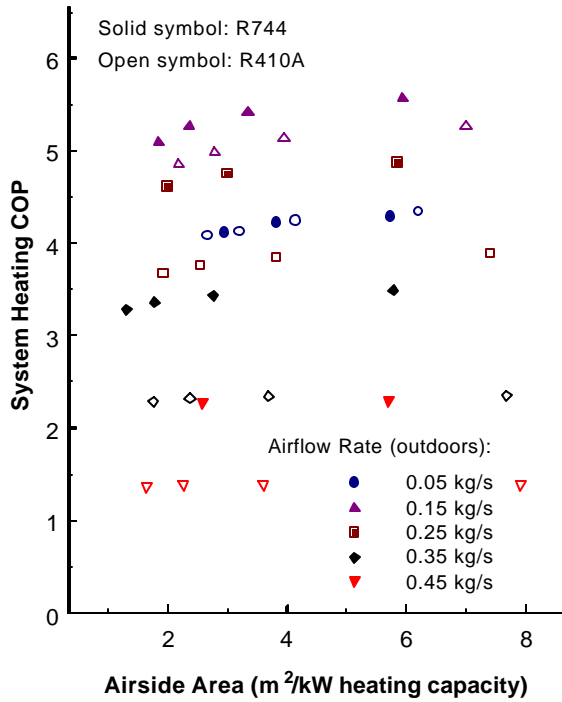


Figure 4.21 Effect of heat exchanger area on system heating COP, 8.3°C outdoor heating condition, 40°C supply air temperature

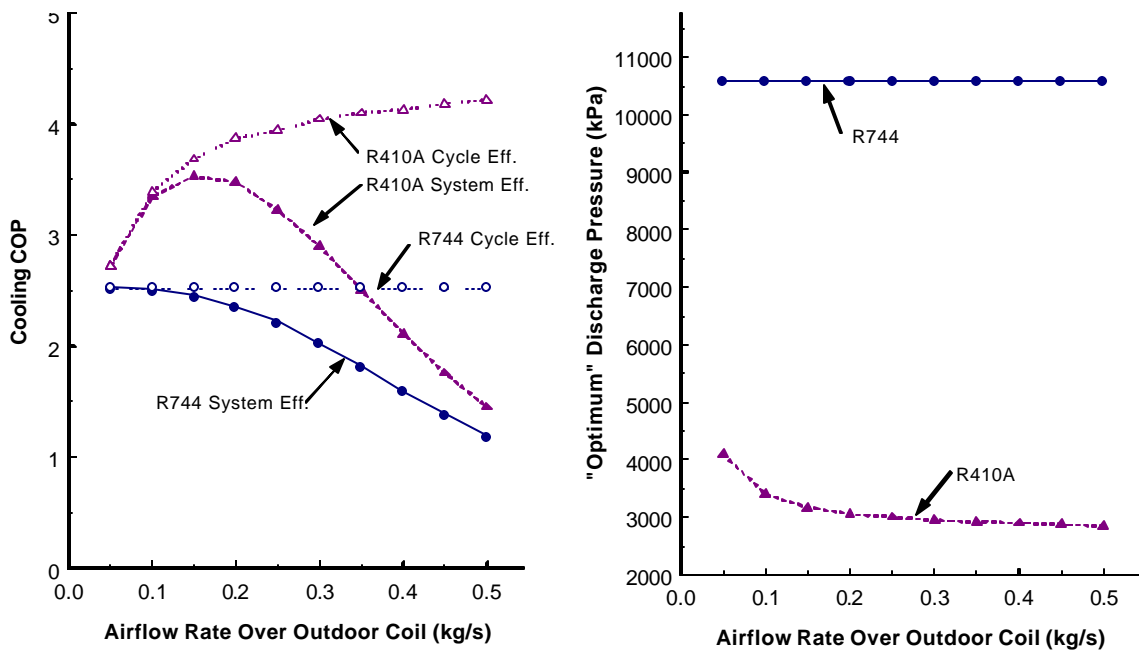


Figure 4.22 Effect of airflow rate on cooling cycle and system efficiency for 45°C outdoor cooling condition, 12°C evaporating temperature

The effect of required heat exchanger area relative to the optimum discharge pressure is different for the two refrigerants. For R744, since the optimum discharge pressure is fixed, increasing the airflow rate increases the

air/refrigerant temperature difference reducing the required heat exchanger area. For R410A, as the optimum discharge pressure is dropped by increasing the airflow rate, the air refrigerant temperature difference decreases and the required heat exchanger area increases. This is shown in Figure 4.23, which shows the effect of heat exchanger area on system COP.

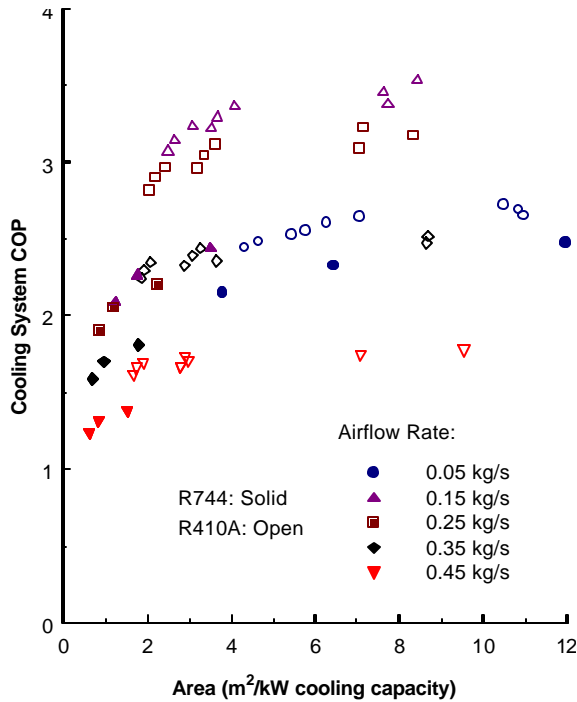


Figure 4.23 Effect of heat exchanger area on system cooling COP, 45°C outdoor cooling condition, 12°C evaporating temperature

4.6 Real cycle conclusions

By specifying the isentropic compressor efficiency, the thermodynamic cycle can be specified with only an evaporating temperature, a condensing pressure and a refrigerant exit temperature from the gas cooler. Additionally, if heat transfer coefficient correlations are included then estimated can be made regarding the size of heat exchanger required for a given cycle efficiency.

In cooling mode, the compression ratios and compressor efficiencies, of the two cycles are comparable. As a result, relative cycle efficiencies are the same as for the ideal cycle, and R410A shows a considerable advantage. If the air flow rates over the heat rejecting coil are matched at reasonable levels, however, then the efficiency advantage of the R410A cycle over R744 is reduced by nearly half.

In heating mode, because of the lower compression ratios for R744, above supply air temperatures of about 40°C the efficiency of R744 is higher than the efficiency of R410A, approximately 10% higher at a supply air temperature of 60°C. For supply air temperatures below 40°C R410A has higher efficiency than R744, approximately 8% higher for a supply air temperature of 35°C. For systems with compressors sized such that the cooling capacity is equal, R744 has higher capacity in heating at low outdoor temperatures. In a typical application,

this increased capacity would have the practical benefit of reduced dependence on lower-efficiency supplementary heating.

The size of the heat exchangers for R744 and R410A are basically the same for R410A and R744 in systems designed for comfort. In heating, at a supply air temperature of 40°C, R744 and R410 have approximately the same efficiency for a given indoor coil size. Above a supply air temperature of 40°C, R744 has higher efficiency for a given size heat exchanger (or equivalently, a smaller heat exchanger would have the same efficiency). In cooling, the comfort condition determines the evaporating temperature and the indoor coil size is predominately a function of the airflow rate. In heating if the fan power required to move air over the outdoor coil in the system COP calculation, the optimum airflow over the outdoor coil is around 0.15 kg/s per kW heating capacity for both R410A and R744. In cooling, in terms of system COP there is an optimum for R410A, but not for R744.

Chapter 5: Seasonal Efficiency

5.1 Annual loads

It has been shown that R410A has higher efficiency in cooling mode while R744 has comparable or higher efficiency in heating mode as well as higher capacity. The higher capacity of R744 in heating mode results in decreased dependence on supplementary heating which has a considerable effect on the overall heating efficiency. As a result, an important component in the comparison of R744 and R410A is the annual estimated heating and cooling requirements.

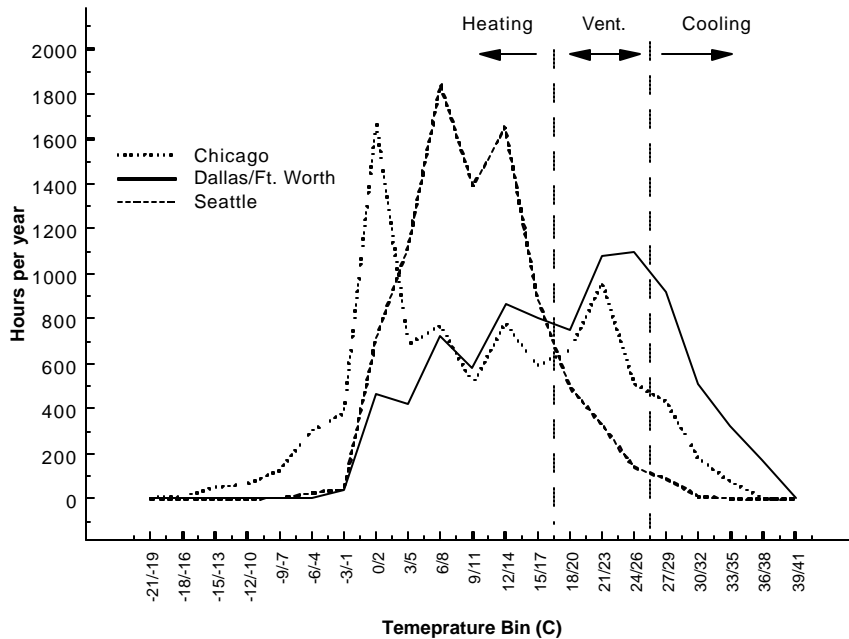


Figure 5.1 Temperature bin data

In order to gauge this effect, R744 and R410A systems are compared based on temperature bin data for three different cities: Dallas/Ft. Worth, Seattle and Chicago. The selected cities are intended to represent three varying climates. Temperature bin data for these cities is shown in Figure 5.1 (ASHRAE, 1997).

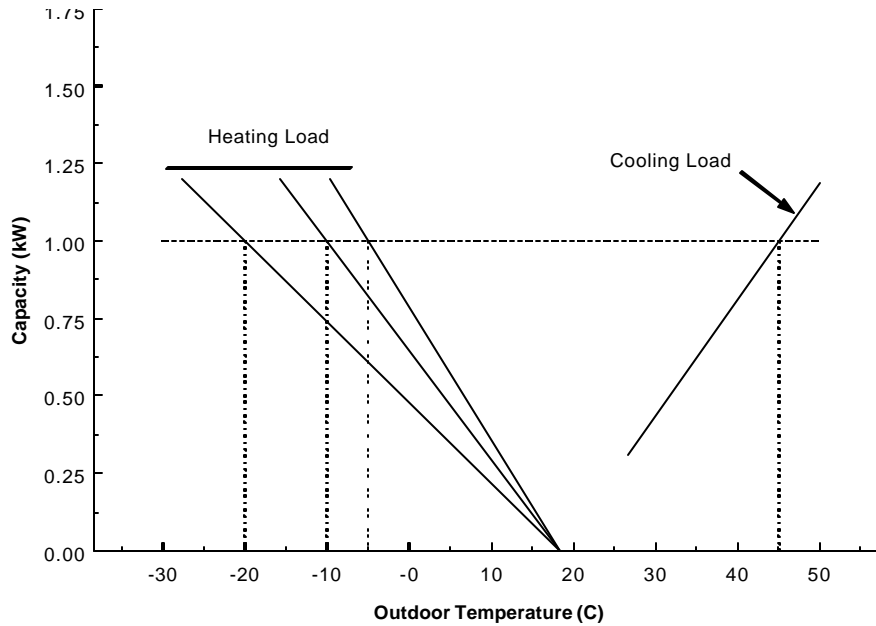


Figure 5.2 Capacity normalization as function of heating capacity and outdoor temperature

The load is approximated as a linear function of temperature with a balance point of 18.3°C. While the actual load for a given outdoor temperature may vary considerably depending on a variety of factors (solar loads, wind speed, etc.), for an annualized approximation the linear load approximation is reasonable. The heating load is normalized as a function of the outdoor temperature at which 1 kW heating capacity is required, as shown in Figure 5.2. The three lines shown for heating loads correspond to various levels of insulation. The cooling load is normalized based on a 1 kW load requirement at 45°C. Since solar radiation and infiltration of hot humid air dominate cooling loads, only one line is shown. Between an outdoor temperature of 18.3°C and 26.6°C it is assumed that ventilation can meet the cooling load.

5.2 Cycle assumptions

It is assumed that the airflow rate over the outdoor coil is 0.15 kg/s per kW cooling capacity at 45°C outdoors. This airflow rate was shown in Figure 5.22 to provide the maximum efficiency in cooling for R410A and is comparable to systems currently available. As a result, it is a reasonable basis of comparison for the two systems. In heating, the evaporating temperature is determined based on the assumption that the air and refrigerant exit temperatures in the outdoor coil are pinched.

In heating mode the return air temperature is assumed to be 21°C, and supply air temperatures of 40 and 60°C are considered. In cooling mode, an evaporating temperature of 12°C is assumed for all conditions to provide sufficient dehumidification.

The compressor is sized such that the 1 kW load at 45°C is met. It is assumed that a variable displacement compressor is used, that the efficiencies are equal to those given in Chapter 4 (Equations 4.1 and 4.2), and that the isentropic and volumetric efficiencies are constant from maximum displacement to one-third maximum capacity. Below one-third of maximum capacity, both systems are assumed to cycle at maximum efficiency to meet the load;

in heating, when the load exceeds the maximum capacity of the system, it is assumed that electric resistance heaters supply supplementary heat with an efficiency of one.

Finally, as discussed in Chapter 4, an internal heat exchanger is assumed to be present on the R744 system, but not on the R410A system.

5.3 Results

The load/capacity and efficiency results based on the above approximations are shown in Figure 5.3, for a 1 kW heating load at -10°C and a supply air temperature of 40°C . In cooling mode, the displacement of the compressor is capable of matching load requirements over most of the outdoor temperature range, and cycling is only necessary below an outdoor temperature of 30°C . In heating, however, varying the compressor displacement meets the load only in a limited portion of the temperature range, with cycling being required above an outdoor temperature of 5°C , and supplementary heating being required below an outdoor temperature of -4°C by R410A, and -8°C by R744. The efficiencies of the two systems are approximately equal, except where the supplementary heating is required and there is a sharp reduction in efficiency. Below -20°C , the heating is supplied predominately by the supplementary heat source. Additionally at this point, for the 60°C supply air case, the refrigerant discharge temperatures begin to approach 200°C and the working limits of the compressor lubricant become a consideration.

Figure 5.4 shows the annualized energy efficiency for the three regions plotted in Figure 5.1 as a function of the outdoor temperature at which the heating load is 1 kW, for a heating supply air temperature of 40°C (the capacity and efficiency for a 1 kW load at -10°C was shown in Figure 5.3). In Dallas/Ft. Worth where cooling loads dominate, R410A is considerably more efficient. In Seattle, where the cooling requirement is relatively small and the majority of the heating load can be met without supplementary heat, the efficiency of the two cycles is nearly equal. In Chicago, R744 show a very slight advantage, except when the outdoor temperature for 1 kW load is low, representing a well-insulated environment.

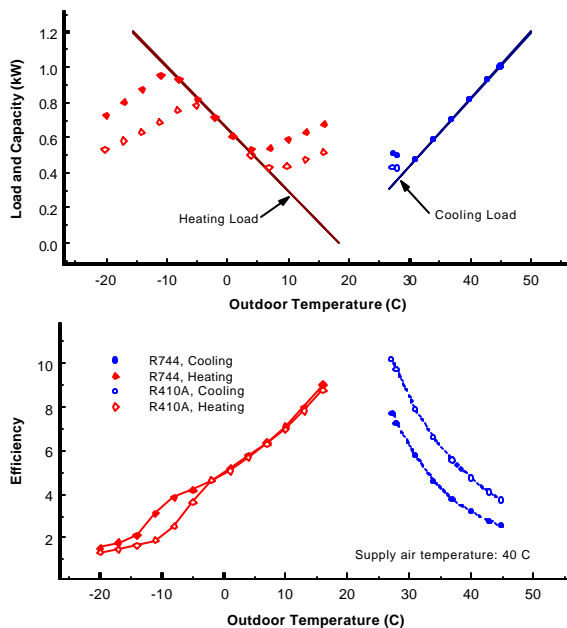


Figure 5.3 Capacity load curve for sample system, 40°C supply air in heating

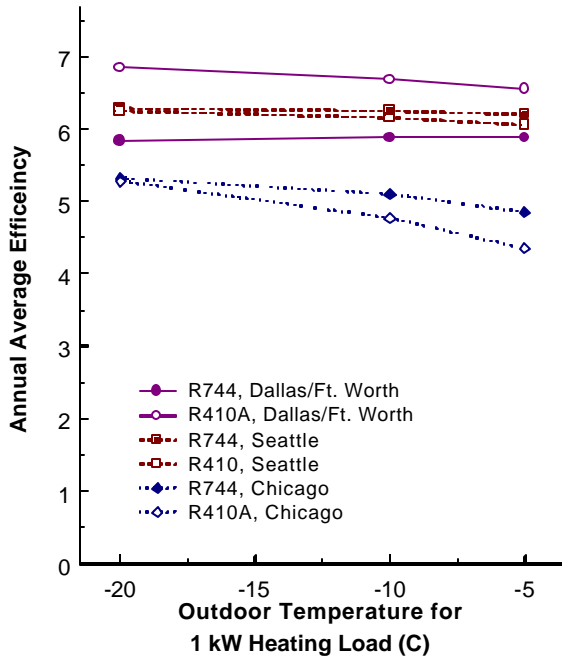


Figure 5.4 Comparison of overall annual efficiency as function of heating load requirement for 40°C supply air

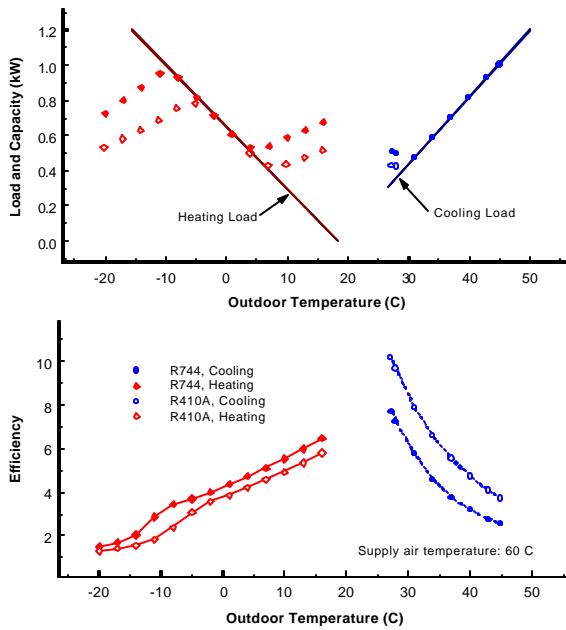


Figure 5.5 Capacity load curve for sample system, 60°C supply air in heating

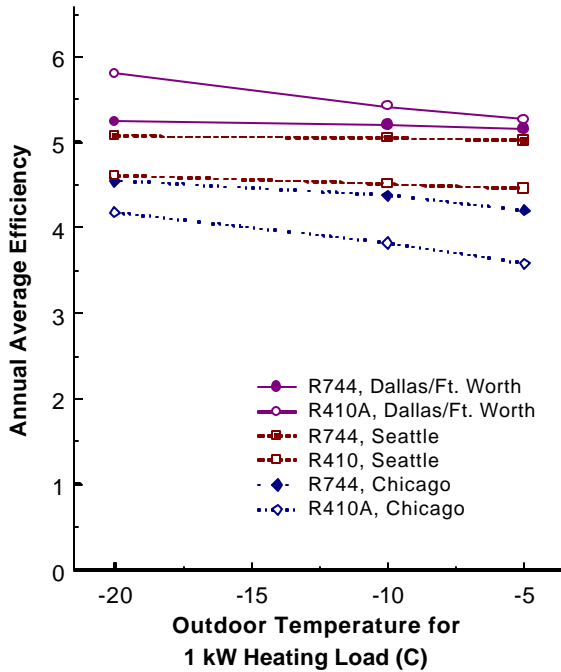


Figure 5.6 Comparison of overall annual efficiency as function of heating load requirement for 60°C supply air

As discussed in Section 4.4.1, the compression ratio for R744 is lower for elevated supply air temperatures, which translates into higher efficiency. This is seen in Figure 5.5, which shows the capacity and efficiency for a 1 kW load at -10°C and a supply air temperature of 60°C. While R410 still shows a dominant advantage for Dallas/Ft. Worth, in Chicago the annual operating efficiency of R744 is about 9-16% higher than R410A depending on the load requirement, and in Seattle R744 is about 10% more efficient than R410A.

Bibliography

- Abersfelder, Guenter, Juergen Maue, Juergen Wertenbach, "Method For Operating an Air Conditioning Cooling System for Vehicles and a Cooling System For Carrying Out the Method", US Patent 5,685,160, Nov. 11, 1997.
- American Society of Heating, Refrigeration and Air-conditioning Engineers, "Handbook of Fundamentals", ASHRAE, 1997.
- Andrade, M.A. and C.W. Bullard, "Controlling Indoor Humidity Using Variable Speed Compressors and Blowers", University of Illinois at Urbana-Champaign, ACRC TR 151, 1999.
- ANSI/ASHRAE Standard 116, "Method of Testing for Seasonal Efficiency of Unitary Air-Conditioners and Heat Pumps", American Society of Heating, Refrigeration and Air -Conditioning Engineers, Inc., 1995.
- ARI Standard 210/240, "Standard for Unitary Air Conditioning and Air Source Heat Pump Equipment", Air Conditioning and Refrigeration Institute, 1989.
- Beaver, A.C., J. M. Yin, C. W. Bullard, P. S. Hrnjak, "Experimental and Model Study of the Heat Pump/Air Conditioning Systems Based on Transcritical Cycle with R744", IIR Congress, Sydney, Australia, 1999a.
- Beaver, A.C., J. M. Yin, C. W. Bullard, P. S. Hrnjak, "An Experimental Investigation of Transcritical Carbon Dioxide Systems for Residential Air Conditioning", University of Illinois at Urbana-Champaign, ACRC CR-18, 1999b.
- Boewe, D., J. M. Yin, Y. C. Park, C. W. Bullard, P. S. Hrnjak, "The Role of the Suction Line Heat Exchanger in Transcritical R744 Mobile A/C Systems", SAE paper 1999-01-0583, 1999.
- Coleman, H.W. and W.C. Steele, Jr., *Experimentation and Uncertainty Analysis for Engineers*, John Wiley & Sons, 1989.
- He, X.D., Sheng Liu, Harry H. Asada, and Hiroyuki Itoh, "Multivariable Control of Vapor Compression Systems", *International Journal of Heating, Ventilating, Air-Conditioning and Refrigerating Research*, vol. 4, no. 3, pp. 205-230, July, 1998.
- Hihara, E., "Heat Transfer characteristics of CO₂", IEA Workshop on Selected Issues on CO₂ as Working Fluid in Compression Systems, Trondheim, Norway, September, 2000.
- Hwang, Y and R. Radermacher, "Theoretical Evaluation of Carbon Dioxide Refrigeration Cycle", *Int. J. of HVAC&R Research*, vol. 4, no. 3, pp. 245-263, July, 1998
- Incorpera, F. P. and D.P. DeWitt, *Fundamentals of Heat and Mass Transfer, Fourth Edition*, John Wiley and Sons, 1996.
- Kirkwood, A.C. and C.W. Bullard, "Modeling, Design, and Testing of a Microchannel Split-System Air Conditioner", University of Illinois at Urbana-Champaign, ACRC TR-149, 1999.
- Klein, S.A. and F.L. Alvarado, *Engineering Equation Solver*, Ver 6.036 (software), F-Chart Software, 2000.
- Krakow, K.I., S. Lin and Z.S. Zeng, "Temperature and Humidity Control During Cooling and Dehumidifying by Compressor and Evaporator Blower Speed Variation", *ASHRAE Transactions*, vol. 101, no. 1, pp. 292-304, 1995.
- Lorentzen, G. and J. Pettersen, "A New, Efficient and Environmentally Benign System for Car Air Conditioning", *Int. J. of Refrigeration*, vol. 16, no.1, pp. 4-12, 1993a.
- Lorentzen, G. and J. Pettersen, Roar R. Bang, "Method and Device for High Side Pressure Regulation in Transcritical Vapor Compression Cycle", US Patent 5,245,836, Sept. 21, 1993b.
- Lorentzen, G. and J. Pettersen, "Transcritical Vapor Compression Cycle Device With A Variable High Side Volume Element", US Patent 5,497,631, Mar. 12, 1996.
- McEnaney, R., Y. C. Park, J. M. Yin, C. W. Bullard, P. S. Hrnjak, "Performance of the Prototype of a Transcritical R744 Mobile A/C System", SAE paper 1999-01-0872, 1999

- Neksa, P, F. Dorin, H. Rekestad, A. Bredesen, A. Serbisse, "Development of Semi-Hermetic CO₂ Compressors", IIR Congress, Sydney, Australia, 1999.
- Park, Y. C., J. M. Yin, C. W. Bullard, P. S. Hrnjak, "Experimental and Model Analysis of Control and Operating Parameters of Transcritical CO₂ Mobile A/C System", VTMS, London, May, 1999.
- Pettersen, J., R. Aarliien, P. Neksaa, G. Skaugen and K. Aflekt, "A Comparative Evaluation of CO₂ and R22 Residential Air-Conditioning Systems in a Japanese Climate", IIR/IEA Workshop in CO₂ Technology in Refrigeration, Heat Pumps and Air Conditioning Systems, Trondheim, Norway, 1997.
- Pita, E. G., *Air Conditioning Principles and Systems: An Energy Approach, Second Edition*, John Wiley and Sons, 1989.
- Pitla, S.S., D. M. Robinson, E.A. Groll and S. Ramadhyani, "Heat Transfer from Supercritical Carbon dioxide in Tube Flow: A Critical Review", *International Journal of Heating, Ventilating, Air-Conditioning and Refrigerating Research*, vol. 4, no. 3, pp. 281-302, July, 1998.
- Richter, M.R., S.M. Song, J.M. Yin, M.H. Kim, C.W. Bullard, P.S. Hrnjak, "Transcritical CO₂ Heat Pump for Residential Application", 4th IIR-Gustav Lorentzen Conference on Natural Working Fluids, Purdue University, July, 2000.
- Robinson, D. and E. Groll, "Efficiencies of Transcritical CO₂ Cycles With and Without an Expansion Turbine", *Int. J. of Refrigeration*, vol. 21, no. 7, pp. 577-589, 1998a.
- Robinson, D. and E. Groll, "Heat Transfer Analysis of Air-to-Carbon Dioxide Two-Phase Heat Absorption and Supercritical Heat Rejection", *Int. J. of HVAC&R Research*, vol. 4, no. 4, pp. 327-345, October, 1998b.
- Robinson, D. M. and E. A. Groll, "Theoretical Performance Comparison of CO₂ Transcritical Cycle Technology Versus HCFC-22 Technology for a Military Packaged Air Conditioner Application", *HVAC&R Research*, vol. 6, no. 4, pp. 325-348, October, 2000.
- Song, S., University of Illinois at Urbana-Champaign, ACRC Technical Report (pending), 2001.
- Stott, S., "Experimental Analysis of a Minimum-TEWI Air Conditioner Prototype", University of Illinois at Urbana-Champaign, ACRC CR-21, 1999.
- Threlkel, J.L., *Thermal Environmental Engineering*, Prentice-Hall, 1962.
- Yin, J. M., Y. C. Park, R. P. McEnaney, D. E. Boewe, A. Beaver, C. W. Bullard, P. S. Hrnjak, "Experimental and Model Comparison of Transcritical CO₂ Versus R134a and R410A System Performance", IIR conference Gustav Lorentzen, Oslo, Proceedings, Preprints, pp. 331-340, 1998.
- Yin, J. M., *Private communication regarding RAC2 simulation*, University of Illinois Air Conditioning & Refrigeration Center, 2000.

Appendix A: System Configuration

A.1 R410A A/C & H/P System

A.1.1 R410A system instrumentation

Refrigerant temperatures were measured with Omega inline grounded type ‘T’ thermocouples. Pressure measurements were made with electronic pressure transducers. Refrigerant mass flow rate and density were measured at the condenser outlet with a coriolis mass flow meter. Inline sight glasses were installed upstream of the expansion valve inlet and at the evaporator exit. Instrument locations are shown in Figure A.1.

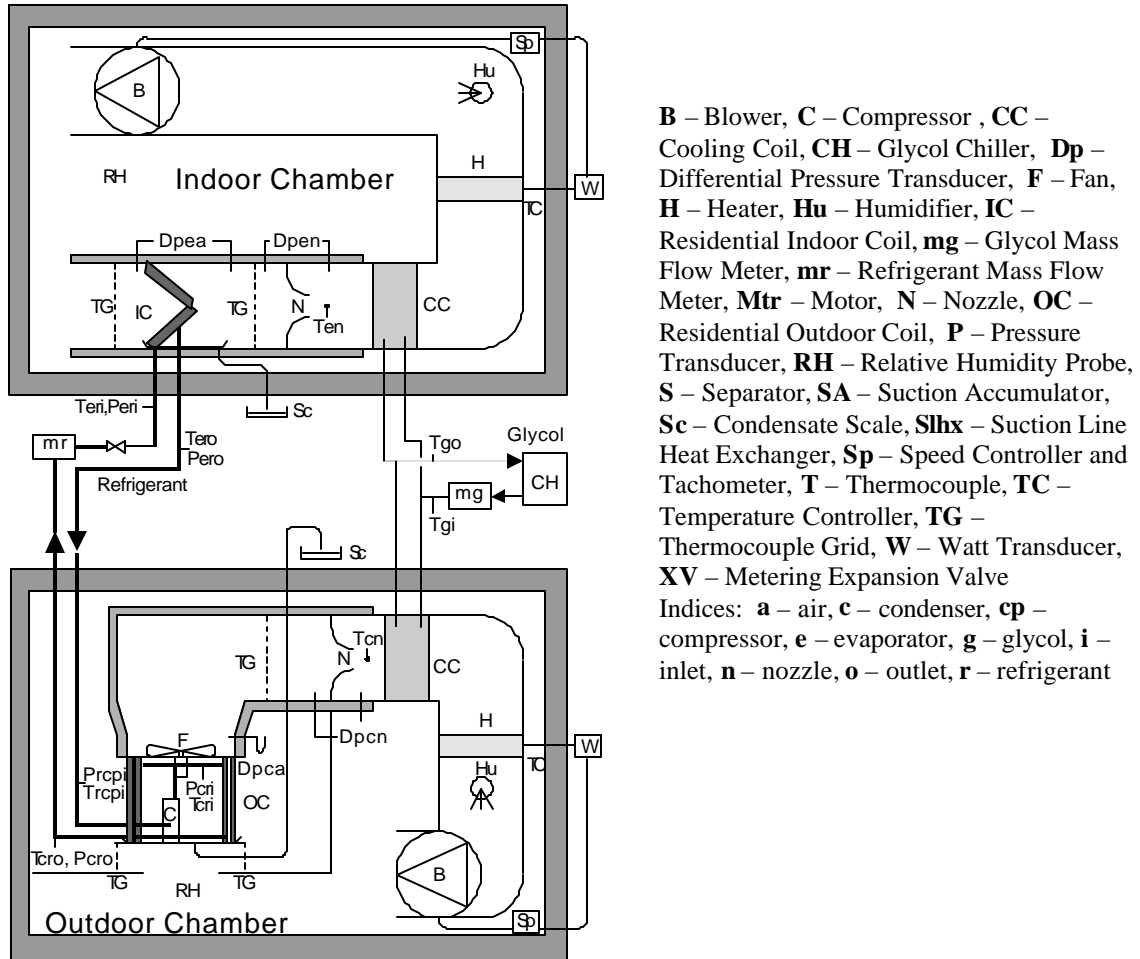
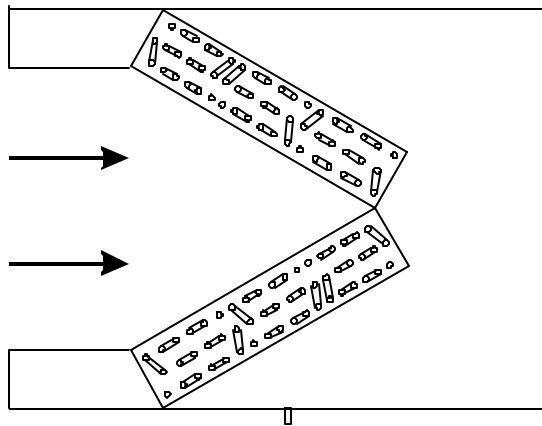


Figure A.1 R410A facility layout showing location of instrumentation

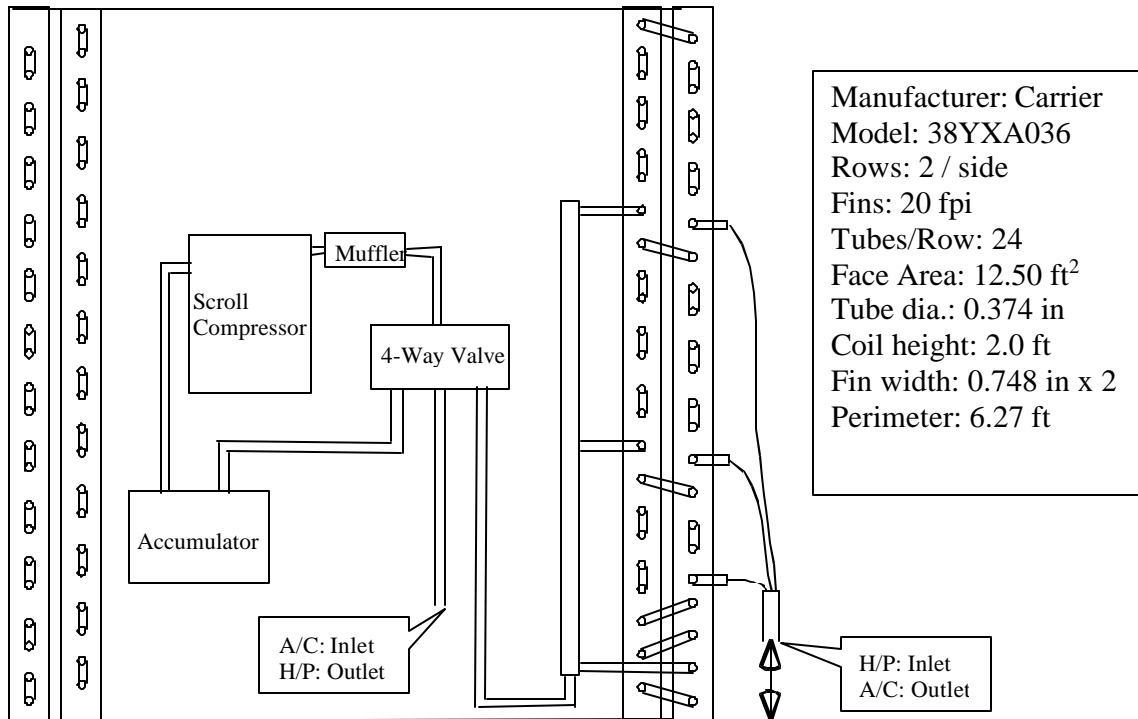
A.1.2 Indoor Coil



Manufacturer: Carrier
 Model: FX4A
 Slope: 30°
 Rows: 3 / Side
 Fins: 15.2 fpi
 Face Area: 4.521 ft²
 Tube Collar Dia: 0.394 in
 Tubes/Row: 18
 Air Flow Rate: 1200 scfm
 Tube Spacing Parallel to Flow: 0.580 in
 Tube Spacing Perp. to Flow: 0.100 in
 Fin Thickness: 0.0045 in
 Fin Height:
 Fin Length:

Figure A.2 Diagram and specifications for the R410A A/C and H/P evaporator coil. This schematic shows the a side view of the evaporator as it is situated in the duct test section B.

A.1.3 Outdoor Coil



Manufacturer: Carrier
 Model: 38YXA036
 Rows: 2 / side
 Fins: 20 fpi
 Tubes/Row: 24
 Face Area: 12.50 ft²
 Tube dia.: 0.374 in
 Coil height: 2.0 ft
 Fin width: 0.748 in x 2
 Perimeter: 6.27 ft

Figure A.3 Diagram and specifications of R410A A/C & H/P outdoor coil and compressor.

A.1.4 Filter Dryer

A Parker Liquid Line Filter Dryer was installed at the exit of the condenser. The filter was included with the Carrier outdoor unit. The model number was 163S.

A.1.5 Mass Flow Meter

The refrigerant mass flow rate was measured with coriolis type mass flow meters manufactured by Micro Motion, model number Elite CMF025.

A.1.6 Compressor

A Copeland scroll type compressor is used with this system. The compressor is located within the outdoor coil, as shown in Figure A.3.

Copeland model # : ZP32K3E – PFV – 230

Copeland serial # : 98F721682

Initial charge: 4.02 kg R410A & POE oil

Power source: 208/230V, single phase, 60Hz

A.1.7 Expansion Valve

The expansion valve for this system was supplied with the indoor unit. It is a short tube orifice type expansion device. The supplied description is: R410A AccuRater® (Bypass Type) Model 70.

A.1.8 Line Sets

9.5 mm o.d. copper tubing was used for the liquid line connection. 19 mm o.d. copper tubing was used for the suction line connection. All joints were brazed with silver solder. The length of both the liquid and suction line sets was 6.7 m. All exposed copper tubing was covered with 9.5 mm thick Armaflex pipe insulation.

A.1.9 Sight Glasses

Inline sight glasses were installed at the condenser exit and evaporator exit in order to be able to visibly check refrigerant conditions. These sight glasses were manufactured by Watsco Components, Inc. and are called Allin™ Liquid Eye Sight Glass. They are an off the shelf product.

A.1.10 Charging Conditions

The system was charged so that the outlet conditions from the indoor coil would match data supplied by the manufacturer for test conditions. At an outlet temperature of 30.3°C the refrigerant pressure was 2475 kPa. These outlet conditions existed for the dry coil test point where the indoor dry bulb temperature was 70°F and an outdoor dry bulb temperature was 47°F.

A.2 R744 RAC1 System Components

A.2.1 System Overview and Schematics of RAC1

A schematic of this system in heat pump mode can be seen in Figure A.4. A description of the RAC1 system in cooling mode is given by Beaver et. al (1999a).

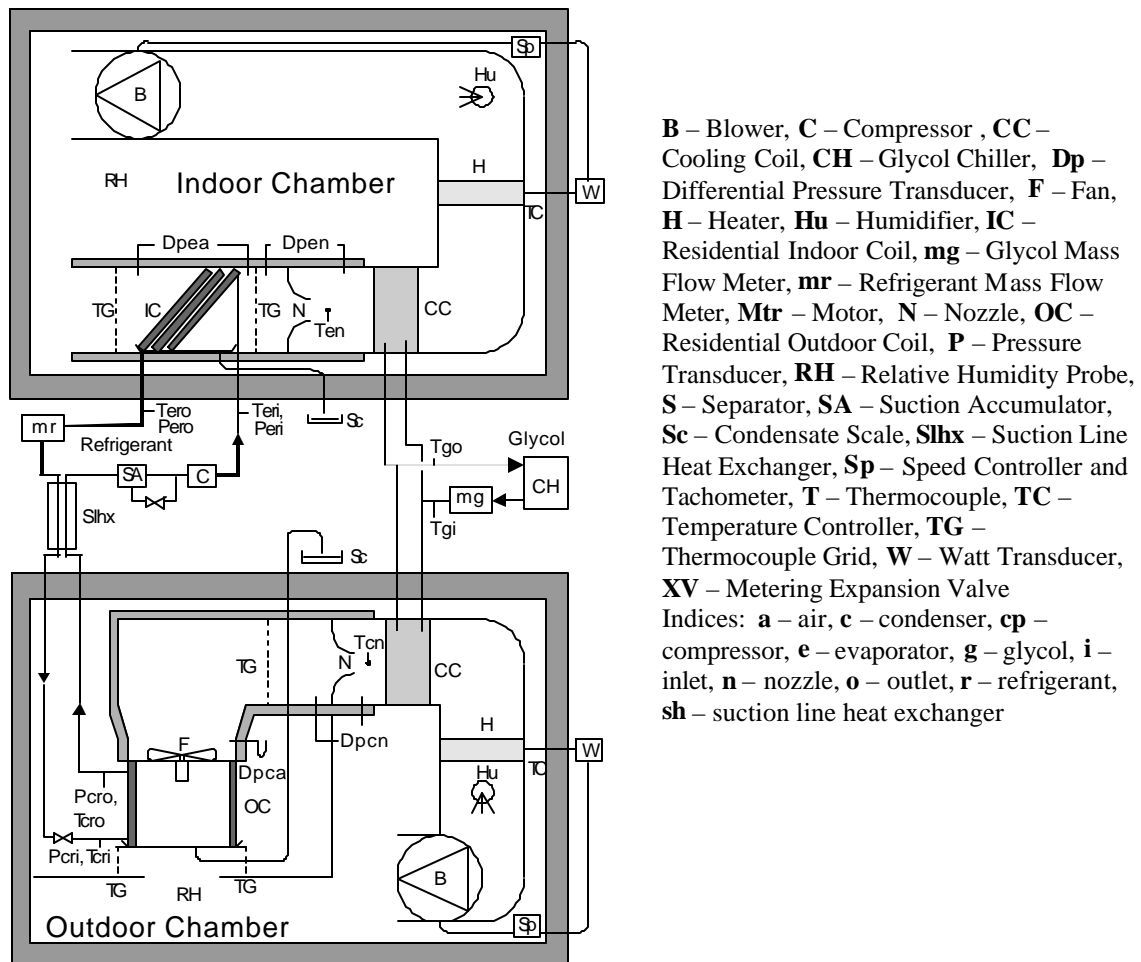


Figure A.4 Schematic of RAC1 CO₂ system

A.2.2 RAC1 Indoor Heat Exchanger

The RAC1 R744 heat exchangers were provided by Hydro Aluminum, sponsor of the project. The design specifications were aimed at matching the geometry of a R410A A/C only system that was tested prior to the A/C/heat pump system used as the baseline. The primary basis for design and comparison is that of an equal core volume. Due to the prescribed thickness of the available microchannel tube, this invariably led to some variations in other heat exchanger parameters. A side by side comparison of some of these parameters can be seen in Table A.1. It is important to note that the R744 heat exchangers were designed around the A/C only R410A system. The heat pump R410A system specifications were released after the R744 heat exchangers had been manufactured.

The R744 heat exchangers incorporate a special header design shown in Figure A.5 that allows for their operation at higher pressures. A schematic of the microchannel tubing can be seen in Figure A.6. The configuration of the heat exchangers in the duct is shown in Figure A.7.

Table A.1 Comparison of indoor heat exchanger specifications.

	R410A –ac only system	R744 (3 slabs combined)	R410 – ac/hp system ("A" coil)
Face area (m ²)	0.32	0.36	0.42
Core volume (m ³)	0.018	0.018	0.024
Core thickness (cm)	5.60	4.95	5.65
Air side area (m ²)	18.6	22.5	27.48
Ref. side area (m ²)	1.0	2.73	1.31
Fin density (fpi)	14.5	17	15.2

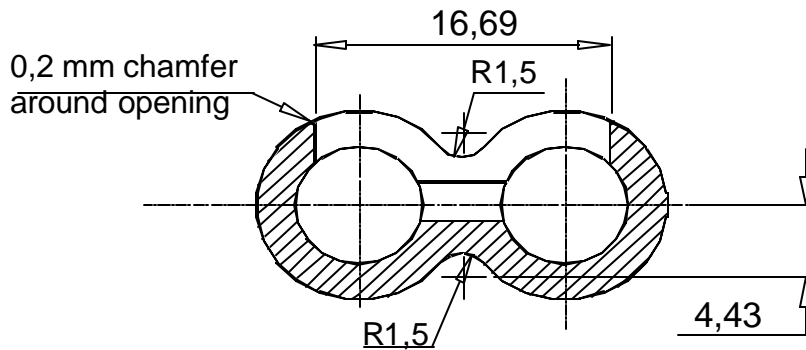


Figure A.5 Cross section of specially designed high pressure R744 heat exchanger header.

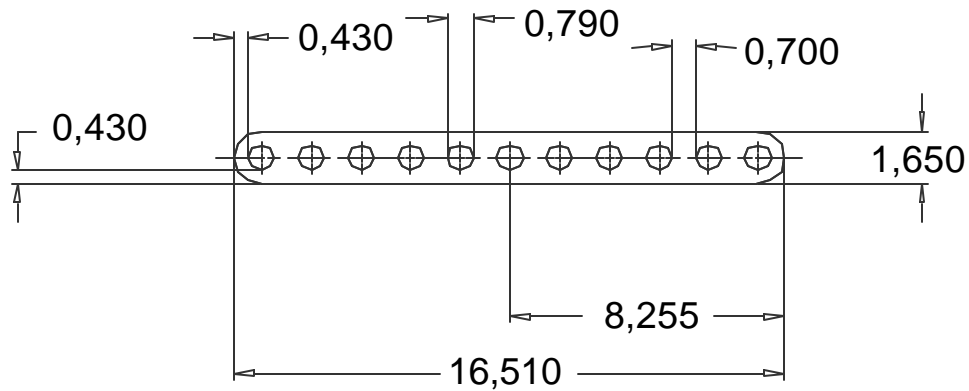


Figure A.6 Cross section of the microchannel tube used in the RAC1 R744 heat exchangers.

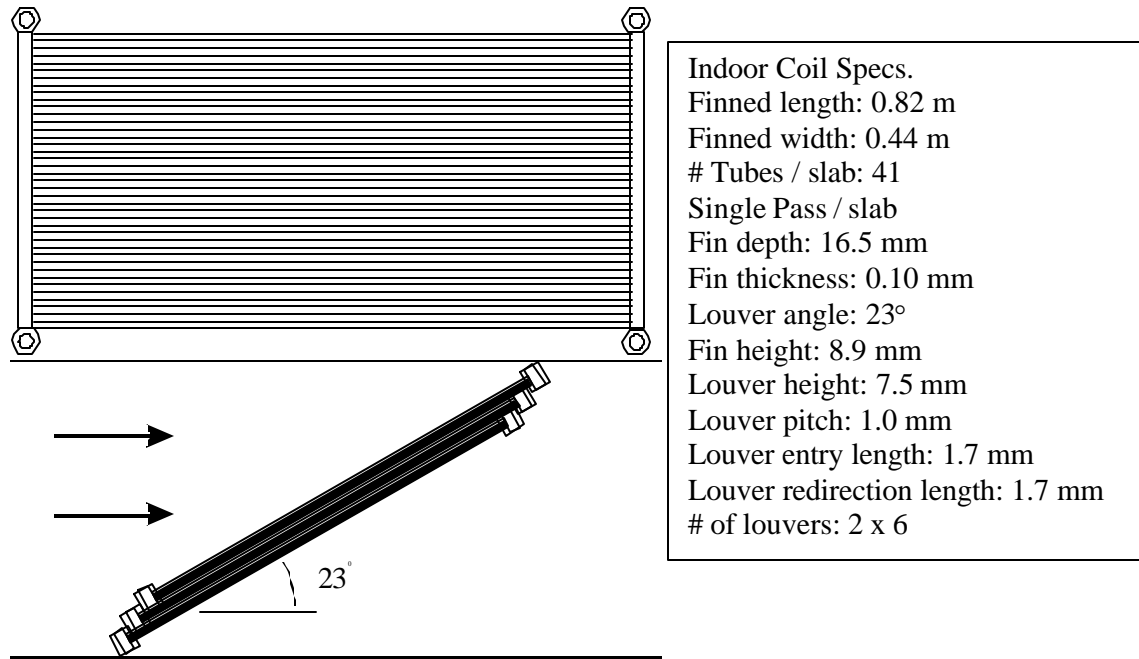
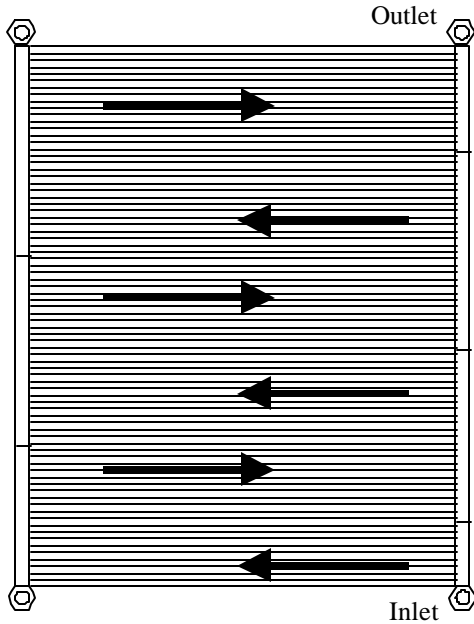


Figure A.7 R744 indoor single pass microchannel heat exchanger slab shown on the top with the arrow showing the direction of refrigerant flow. The bottom schematic shows three single slab evaporators as they are placed in the duct test section.

A.2.3 RAC1 Outdoor Heat Exchanger

In order to simulate the U-shaped heat exchanger of the R410A system, three flat microchannel heat exchangers are connected in parallel and placed together to form three sides of a box. The backside of this set of heat exchangers is covered with plywood. The same fan that was used with the R410A outdoor unit was also mounted to the top of this set of heat exchangers.

The heat exchanger slabs for the outdoor coil are comprised of the same microchannel tube and header parts that made up the indoor heat exchanger slabs (see Figures A.5 and A.6). Each heat exchanger slab uses 80 total microchannel rows over 6 passes. More detailed specifications and a schematic of one of these slabs can be seen in Figure A.8. A comparison of the key parameters between the baseline and R744 system is shown in Table A.2.



Outdoor Coil Specs.
 Finned length: 0.626 m
 Finned height: 0.850 m
 # Tubes / slab: 80
 Six Passes / slab
 #Tubes / pass : 16/15/14/14/11/10
 Fin depth: 16.5 mm
 Fin thickness: 0.10 mm
 Louver angle: 23°
 Fin height: 8.9 mm
 Louver height: 7.5 mm
 Louver pitch: 1.0 mm
 Louver entry length: 1.7 mm
 Louver redirection length: 1.7 mm
 # of louvers: 2 x 6

Figure A.8 R744 outdoor six pass microchannel heat exchanger slab.

Table A.2 Comparison of outdoor coil specifications for the three tested systems.

	R410A –A/C only system	R744 (3 slabs combined)	R410A – A/C & H/P system
Face area (m ²)	1.43	1.60	1.16
Core volume (m ³)	0.026	0.026	0.043
Core thickness (cm)	1.85	1.65	3.70
Air side area (m ²)	54.1	50.4	66.9
Ref. side area (m ²)	1.5	4.1	3.38
Fin pitch (fins / in.)	24	23	20

A.2.4 Compressor and Compressor Motor

A 3 kW Dorin CO₂ compressor is used with this system. The compressor is located outside of the environmental chambers, as shown in Figure A.4.

- Dorin model # : CD4.0275
- Dorin serial # : 99061057D
- Displacement: 2.7 m³/h at 1450 rpm
- Oil: Mobil EAL POE-100-KG 1.8
- Power source: 380V, three phase, 50Hz

A.2.5 Line Sets

On the high-pressure side, 9.5 mm o.d. copper tubing was used for all connecting lines. The inside diameter was 6.4 mm. All connections used two ferrule compression fittings and the total length of copper pipe from the compressor exit to the evaporator inlet was 10.4 m. On the low-pressure side, 15.9 mm o.d. soft copper tubing was used for all connecting lines. The inside diameter was 12.7 mm, and the total length was 9.5 m from the evaporator exit to the compressor inlet.

A.2.6 Sight Glasses

Special high pressure sight glasses were used in the R744 system. They were made by PresSure® Products and called Bull's-Eye See-Thru sight glasses. The standard model was used for locations between the expansion device and the compressor inlet. This model had a maximum operating pressure of 6.9 MPa. A heavy duty model was also specially manufactured for the high-side locations. These sight glasses had a maximum operating pressure of 20.7 MPa. A picture of one of the sight glasses can be seen in Figure A.9.

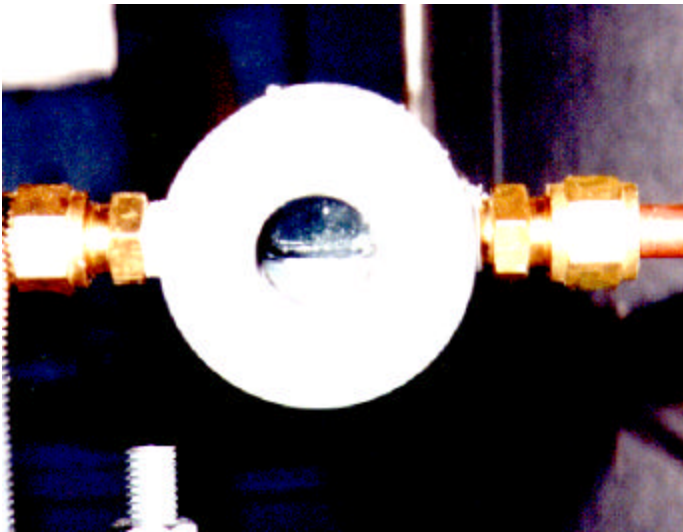


Figure A.9 R744 sight glass. Note the presence of liquid R744 at the bottom of the viewing area.

A.2.7 Suction Accumulator

A special high-pressure suction accumulator was designed by PresSure® Products for use in the R744 system. A picture of this accumulator can be seen in Figure A.10. The maximum rated operating pressure for this unit was 6.9 MPa. It was designed with a sight glass running the height of the unit on both the front and rear of the device. An additional round sight glass was located on the bottom of the unit. The presence of these sight glasses allowed for the monitoring of the levels of oil, liquid CO₂, and vapor CO₂ within the accumulator chamber. The accumulator had one inlet and two exits. The inlet was designed to prevent the fast moving entering mixture from disturbing the liquid and oil layers as much as possible. One exit was located at the top of the chamber and was used to remove refrigerant vapor. The other exit is located at the bottom of the chamber and is used to remove both oil and liquid CO₂.

A.2.8 Suction Accumulator Oil-Bleed Valve

To control the relative return of oil (and some associated refrigerant) the compressor, a valve controls the liquid line exiting the suction accumulator. By opening the valve the amount of liquid returning to the compressor is increased and the exit quality from the evaporator decreased. The valve used is a 316 stainless steel rising plug valve manufactured by Whitey, part number SS-5PDF8. The maximum working pressure for the valve is 6000 psi.

A.2.9 Expansion Valve

A manual expansion valve was used for all R744 systems. They are supplied by Hoke® and are called Bar Stock Metering Valves, model number 2311F4B. They are supplied with a micrometer vernier handle and have a maximum operating pressure of 20.7 MPa.

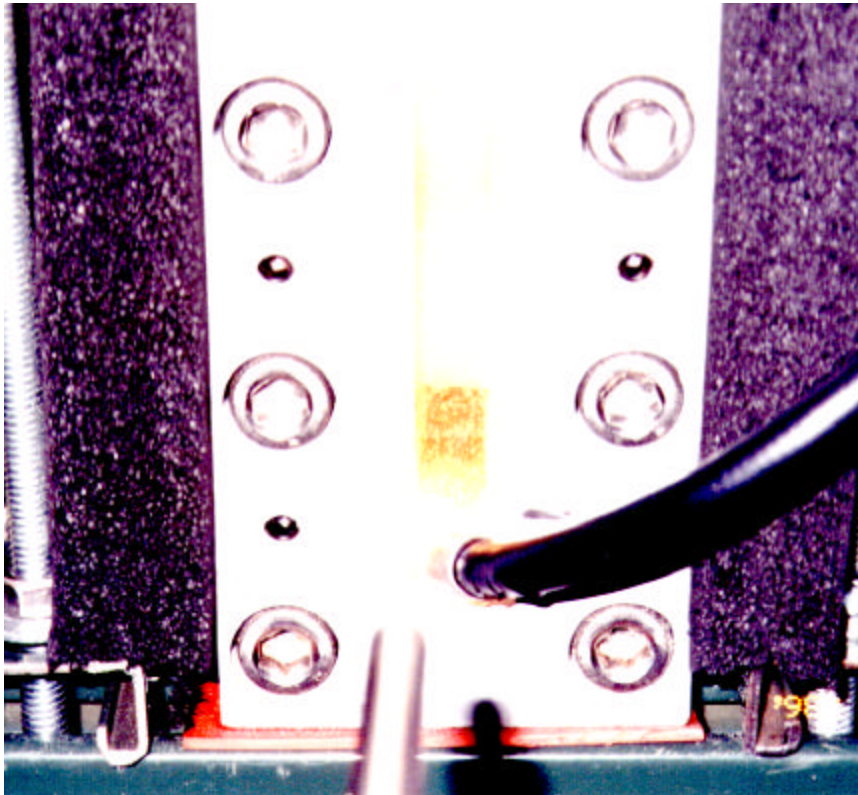


Figure A.10 The R744 suction accumulator. The black tube pointed at the bottom of the viewing area is actually a fiber optic light source used to improve visibility

A.2.10 Charging Conditions

The R744 system was charged with an amount of dry CO₂ sufficient to keep a visible level of liquid refrigerant in the suction accumulator. The level would be allowed to fluctuate as testing condition changed, but refrigerant would be added if the accumulator chamber completely emptied and refrigerant would be removed if the refrigerant level rose above the level of the inlet pipe.

Appendix B: Effect of Suction Accumulator Configuration/Indoor Heat Exchanger Orientation on RAC1 R744 Heat Pump Performance

B.1 System configuration

It is likely that the full benefit of the suction accumulator and suction line heat exchanger in the R744 heat pump system was not realized in the experimental comparison of R744 and R410A. This can be attributed to the placement of the suction line/vapor line intersection after the suction accumulator below the liquid level in the suction accumulator, as shown in Figure B.1. As a result, the intersection of the vapor and liquid lines may have been flooded, neutralizing the effect of the suction accumulator and allowing refrigerant with a low exit quality to pass into the internal heat exchanger. Further testing (after raising the intersection above the liquid level) suggested that better control over the exit quality from the evaporator may result in a 5-10% improvement in system efficiency at the ARI rating condition, matching and slightly surpassing the efficiency of R410 for matched heating capacity.

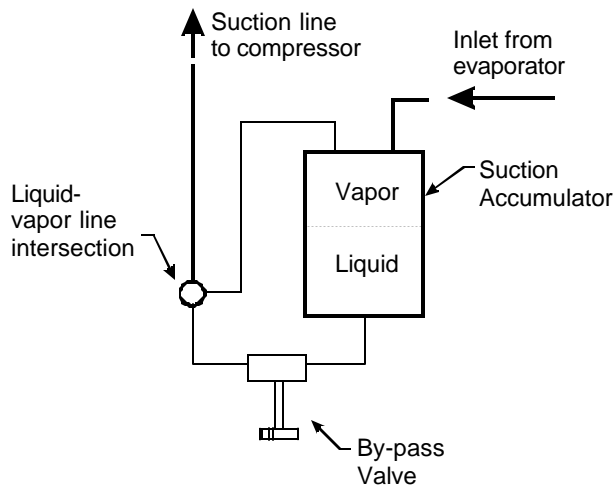


Figure B.1 Arrangement of suction accumulator for R744 RAC1 comparison with R410A: liquid-vapor lines intersect below level in accumulator

A study by Song et al. (2001) showed that the angle of attack of the indoor coil has little effect on the heat transfer performance of the coil, but has considerable effect on the air pressure drop over the coil. As a result, placing the indoor coil perpendicular to the airflow has the potential of reducing the fan power required by the system while not affecting the capacity of the coil. Based on these results, the R744 indoor coil was rotated 90° and placed perpendicular to the airflow. Subsequent testing showed as much as a 10% improvement in the efficiency of the system, with the efficiency calculated independent of the fan power. This was an unexpected result, as, based on Kim's work, orientation of the coil should not have influenced the capacity of the coil.

Further testing of the system indicated that the improved results were dependent on the charging conditions of the system. The presence of the suction accumulator should reduce performance dependence on charging, which indicates that the suction accumulator was not functioning properly.

The following results compare the original R744 data which was used in the comparison with R410A with later results with the indoor coil vertical both with the suction accumulator the same as it was during the R410A

comparison and reconfigured to eliminate the gas-vapor line flooding. All of the following results are for the ARI 21°C/8.3°C indoor/outdoor heat pump rating condition.

B.2 Experimental Results

Figure B.2 shows a comparison of the capacity and heating COP of the R744 system for the R744/R410A comparison and the vertical indoor coil with the suction accumulator adjusted and unadjusted. The capacity shown in Figure B.2 is based on the indoor chamber energy balance, which is believed to be the most accurate balance (during the experiments with the vertical coil runs the glycol energy balance agreed with the electrical input to the chamber within 1.5%). The capacity of the re-orientated coil/no suction accumulator adjustment is about 5% higher than the other two cases, while the efficiency of both the re-orientated cases is between 5 and 10% higher than the R744/R410A comparison results. From Figure B.3, which shows the compressor work for each of the points plotted in Figure B.2, it is evident that higher efficiency for the re-orientated coil/no suction accumulator adjustment is primarily from the increased capacity. The improvement for the re-orientated/suction accumulator adjusted case is primarily the result of a decrease in the compressor power.

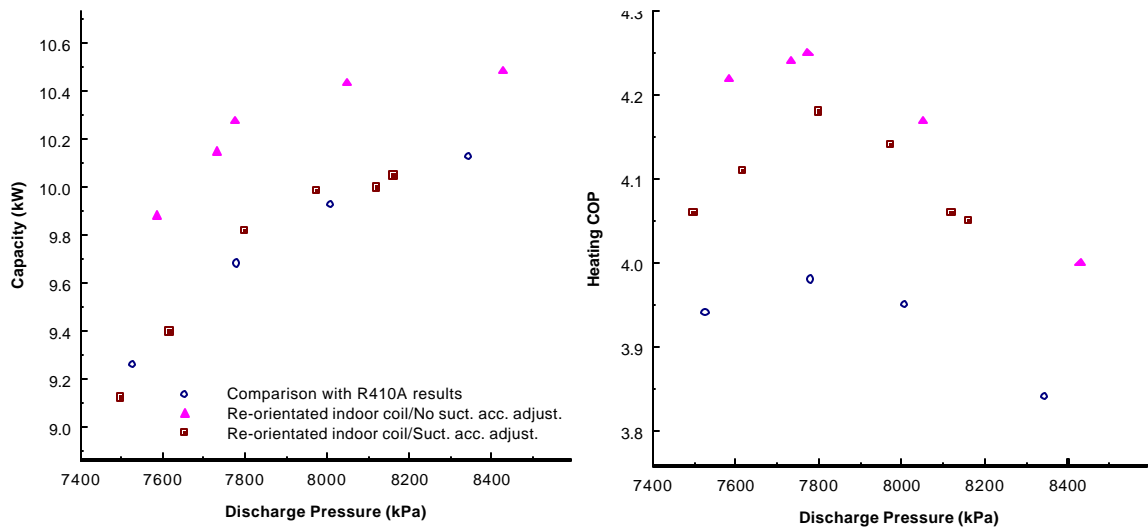


Figure B.2 Comparison of capacity and efficiency with re-orientation of indoor coil and adjustment of suction accumulator

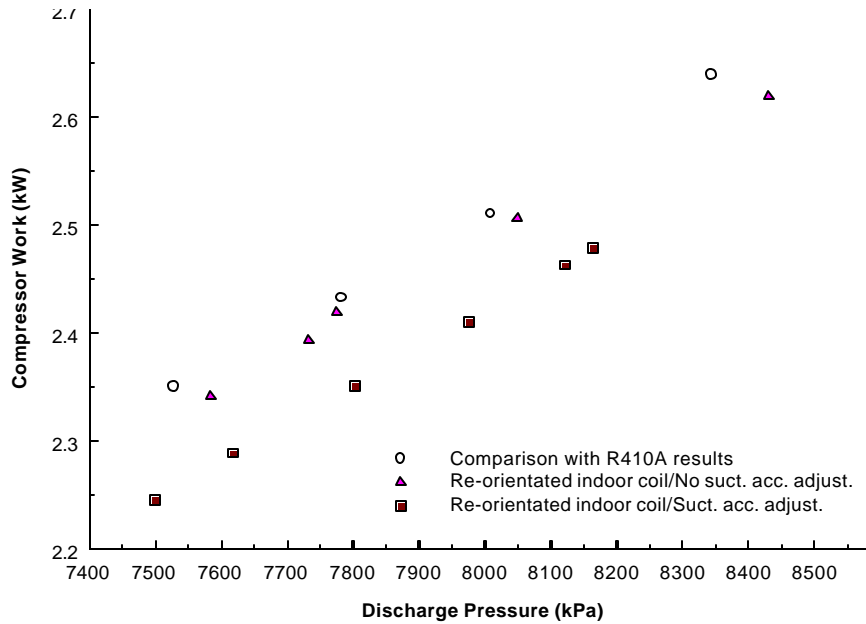


Figure B.3 Compressor power for capacity/efficiency results

Because of the timing of the tests and the configuration of the system and chambers, the results compared with R410A were run with dry outdoor coils while condensate may have been present on the outdoor coil during the re-orientated coil tests. However, this does not appear to have influenced the evaporating temperature in the outdoor coil as shown in Figure B.4. Since the outdoor coil in the R744 system is fed by three manual expansion valves (Appendix A), it was not possible to keep the outdoor chamber sealed during testing. As a result, each time the valves were adjusted air from the room would leak into the chamber. The R744/R410A tests were run in March when this air was relatively dry, as compared to the re-orientated coil tests that were run in June and July. Since the source of the condensate on the outdoor coil was from intermittent leakage of room air and the evaporating temperatures are comparable, it is not believed that the difference between a wet and dry outdoor coil explains the improved capacity seen in the re-orientated coil results. Difficulty in exactly duplicating the dry testing conditions, however, was one consideration in not re-running the full R410A comparison test matrix.

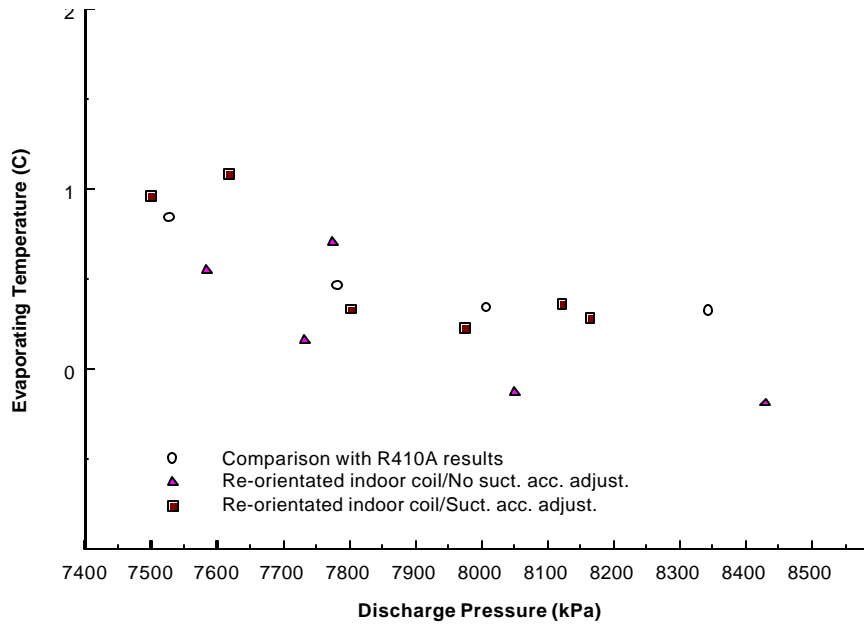


Figure B.4 Evaporating temperature (at inlet to evaporator)

To get an idea of the effectiveness of the suction accumulator, we can look at the estimated ratio of heat transfer in the suction line heat exchanger from the high pressure side to the low pressure side. Since the refrigerant on the low-pressure side is assumed to be vapor, a change of phase of liquid in the suction line heat exchanger will reduce the calculated heat transfer and result in a ratio greater than one. Figure B.5 shows the ratio of high-pressure side to low-pressure side heat transfer in the suction accumulator. The results from the re-orientated/no suction accumulator adjustment are very close to one indicating that very little phase change occurred within the suction line heat exchanger and that the system was optimally charged. Except for the lowest and highest discharge pressure points in the re-orientated/suction accumulator adjusted data, which were both taken after additional charge was added to the system, there appears to be slightly less of a dependence on the discharge pressure as compared to the results compared with R410A. This indicates that the exit quality from the suction accumulator is more consistent since the vapor line/liquid line intersection was relocated. Also, to note, during the re-orientated coil/suction accumulator adjusted testing, to prevent surging (spikes in the refrigerant mass flow rate), the suction accumulator bypass valve (Appendix A, section 2.8) was open $\frac{1}{4}$ of a turn more than in previous tests. This valve may not have been adjusted optimally during these runs. For reference, in earlier tests the valve was open $\frac{1}{8}$ of a turn from fully closed.

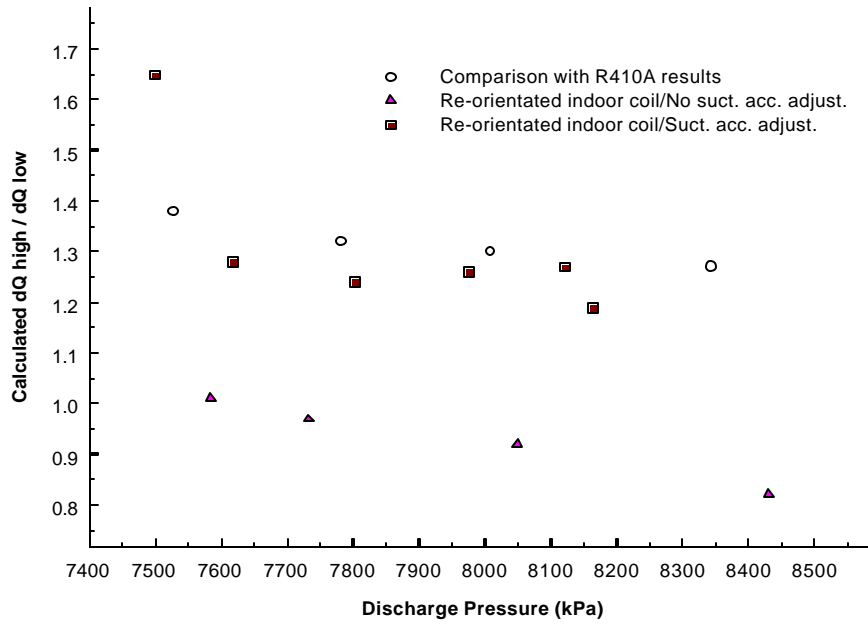


Figure B.5 Ratio of calculated heat transfer in internal heat exchanger from high pressure side to low pressure side assuming no phase change

B.3 Conclusion

To summarize, there is reason to believe that the R744 system in the R744/R410A comparison may not have had full benefit from the suction accumulator because of the installation of the suction accumulator. Further tests suggest that this may have reduced the efficiency of the R744 system by about 5-10%.

Appendix C: Indoor Chamber Energy Balance

C.1 Determination of specific heat constants

The data reduction programs determine the change in enthalpy of the glycol cooling loop based on the inlet and exit temperatures of the glycol and the integral of the linear relationship between temperature and specific heat, as given by:

$$\Delta Q_{glycol} = \dot{m}_{glycol} \left(A \cdot (T_{out} - T_{in}) + \frac{B}{2} \cdot (T_{out}^2 - T_{in}^2) \right) \quad (C.1)$$

The constants A and B for this equation are determined based on a linear fit of specific heat values calculated over an appropriate range of temperatures for a given concentration. The *Fluidfile* software from Dow Chemical (installed on the data acquisition PC in MEL 361) will calculate the concentration of a glycol solution given a temperature and density, and can calculate the specific heat of a solution given the concentration.

The concentration of the glycol can be determined from either the density measured by the Micromotion flow meter and thermocouples in the loop or from a sample using a thermometer and hydrometer (both methods can be used in combination to ensure accuracy). With these values, the concentration of the solution can be calculated from *Fluidfile*. Once the concentration is known, a series of temperature and specific heat values can be generated using *Fluidfile* and a linear fit can be determined.

C.2 Testing and results

Table C.1 shows the results of chamber heat balance tests run to check the accuracy of the glycol energy balance results from the R410A baseline heat pump data taken during the last week of November, 1999. In that data, the chamber energy balance had a consistently higher capacity at the test points than the capacity calculated by other means. The mass flow rates and temperature ranges of the original data are included for comparison with the test points.

The tests consisted of running just the glycol loop, blower and heater (to maintain a chamber temperature of 70°F—the same temperature as for the R410A data) and calculating the energy balance based ON the heat input of the blower and heater and the heat removal by the glycol loop. The tests were conducted on three different days (11/30/99, 12/6/99 and 12/12/99) at three different flow rates and temperature inlets. In order to eliminate errors due to infiltration, for the first test on 12/12/99 the feed through for the instrumentation wires was blocked and for the second test, in addition to blocking the feed through, the edges of the removable door were taped.

Table C.1 Summary of energy balance results

Original Heat Pump Tests:

	17701112rpm.xls	17701200rpm.xls	35701200rpm.xls	47701096rpm.xls	47701200rpm.xls	62701200rpm.xls
Mgi	730	734	745.5	746.9	749.5	752.5
Tegi	1.775	2.54	4.38	4.94	5.29	5.29
Tego	7.827	8.699	10.73	11.41	11.81	11.81

Calculated with A=3.45, B=0.002956

	Heat Bal I (11/30)	Heat Bal II (11/30)	Heat Bal I (12/6)	Heat Bal II (12/6)	Heat Bal I (12/12)	Heat Bal II (12/12)
Mgi	258.2	288.6	368.6	366.8	368.2	368.6
Tegi	11.67	12.72	5.273	4.56	2.2	2.17
Tego	15.61	15.85	11.55	11.08	9.6	9.6
Qglycol (W)	3546	3161	8035	8313	9439	9432
We-Qetr (W)	3434	3052	7602	7904	8905	8882
Difference (W)	112	109	433	409	534	550
Diff/Qglycol	3.16%	3.45%	5.39%	4.92%	5.66%	5.83%

With Revised Cp Values for Glycol: A=3.1618, B=0.003967

Mgi	258.2	288.6	368.6	366.8	368.2	368.6
Tegi	11.67	12.72	5.273	4.56	2.2	2.17
Tego	15.61	15.85	11.55	11.08	9.6	9.6
Qglycol (W)	3267	2914	7388	7642	8670	8664
We-Qetr (W)	3434	3052	7602	7904	8905	8882
Difference (W)	-167	-138	-214	-262	-235	-218
Diff/Qglycol	-5.11%	-4.74%	-2.90%	-3.43%	-2.71%	-2.52%

The first set of results is the energy balance calculated using the same constant values for the determination of the specific heat as were used in the R410A data. Following the tests, the concentration of the glycol was determined by measuring the specific gravity of the solution with a hydrometer and the constants for the specific heat calculation were recalculated based on those results, summarized in Table C.1. The second set of results presents the energy balance using the revised constants for the specific heat.

The data shows a large shift (approx. 0.8 kW at high flow rates) in the calculated energy removal rate of the glycol based on the revised values for The specific heat. This reduces the calculated amount of heat that is removed by the glycol. In the original R410A data, this would bring the capacity results from the glycol energy balance more in line with the capacity calculated by other methods. At higher flow rates and lower inlet/outlet temperatures, the difference between the heat input and removal to the system is smaller (as a percentage) than at the lower flow rates—a switch from the results calculated using the original constants for the glycol specific heat calculation.

C.3 Error analysis:

For the baseline R410A data from the Carrier system, the calculated precision of the chamber calorimeter balance was calculated to be ± 470 W, determined as follows.

The theoretical uncertainty in the specific heat is based on the uncertainty in the concentration. The uncertainty in the concentration (C) is a function of the uncertainty in the temperature (T) and density (ρ) measurements and can be estimated can be estimated from (Coleman et al., 1989):

$$\left(\frac{P_C}{C}\right)^2 = \left(\frac{1}{C} \frac{\partial C}{\partial T} P_T\right)^2 + \left(\frac{1}{C} \frac{\partial C}{\partial \rho} P_\rho\right)^2 \quad (C.2)$$

Where P_T , P_C , P_F are the uncertainties associated with the temperature, concentration and density, respectively. The values for the precision of the measurement were taken to be $\pm 1^\circ\text{C}$ for the thermocouple and 0.5 kg/m^3 for the density (manufacturers spec). Since the function relating temperature and density to concentration is unknown, the partial derivatives are calculated by fitting a line to a set of values which are obtained by holding one variable constant while determining the concentration as the other variable takes on values over a range. Plots illustrating this are shown in Figures C.1 and C.2. The slope of the best fit line was taken to be the partial derivatives in Equation C.1. From this calculation the uncertainty in the concentration of the glycol solution is calculated to be 0.5%.

The effect of uncertainty in the concentration on the uncertainty in the specific heat over a range of temperatures was calculated two ways. The first paralleled the method used to determine the uncertainty in the concentration: computing a partial derivative of specific heat with respect to concentration off the slope of a line of best fit and multiplying this times the precision of the concentration. The plot used to determine the value for the partial derivative is shown in Figure C.3. The resulting uncertainty in the specific heat, ultimately based on the uncertainty in the temperature and density measurements is calculated to be $\pm 0.01 \text{ kJ/kg K}$. To verify this value, the specific heat corresponding to $+0.5\%$ and -0.5% of the estimated concentration was evaluated over a range of temperature (-20°C to $+20^\circ\text{C}$). The difference between the values which (varied by 1%) was 0.02 kJ/kg K which verifies the results from the first approach.

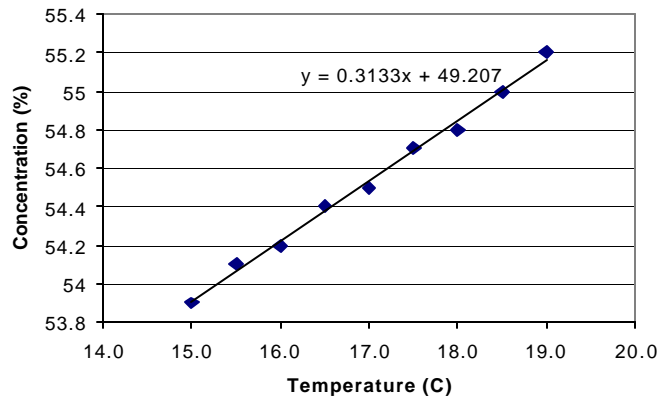


Figure C.1 Calculated concentration dependence on temperature with fixed density

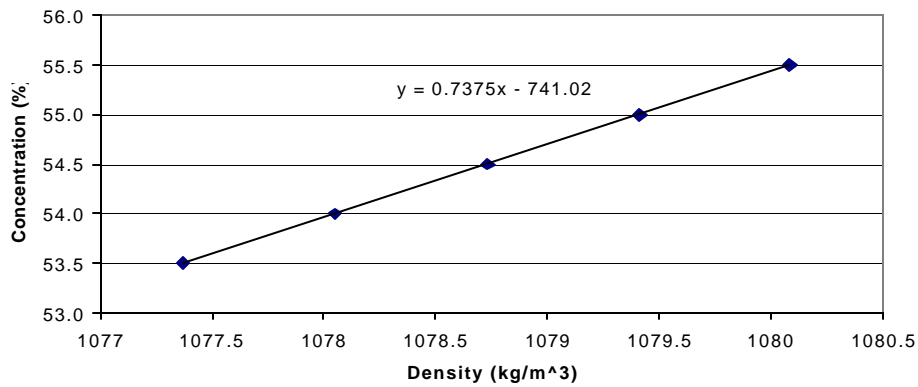


Figure C.2 Calculated concentration dependence on density with fixed temperature

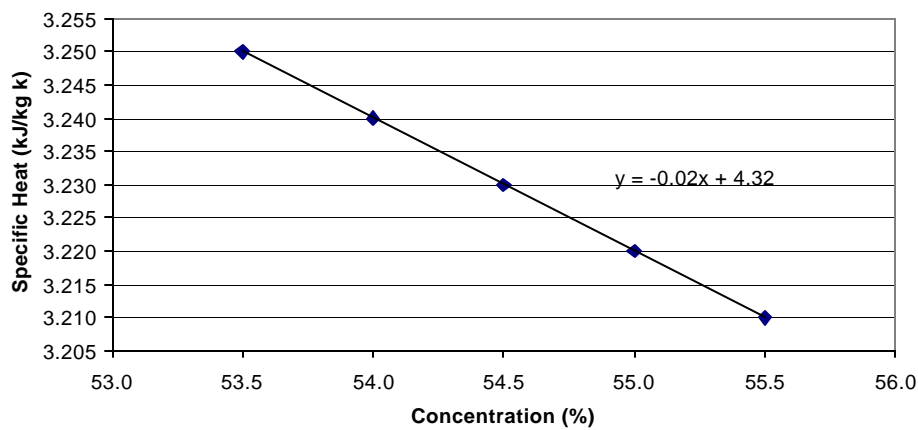


Figure C.3 Calculated specific heat dependence on concentration

For glycol, the dependence of specific heat on temperature is a linear relationship. In order to calculate the heat removal rate by the glycol in the data reduction, an inlet and exit enthalpy is determined by integrating this line. Therefore, the uncertainty in the heat removal rate is a function of the uncertainty of the linear relationship between temperature and specific heat. This relationship is determined by fitting a line to a group of specific heats calculated for different temperatures of a fixed concentration in *FluidFile*. As a result, the uncertainty of the heat removal rate is a function of the uncertainty in the slope and intercept values determined by the best fit of this line. Because a change in concentration primarily shift the line up or down rather than changing the slope, it is assumed that the uncertainty in the intercept is equal to the uncertainty in specific heat, which results from the uncertainty in the concentration. As a result the uncertainty in the coefficients from the best fit line are equal to ± 0.01 kJ/kg K on the intercept (A), and to the statistical uncertainty of the slope of the line of best fit for the slope (B).

With the uncertainties in the constants A and B determined, as before the propagation of error in the heat removal rate is calculated by:

$$\left(\frac{P_{\Delta Q}}{\Delta Q}\right)^2 = \left(\frac{1}{\Delta Q} \frac{\partial \Delta Q}{\partial \dot{m}} P_m\right)^2 + \left(\frac{1}{\Delta Q} \frac{\partial \Delta Q}{\partial A} P_A\right)^2 + \left(\frac{1}{\Delta Q} \frac{\partial \Delta Q}{\partial B} P_B\right)^2 + \left(\frac{1}{\Delta Q} \frac{\partial \Delta Q}{\partial T_{out}} P_{T_{out}}\right)^2 + \left(\frac{1}{\Delta Q} \frac{\partial \Delta Q}{\partial T_{in}} P_{T_{in}}\right)^2 \quad (C.3)$$

To gauge the relative importance of each term above, the relative contribution for each term in Equation C.3 is listed in Table C.2 for the R410A baseline rating condition results. From the results in Table C.2 it is evident that the error in the glycol calculation is almost entirely dependent on the uncertainty in the thermocouple readings, and that the contribution from the uncertainty in the calculated constants for specific heat is relatively minor.

Table C.2 Relative contribution to overall error from each source for the R410A baseline rating condition (8.3°C outdoor/21.1°C indoor)

Source	Uncertainty	Contribution
Mass flow meter (P_m)	$\pm 0.12\%$ of reading	0.31%
Intercept of Spec Heat (P_A)	± 0.01 kJ/kg K	2.1%
Slope of Spec Heat (P_B)	$\pm 9.42 \times 10^{-6}$	-----
Temperature ($P_{T_{out}}$ & $P_{T_{in}}$)	$\pm 0.1^\circ\text{C}$	97.6%

Appendix D: Vapor Compression Cycle Control/Distribution

D.1 Low pressure receiver in subcritical / transcritical cycle

The objective of the low-pressure receiver, illustrated in Figure D.1, is to separate liquid from vapor sending only vapor to the compressor, and to provide a reservoir of refrigerant to accommodate changing operating conditions and system leakage over time. The thermodynamic cycle for a system with a low-pressure receiver is the same in subcritical and transcritical cycles.

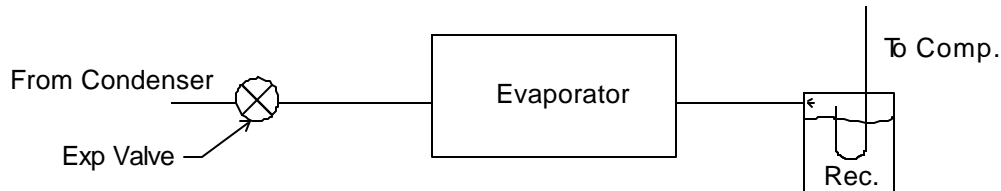


Figure D.1 Low pressure receiver

In the ideal cycle, only vapor exits the receiver. As a result, if refrigerant entering the receiver has a quality less than one, the liquid content of the refrigerant will remain in the receiver and only the vapor will pass. This will reduce the charge of refrigerant in the system. For the same heat transfer in the evaporator, the lower mass flow will exit with a higher quality until at steady state the quality of the refrigerant entering the receiver (exiting the evaporator) will be one. Similarly, if the refrigerant entering the receiver is superheated, the temperature and pressure of the refrigerant reservoir will rise. This will increase the amount of charge in the system, reducing the superheat of the refrigerant until at steady state the entering quality is one. In this way the low-pressure receiver modulates the mass flow of refrigerant through the system so that the quality of refrigerant entering the receiver is one.

In a real cycle, a controlled amount of liquid needs to be allowed past the receiver to ensure lubricant return—this is typically done by placing a small hole in the bottom of the “j” on the compressor suction line.

In the transcritical cycle, increasing the discharge pressure while maintaining a constant gas cooler outlet temperature until the effect of additional work required by the compressor offsets that of the additional refrigerating effect can increase COP. This is in contrast to the subcritical cycle in which COP is maximized at the lowest compressor discharge pressure. Control of high side pressure in the transcritical cycle with the expansion device was patented by Sinvent (Lorentzen et al., 1993), and, although not required, the “preferred embodiment” in the patent features a low side receiver. With a low-pressure receiver, maximum cycle efficiency can be accomplished by controlling one valve, the expansion valve, which sets the high side pressure.

Stating that low side receiver/expansion valve control is effective only in systems from 2-10 kW, Mercedes-Benz patented transcritical system control based on varying the capacity of the compressor (Abersfelder et al., 1997). Varying the compressor capacity allows for the capacity of the cycle to be efficiently maintained over a wider range of system capacities. If maximum efficiency is to be achieved over all conditions, then a controllable expansion device as described by in the Sinvent patent needs to be incorporated into the variable compressor cycle

as well. Again, although not required, Abersfelder sites the same benefits of using a low pressure receiver as Lorentzen and incorporates one into the system.

D.2 High Pressure Receiver

D.2.1 Subcritical Cycle

The high pressure receiver in subcritical systems plays a role similar to the low pressure receiver, shown in Figure D.2. The objectives of the high pressure receiver are to fix the exit quality of the refrigerant exiting the condenser, to separate the liquid and vapor sending only liquid to the expansion valve, and to provide a reservoir of refrigerant for changing operating conditions and system leakage over time.

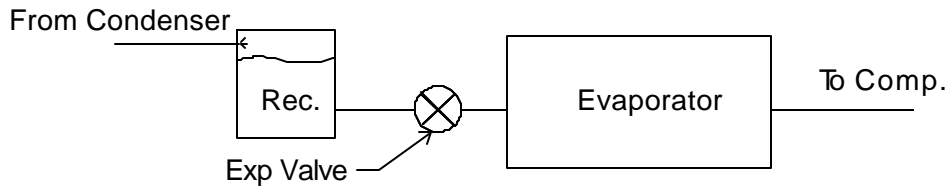


Figure D.2 High pressure receiver

With the high-pressure receiver, the vapor above the refrigerant reservoir determines the condensing pressure. If the refrigerant exiting the condenser has a quality greater than zero, then the excess vapor (since only liquid is removed from the receiver) will drive the pressure inside the receiver up which will increase the condensing pressure and temperature. The increased condenser temperature results in higher heat transfer inside the condenser, which will move the quality of the exiting refrigerant to zero. If the refrigerant exiting the condenser is subcooled, the refrigerant stream will cool the reservoir dropping the condenser pressure and temperature. The decreased temperature of the condenser will decrease the heat transfer rate, eliminating the subcooling.

A comparison of the effect of a high and low pressure receiver on an ideal subcritical R410 cycle are shown in Figure D.3. This plot shows the efficiency and refrigerant mass flow rate for an ideal cycle operating at an evaporation temperature of 8°C. The exit from the condenser for the high pressure receiver case is of quality zero and at the saturation temperature; for the low pressure receiver, the refrigerant exit temperature from the condenser is 21°C, typical of heat pump operation. Significant subcooling occurs in the low pressure receiver case. With a high pressure receiver, as the discharge pressure increases the refrigerant mass flow required to maintain the same system capacity increases. This results from the fact that the line of constant entropy is steeper than the line of zero quality on an R410A property plot. As a result, if the exit from the condenser is fixed at quality one by a high side receiver, the enthalpy difference between compressor exit and condenser exit decreases at higher discharge pressure. The net effect is reduced ideal cycle performance as compared to an ideal system operating with a low pressure receiver.

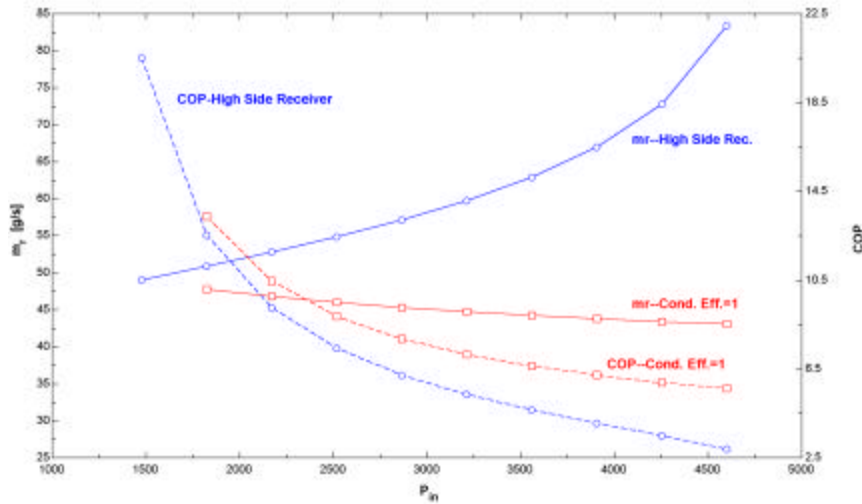


Figure D.3 Comparison of effect of high and low pressure receiver on ideal R410A subcritical cycle

D.2.2 Transcritical cycle

In the transcritical cycle, there can be no separation of liquid and vapor at the exit of the gas cooler, as the supercritical fluid is single phase. As a result, the receiver would not serve to regulate the gas cooler pressure. Additionally, since the exit from the gas cooler is supercritical liquid, the receiver's purpose as a refrigerant reservoir would be limited, as a large increase in pressure would be necessary for a small volume of refrigerant storage. This limitation could be overcome with a patented variable volume high side receiver (Lorentzen and Petterson, 1993).

D.3 Flash gas bypass in subcritical / transcritical cycle

Flash gas bypass plays the same role in the subcritical and transcritical cycles. Flash gas bypass can be used to separate liquid from vapor of the refrigerant entering the evaporator. The benefit for R744 systems is substantial because it minimizes distribution problems in the headers of microchannel heat exchangers, which are used to accommodate the high pressures of carbon dioxide. Flash gas bypass not only results in better distribution through the header, but at the same time allows for control of the evaporator exit quality. By placing the receiver after the expansion valve, separation of liquid and vapor can occur which would not happen if the receiver were placed before the expansion valve (as in a high-pressure receiver). This low-pressure receiver also allows for the accumulation of excess refrigerant in the cycle.

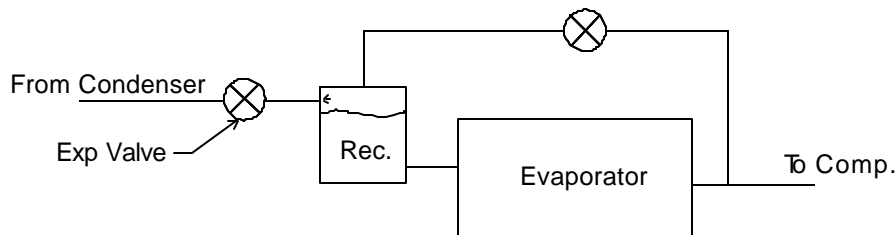


Figure D.4 Flash Gas Bypass

The disadvantage of this configuration is that it requires two valves for control. An additional valve (or possibly fixed orifice) on the vapor line controls the evaporator exit state. Depending on the adjustment of the valve on the vapor line, the mass flow through the vapor line and evaporator, and the evaporating temperature and pressure, will adjust so that the pressure drop across both lines equilibrates. For a closed loop system, a sensor at the evaporator exit provides feedback for control of the valve: for example, a thermostatic expansion valve could be used on the vapor line or the combination of a thermocouple, electronic expansion valve and controller could be used. Adjustment of the throttling valve works similarly to the low-pressure receiver system, where refrigerant is moved to or from the condenser to determine the high side pressure.

By removing vapor from the refrigerant and sending only liquid to the evaporator, distribution in the header of the evaporator is improved. This results in more uniform distribution of refrigerant in the heat exchanger, which maximizes the evaporator's effectiveness.

Appendix E: Psychrometrics and Sensible Heat Ratio

E.1 Sensible heat ratio in terms of log-mean differences

The sensible heat ratio is defined as:

$$SHR = \frac{q_{sensible}}{q_{sensible} + q_{latent}} \quad (E.1)$$

For sensible heat transfer, based a resistance network and the log-mean difference is:

$$\frac{1}{UA} = \frac{\mathbf{a}}{h_{ref}A_{air}} + \frac{1}{h_{air}A_{air}} \quad (E.2)$$

$$q_{sensible} = \frac{h_{ref}h_{air}A_{air}}{h_{ref} + \mathbf{a}h_{air}} \cdot LMTD \quad (E.3)$$

Localized mass transfer is given by:

$$q_{latent} = h_{mass}A(\mathbf{w}_{air} - \mathbf{w}_{sat})h_{fg} \quad (E.4)$$

As a result, incorporating the heat/mass transfer analogy, the overall latent heat transfer based on log-mean difference is:

$$h_{mass} = \frac{h_{heat}}{c_{p,m}Le^{2/3}} \quad (E.5)$$

$$\frac{1}{UA} = \frac{1}{h_{mass}A} = \frac{c_{p,m}Le^{2/3}}{h_{air}A_{air}} \Rightarrow UA = \frac{h_{air}A_{air}}{c_{p,m}Le^{2/3}} \quad (E.6)$$

$$q_{latent} = \frac{h_{air}A_{air}}{c_{p,m}Le^{2/3}} \cdot LMwD \cdot h_{fg} \quad (E.7)$$

Combining the above, the sensible heat ratio is determined by:

$$SHR = \frac{1}{1 + \frac{LMwD \cdot h_{fg} \cdot (h_{ref} + \mathbf{a}h_{air})}{LMTD \cdot c_{p,m} \cdot Le^{2/3} \cdot h_{ref}}} \quad (E.8)$$

Based on the previous equations the required heat exchanger area can be calculated by:

$$A_{air} = \frac{q_{total}}{h_{air} \left(\frac{h_{ref}LMTD}{h_{ref} + \mathbf{a}h_{air}} + \frac{LMwD \cdot h_{fg}}{c_{p,m}Le^{2/3}} \right)} \quad (E.9)$$

E.2 Psychrometric relationship

From the expression for sensible heat ratio it is evident that this is independent of capacity, which can be explained based on psychrometric considerations. Since the latent and sensible heat transfer is a function of the

same air flow rate, psychrometrically the sensible heat ratio is the ratio between the latent and sensible change in enthalpy. The enthalpy ratio fixes the slope of a cooling line on a psychrometric chart (Pita, 1989). As shown in Figure E.1, the inlet condition and slope of the relative change in enthalpy then uniquely defines the evaporator surface temperature as the intercept of this line with the saturation curve on a psychrometric plot. In the equations above, the relative latent and sensible changes in enthalpy are defined in terms of the heat transfer coefficients and log-mean differences. As a result, the evaporating temperature for a given SHR is dependent only on the inlet conditions, and the air mass flow rate can be adjusted for capacity.

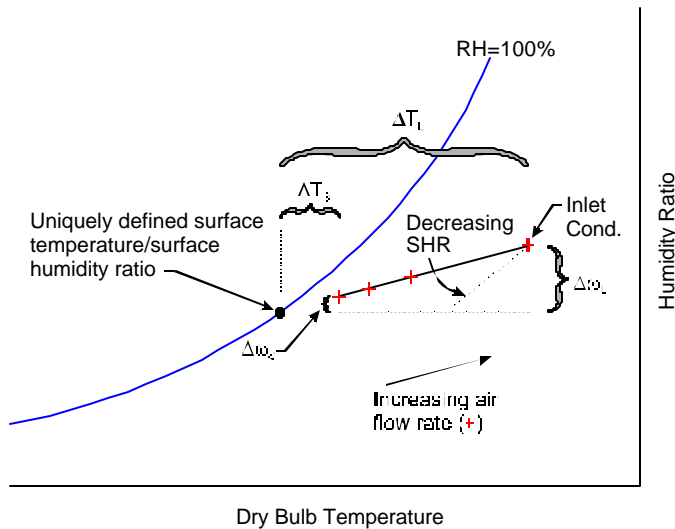


Figure E.1 Graphic psychrometric determination of evaporator surface temperature

E.3 EES program

The following EES program calculates the required evaporating temperature from given inlet air conditions and SHR based on the equations above. Additionally, the air-refrigerant temperature difference at the exit from the evaporator can be specified, which determines the air exit enthalpy; from that, the required air flow rate and heat exchanger area for a given capacity can be calculated. The program is arranged to simulate the effect of a variable speed fan by adjusting the air side heat transfer coefficient as $Re^{0.8}$.

EES listing:

"!Main psychrometric program"

"Sensible heat ratio and air flow requirements"

P_atm = 101

RH = 0.5 "Relative humidity"

Teai = 27

DELTAT_air = 1 "assume 1 degree approach on air side"

SHR=0.75 "sensible heat ratio"

m_dot_air_max=0.1

Q_supplied = 1 "Total heat transfer in kW"

Le=1

$h_{2\text{phase}}=10000$ "Refrigerant side heat transfer coefficient, [W/m² K]"
 $h_{\text{ev_air}}=90*(m_{\text{dot_air}}/m_{\text{dot_air_max}})^{0.8}$ "Air side heat transfer coefficient, [W/m² K]"
 $\alpha=7.8$ "Fin to refrigerant area ratio"

$T_{\text{dp_in}} = \text{dewpoint}(\text{airh2o}, P=P_{\text{atm}}, T=\text{Teai}, R=\text{RH})$
 $T_{\text{dp_out}}=\text{dewpoint}(\text{airh2o}, P=P_{\text{atm}}, T=\text{Teao}, R=\text{RH}_o)$

"First calculate air outlet temperature and humidity for various mass flow rates at given SHR"

$\text{cfmperton} =$
 $m_{\text{dot_air}}*\text{volume}(\text{air}, T=\text{Teai}, P=P_{\text{atm}})*\text{convert}(m^3/s, ft^3/min)/((q_s+q_{\text{lat}})*\text{convert}(kW, ton))$
 $q_s + q_{\text{lat}} = Q_{\text{supplied}}$
 $\text{SHR} = 1/(1+q_{\text{lat}}/q_s)$
 $q_s = m_{\text{dot_air}}*\text{specheat}(\text{air}, T=\text{Teai})*(Teai - Teao)$
 $q_{\text{lat}} = m_{\text{dot_air}}*(\omega_i - \omega_o)*h_{\text{fg}}$
 $h_{\text{fg}} = (\text{enthalpy}(\text{water}, x=1, T=\text{Teao}) - \text{enthalpy}(\text{water}, x=0, T=\text{Teao}))$
 $c_{\text{pm}} = 1.02$
 $\omega_i = \text{humrat}(\text{airH2O}, T=\text{Teai}, R=\text{RH}, P=P_{\text{atm}})$
 $\omega_o = \text{humrat}(\text{airH2O}, T=\text{Teao}, R=\text{RH}_o, P=P_{\text{atm}})$

"Results showed that outlet air conditions are essentially independent of air flow rate"

"Now calculate relation between outlet air temperature and humidity, consistent with heat/mass transfer relation"

$\text{SHR} =$
 $1/(1+(h_{\text{fg}}*\text{LMwD}*((h_{2\text{phase}}+\alpha*h_{\text{ev_air}})/1000))/(c_{\text{pm}}*Le^{(2/3)}*(h_{2\text{phase}}/1000)*\text{LMTD}_a))$
 $\text{LMTD}_a = (L_t - S_t)/\ln(L_t/S_t)$
 $L_t = Teai - T_{\text{surf_ev}}$
 $S_t = Teao - T_{\text{surf_ev}}$

$\text{LMwD} = (L_w - S_w)/\ln(L_w/S_w)$
 $L_w = \omega_i - \omega_s$
 $S_w = \omega_o - \omega_s$
 $\omega_s = \text{humrat}(\text{airH2O}, T=T_{\text{surf_ev}}, R=1, P=P_{\text{atm}})$

$\text{DELTAT}_{\text{approach}} = \text{DELTAT}_{\text{air}} + \text{DELTAT}_{\text{ref}}$
 $T_{\text{surf_ev}} = T_{\text{ero}} + \text{DELTAT}_{\text{ref}}$
 $Teao = T_{\text{surf_ev}} + \text{DELTAT}_{\text{air}}$

$h_{\text{in}} = \text{Enthalpy}(\text{airH2O}, P=P_{\text{atm}}, T=\text{Teai}, W=\omega_i)$
 $h_{\text{out}} = \text{Enthalpy}(\text{airH2O}, P=P_{\text{atm}}, T=\text{Teao}, W=\omega_o)$

$\text{DELTAT}_{\text{ref}} = Q_{\text{supplied}}/(h_{2\text{phase}}/1000*A_{\text{ev_logmean}}/\alpha)$

$A_{\text{ev_logmean}} = Q_{\text{supplied}}/(h_{\text{ev_air}}/1000*((h_{2\text{phase}}/1000*\text{LMTD}_a)/(h_{2\text{phase}}/1000+\alpha*h_{\text{ev_air}}/1000)+(\text{LMwD}*h_{\text{fg}})/(c_{\text{pm}}*Le^{(2/3)})))$ "Evaporator air-side area"

E.4 Results

In Figure E.2 the required evaporating temperature is plotted as a function of SHR for two inlet conditions, based on the following assumptions (typical for R744):

h_{ref} :	10,000 W/m ² K
$h_{\text{air,max}}$:	90 W/m ² K
α :	7.8
Le :	1

The sharp decay of the evaporating temperature as the SHR is decreased in Figure E.2 can be explained in terms of the psychrometric plot: as the SHR is decreased, the slope of the line gets steeper, which, when coupled with the curve of the saturation line, produces the sharp decay.

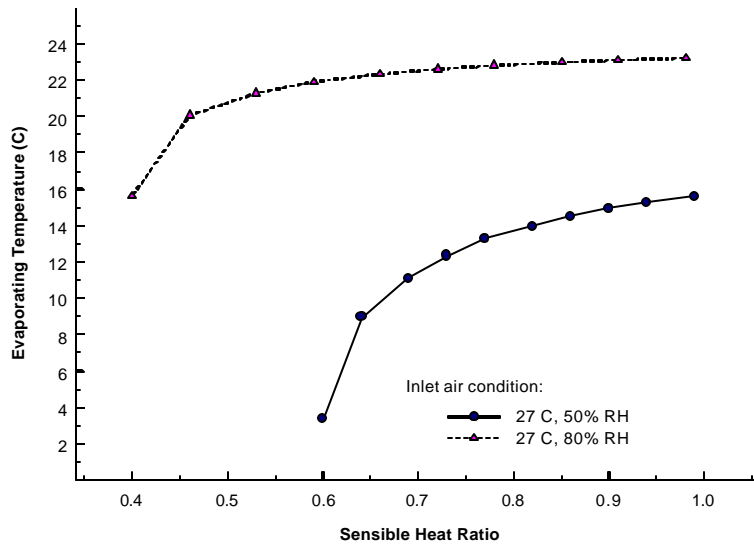


Figure E.2 Evaporating temperature dependence on inlet conditions for a given sensible heat ratio (R744)

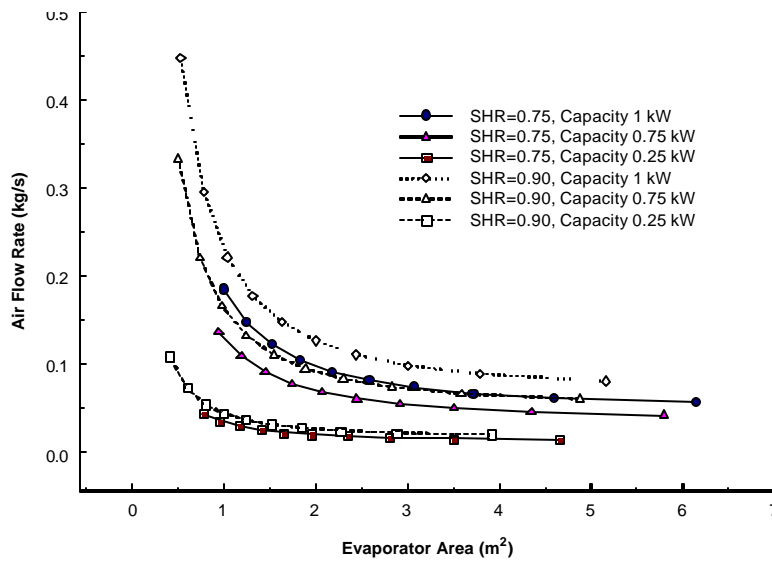


Figure E.3 Capacity control for finite heat exchange area by varying air flow rate (R744)

Since the evaporating temperature for a given SHR is independent of air flow rate, a specified SHR can be met from a fixed sized heat exchanger for a range of capacities by adjusting the air flow rate. Changing the airflow rate changes the air side heat transfer coefficient which then changes the area required for the same heat transfer. As a result, by controlling both the compressor displacement and airflow rate the SHR can be adjusted for a fixed area heat exchanger. This is shown in Figure E.3 where the relationship between airflow rate and evaporator area is shown for three capacities and two sensible heat ratios, based on the assumptions above.